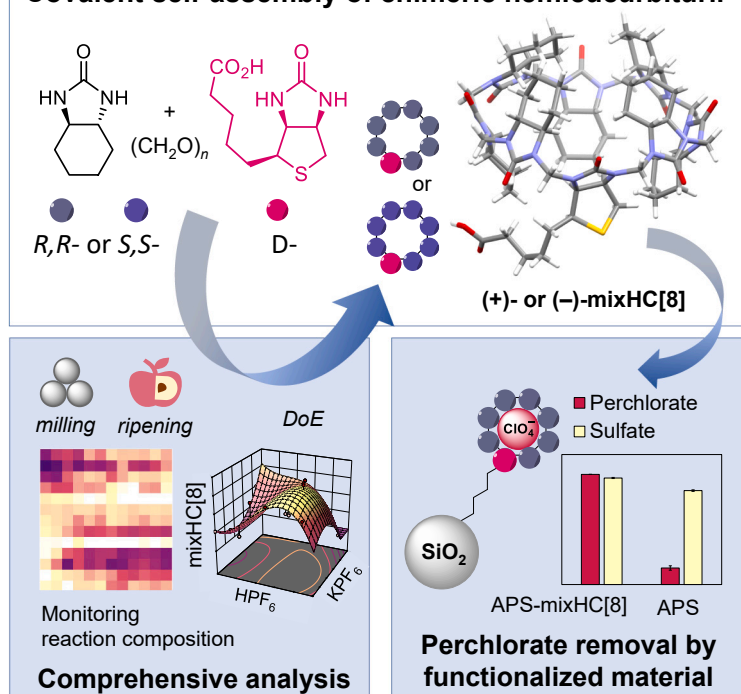


Article

Mechanochemically driven covalent self-assembly of a chiral mono-biotinylated hemicucurbit[8]uril

Covalent self-assembly of chimeric hemicucurbituril



Elina Suut-Tuule, Tatsiana Jarg, Priit Tikker, ..., Kari Rissanen, Dzmitry Kananovich, Riina Aav

riina.aav@taltech.ee

Highlights

Dynamic covalent chemistry in solid state delivers chimeric hemicucurbit[8]urils

Two major products are amplified from ca. 50,000 possible compounds

Mechanochemistry and anionic templation drive covalent self-assembly

Silica modified by biotinylated macrocycle is suitable for perchlorate capture

Suut-Tuule and Jarg et al. demonstrate that mechanochemistry enhances reactivity and significantly improves selectivity in the solid-state synthesis of mono-biotinylated hemicucurbit[8]urils. The application of the chimeric macrocycle is showcased by its immobilization on silica and subsequent use as a selective solid-phase extraction material for perchlorate removal.

Suut-Tuule et al., Cell Reports Physical Science 5, 102161

September 18, 2024 © 2024 The Author(s).
Published by Elsevier Inc.

<https://doi.org/10.1016/j.xcrp.2024.102161>



Article

Mechanochemically driven covalent self-assembly of a chiral mono-biotinylated hemicucurbit[8]uril

Elina Suut-Tuule,^{1,8} Tatsiana Jarg,^{1,8} Priit Tikker,² Ketren-Marlein Lootus,¹ Jevgenija Martõnova,¹ Rauno Reitalu,¹ Lukas Ustrnul,¹ Jas S. Ward,³ Vitalijs Rjabovs,^{4,5} Kirill Shubin,⁶ Jagadeesh V. Nallaparaju,¹ Marko Vendelin,⁷ Sergei Preis,² Mario Öeren,¹ Kari Rissanen,³ Dzmitry Kananovich,¹ and Riina Aav^{1,9,10,*}

SUMMARY

Solution-based synthesis of complex molecules with high efficiency leverages supramolecular control over covalent bond formation. Herein, we present the mechanosynthesis of chiral mono-biotinylated hemicucurbit[8]urils (mixHC[8]s) via the condensation of D-biotin, (R,R)- or (S,S)-cyclohexa-1,2-diylurea, and paraformaldehyde. The selectivity of self-assembly is enhanced through mechanochemistry and by fostering non-covalent interactions, achieved by eliminating solvents and conducting the reaction in the solid state. Rigorous analysis of intermediates reveals key processes and chemical parameters influencing dynamic covalent chemistry. The library of ca. 50,000 theoretically predicted intermediates and products leads to covalent self-assembly of chiral hemicucurbiturils. Mechanochemically prepared diastereomeric (–)- and (+)-mixHC[8]s are suitable for anion binding and derivatization. Immobilization of the macrocycles on aminated silica produces a functional material capable of selective capture of anions, as demonstrated by efficient perchlorate removal from a spiked mineral matrix.

INTRODUCTION

The spontaneous organization of molecular species relies on non-covalent interactions, resulting in intricate aggregates. Such supramolecular self-assembly can facilitate the formation of covalent bonds leading to complex molecules and may be exceptionally responsive to minor changes in the reaction conditions, resulting in the amplification of particular products.¹ In the case of increased molecular crowding, the dynamics of an interaction between species is accelerated compared to a dilute environment, which has been demonstrated for strongly hydrogen-bonded base pairs of nucleic acids.² Furthermore, in the solid state at extreme concentrations, unobstructed by solvent, the number of non-covalent interactions between counterparts increases, enabling the formation of products that are less favored in solution.^{3,4} Mechanochemical activation enhances chemical reactivity and provides a solvent-free sustainable approach in chemical syntheses.^{5–7}

Single-bridged cucurbituril-type molecular containers, hemicucurbit[n]urils (HC[n]s) are renowned for their anion-binding properties and typically assembled from urea monomers in a one-pot reaction with dynamic covalent chemistry (DCC).^{8–10} Although the size of the macrocycle can be controlled by anion templation,^{8,11–15} HC[n]s prevalently consist of six units.^{12,16,17} Up to date, 8-membered HC[n]s have been synthesized exclusively from chiral C₂-symmetric cyclohexa-1,2-diylurea (CU)

¹Tallinn University of Technology, Department of Chemistry and Biotechnology, 12618 Tallinn, Estonia

²Tallinn University of Technology, Department of Materials and Environmental Technology, 19086 Tallinn, Estonia

³University of Jyväskylä, Department of Chemistry, 40014 Jyväskylä, Finland

⁴National Institute of Chemical Physics and Biophysics, 12618 Tallinn, Estonia

⁵Institute of Chemistry and Chemical Technology, Riga Technical University, 1048 Riga, Latvia

⁶Latvian Institute of Organic Synthesis, 1006 Riga, Latvia

⁷Tallinn University of Technology, Department of Cybernetics, 12618 Tallinn, Estonia

⁸These authors contributed equally

⁹X (formerly Twitter): @RiinaAav

¹⁰Lead contact

*Correspondence: riina.aav@taltech.ee
<https://doi.org/10.1016/j.xcrp.2024.102161>



monomers, and the corresponding (*R,R*)- and (*S,S*)-cyclohexanohemicucurbit[8]urils (cycHC[8]s) can be assembled both in solution¹⁸ and the solid state.¹⁷ Their larger cavity expands the range of applications, and the insertion of another functional monomer, such as D-biotin, into the cycHC[8] scaffold can further enhance receptor versatility. Biotin is a naturally occurring and commercially available compound with a carboxylic group suitable for derivatization. Furthermore, it has previously been used in the synthesis of chiral macrocycles.¹³ So far, the reported chimeric HC[*n*]s assembled from non-equivalent urea monomers have been limited to 6-membered hybrid HC[*n*]s prepared in solution via multi-step approaches^{19,20} and mono-functionalized bambus[6]urils obtained in a one-pot reaction.^{21–23} The difficulties in the single-step formation of non-uniformly composed macrocycles arise from a plethora of possible linear and cyclic intermediates. Consequently, arranging a chaotic mixture into a well-organized molecule presents considerable challenges, and the number of combinations increases with the number of monomeric units.

Mechanochemistry has been utilized in the synthesis of several macrocycles,^{17,24–30} inducing covalent assembly of uniformly structured monomers. As mechanosynthesis enables overcoming the solubility barriers and promotes reactions between compounds with drastic polarity differences, its potential can be exploited even further. To the best of our knowledge, there have been no reports describing covalent self-assembly of macrocycles from mixtures of various monomers in the solid state. The formation of chiral chimeric HC[*n*]s via DCC in the solid state could pave the way to novel synthetic approaches, unlocking access to versatile applications.

The present work describes a mechanochemically activated solid-state condensation of (*R,R*)- or (*S,S*)-CU, D-biotin ((*S,S,R*)-B), and paraformaldehyde and their selective covalent self-assembly into the enantiopure mono-biotinylated HC[8]s (–)-((*S,S,R*)(*R,R*))-mixHC[8] or (+)-((*S,S,R*)(*S,S*))-mixHC[8], along with homomeric cycHC[8]s. The challenges of assembling a chimeric mono-functionalized 8-membered macrocycle are related to the number of possible combinations of monomeric units and their chemical reactivity. Fine-tuning of the reaction conditions enabled amplification of the two major products, chimeric mixHC[8] and homomeric cycHC[8], among 498 potential 8-membered HC[*n*]s³¹ (Figure 1; theoretical number of linear cyclic oligomers in the supplemental experimental procedures; Data S1).

The covalent assembly process is essentially solvent free and has a very low process mass intensity (PMI; the mass of all used reagents per formed product³²). The most significant chemical and technical factors affecting macrocyclization were identified with response surface methodology (RSM) and thorough analysis of intermediates by high-performance liquid chromatography-mass spectrometry (HPLC-MS) provided mechanistic insight into this complex process. The affinity of mixHC[8] for selected anions and the subtle differences in the binding properties of the two chimeric diastereomers were determined by isothermal titration calorimetry (ITC) and characterized by single-crystal X-ray crystallography (SC-XRD) and modeling studies. Furthermore, a practical example of the selective anion capture by silica-immobilized mixHC[8] was demonstrated in the efficient removal of perchlorate from a spiked mineral matrix.

RESULTS AND DISCUSSION

Covalent assembly of hemicucurbiturils in the solid state

The first attempts to synthesize mono-functionalized mixHC[8] in solution according to the protocol developed for cycHC[8]¹⁸ were promising. The condensation of

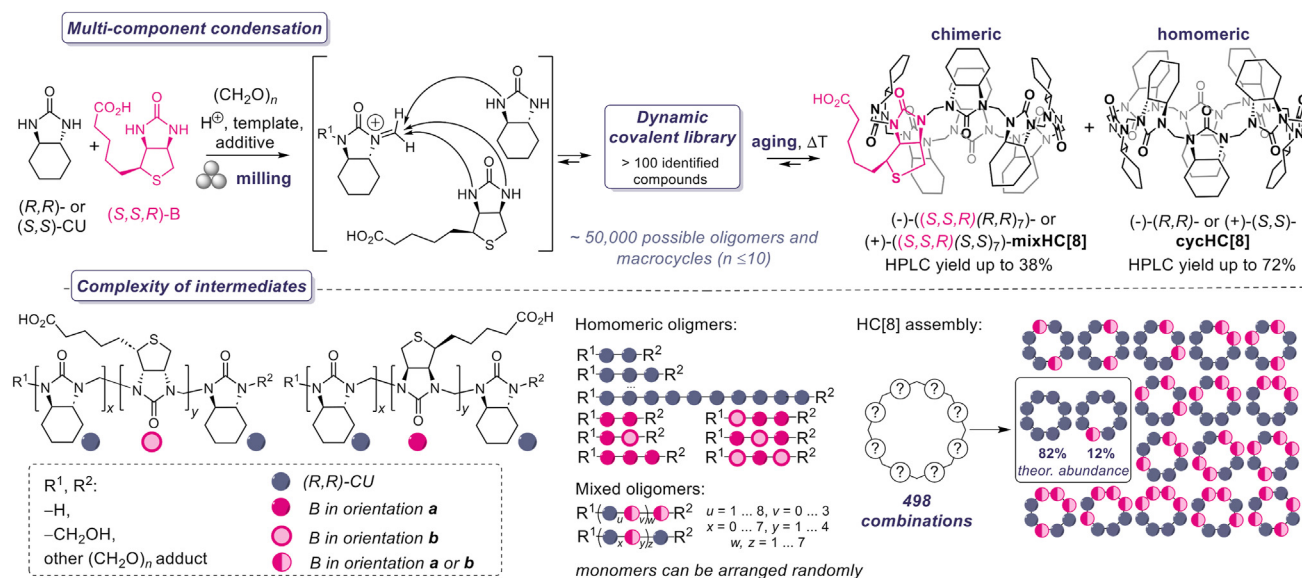


Figure 1. Synthetic scheme and complexity of intermediates during formation of the HC[8]s studied in this work

Multi-component condensation of (*S,S,R*)-biotin (B) and (*R,R*)- or (*S,S*)-cyclohexa-1,2-diylurea (CU) to homomeric cycHC[8]s and chimeric mixHC[8]s. The complexity of the intermediates in the DCL is expressed via possible numbers of oligomers, HC[8]s, and the abundance of major HC[8]s resulting from the 1:7 (B:CU) ratio of starting materials (theoretical number of linear cyclic oligomers in the supplemental experimental procedures; Data S1). The best reaction conditions afford 38% and 34% yields of mixHC[8] and cycHC[8], respectively: 1 equiv B, 7 equiv CU, 8 equiv (CH₂O)_n in the presence of 2 equiv HPF₆ and 1 equiv KPF₆, milled at 30 Hz for 60 min and aged at 60°C for 3 h (Table S15). The highest yield (72%) of cycHC[8] was observed under the following conditions: 1 equiv B, 15 equiv CU, 16 equiv (CH₂O)_n in the presence of 3 equiv HClO₄, milled at 30 Hz for 60 min and aged at 45°C for 24 h (Table S2).

biotin and CU taken in stoichiometric 1:7 molar ratio with paraformaldehyde, mediated by trifluoroacetic acid in acetonitrile, produced mixHC[8] and cycHC[8] in 9% and 38% yields, respectively (see synthesis in solution in the supplemental experimental procedures; Data S1). The ratio of the macrocycles did not reflect the statistical distribution based on the starting monomer ratio, which implied a strong influence of the chemical parameters. In solution-based synthesis, compatibility between the solvent and reagents governs the fast diffusion and mixing of starting materials, intermediates, and products, as well as their reactivity. Poor solubility can obstruct reactions, especially in DCC, due to suppressed exchange between reactants. We envisioned that mixHC[8]s may be assembled with higher efficiency in the solid state, where solubility is not critical, non-covalent interactions are not obstructed by the solvent, and templation is enhanced due to a high concentration of reactants.³ According to the previous study,¹⁷ covalent self-assembly in the solid state required just a minute amount of a liquid additive^{33–35} to facilitate proton transfer and delivery of the anionic template, as well as to promote conformational flexibility. The complexity of the dynamic covalent library (DCL) drastically increases in multi-component reactions; for instance, the incorporation of non-C₂ symmetric (*R,S*)-CU units resulted in higher stereochemical diversity and the formation of several diastereomeric HC[*n*]s (i.e., *cis*-cycHC[6] and inverted-*cis*-cycHC[6]).³⁶ Similarly, condensation of chiral CU and non-C₂ symmetric biotin into linear and cyclic oligomers can be realized via various combinations, considering the possibility of different orientations of the biotin unit (Figure 1). For instance, all forms with a length of 2 to 10 monomers result in ca. 50,000 cyclic and linear oligomers. However, the number of possible products can be decreased by templation. Variation of position, orientation, and number of B and CU monomers leads to 498 potential 8-membered macrocycles³¹ (Figure 1; theoretical number of linear cyclic oligomers in the

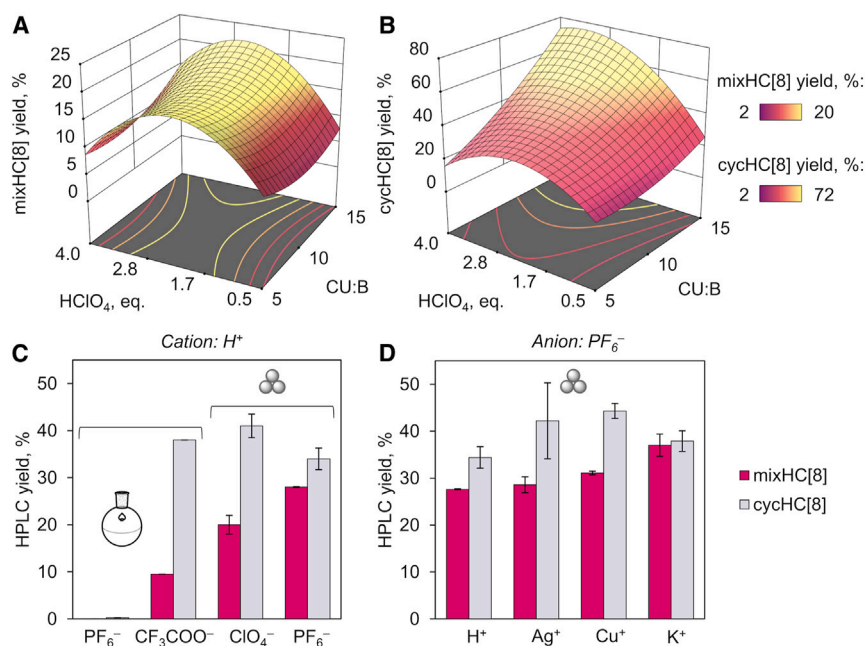


Figure 2. 3D response surfaces and bar charts expressing the formation of HC[8]s

(A and B) 3D response surfaces displaying the influence of the ratio of monomers and loading of aq. HClO₄ on the HPLC yields of (A) mixHC[8] and (B) cycHC[8].

(C and D) Bar charts comparing the effect of the acid anions (CF₃COO⁻, ClO₄⁻, and PF₆⁻) in solution and the solid state (C) and hexafluorophosphate salt cations (Ag⁺, Cu⁺, K⁺) in the solid state (D) on the yields of cycHC[8] (gray) and mixHC[8] (magenta). Error bars on HPLC yields express standard deviation between reproduced reactions (n= 2–8). For more details, see Table S7.

supplemental experimental procedures; Data S1). Full conversion of the 1:7 ratio of B and CU into HC[8]s is expected to direct 498 combinations to 12% and 82% of mixHC[8] and cycHC[8], respectively (Figure 1; Table S1).

The fact that solution-phase synthesis did not result in a statistical ratio of more favored HC[8]s encouraged us to study if the selectivity of mono-biotinylated mixHC[8] formation can be increased via tuning the conditions of the mechanosynthesis. To investigate the effect of multiple reaction parameters on the assembly of 8-membered macrocycles, we utilized RSM for experimental design and screening of reaction conditions.³⁷ The HPLC yields of mixHC[8] and cycHC[8] obtained after the aging step were plotted as 3D response surfaces, highlighting the conditions favorable for the assembly of mixHC[8] compared to cycHC[8] (Figures 2A, 2B, S3, and S4; Tables S2–S6). The ratio of monomers, loading of aqueous mineral acid (HClO₄), milling duration, and aging temperature, which affect macrocyclization,⁸ were simultaneously explored.

The formation of mixHC[8] and cycHC[8] proved to be sensitive to the monomer ratio and acid loading (Figures 2A and 2B). Variations of the monomer ratios within the range of 1:5 to 1:15 did not significantly affect the yield of chimeric mixHC[8] (Figure 2A; Table S2); however, using an excess of CU clearly resulted in the enhanced generation of cycHC[8] (Figure 2B; Table S2). The quantity of HClO₄ appeared to be the vital parameter affecting the formation of mixHC[8]. The highest yields of mixHC[8] were attained within the specific range of HClO₄ loadings of 1.2–3.0 equiv (Figure 2A), while cycHC[8] was less dependent on the quantity of acid catalyst. This observation highlights the difference in formation of mixHC[8] and cycHC[8] in

response to varied reaction conditions. The impacts of milling time and aging temperature appeared to be less significant, and the optimal temperature for ripening mixHC[8] was found to range from 40°C to 65°C. RSM helped to reach a 20% yield of mixHC[8] under standard conditions—3 equiv of template, 1 h ball milling followed by 24 h aging at 60°C—selected for further optimization studies.

It was hypothesized that an alternative template could amplify the formation of the target macrocycle. The binding studies for the cycHC[8] receptor revealed the following ranking of anion affinity: $\text{SbF}_6^- > \text{PF}_6^- > \text{ReO}_4^- > \text{ClO}_4^-$.¹¹ The use of hexafluoroantimonate (SbF_6^-) as a template did not seem practical since HSbF_6 mainly exists as the HF/SbF_5 superacid system.^{38,39} Hexafluorophosphate (PF_6^-), on the other hand, serves as an efficient template for the synthesis of homomeric cycHC[8] in solution.¹⁸ Due to its advantageous templating potential, HPF_6 was chosen as an alternative reagent to mediate the solid-state synthesis of mixHC[8]. In addition, it is safer to handle than perchlorates, which are known for their undesirable oxidative, flammable, and explosive hazards.^{40,41} Interestingly, the use of HPF_6 resulted in decreased formation of homomeric cycHC[8], contrary to an improved yield (28%) of mixHC[8] (Figure 2C; Table S7). Since the mixHC[8] assembly was highly sensitive to the quantity of acid (Figure 2A), we tested three hexafluorophosphate salts (AgPF_6 , $[\text{Cu}(\text{CH}_3\text{CN})_4]\text{PF}_6$, and KPF_6) as additives to partially substitute the acid while keeping the amount of template anion constant (Figure 2D; Table S7). Additionally, we anticipated that the Ag^+ and Cu^+ cations could serve as potential promoters for the generation of mixHC[8] due to their affinity for biotin.^{42–44} As depicted in Figure 2D, the Ag^+ and Cu^+ salts had a negligible effect on the formation of mixHC[8] while improving the yield of homomeric cycHC[8] compared to the reaction with HPF_6 . The latter points at the effective decrease in the concentration of antagonistic⁴⁵ CU-rich mixed oligomers, which reassembled and provided CU to cyclize into cycHC[8]. The best result was achieved with KPF_6 , which afforded the highest yield of mixHC[8] (37%) with the accompanying formation of cycHC[8] (38%) (Figure 2D). Further variation of $\text{HPF}_6/\text{KPF}_6$ equivalence by RSM, however, did not improve the formation of mixHC[8] (Tables S8–S12; Figure S8). It was additionally confirmed that the stoichiometric ratio of the starting monomers provided the best mixHC[8] yield (Table S13). Once the key chemical parameters had been identified, the durations of ball milling and aging at moderately elevated temperatures were optimized, leading to the best 38% yield of mixHC[8] in a 4 h total reaction time (Tables S14 and S15; for conditions, see the Figure 1 caption).

The changes in the content of intermediates and products were analyzed by HRMS. Altogether, over 100 reaction species were identified in the crude reaction mixtures during different stages of covalent assembly and mapped based on MS signal intensities (Figures 3A and S9–S13; Tables S16 and S29; MatchMass tool⁴⁶). The results display the dynamic changes in the composition of the reaction mixture during milling and aging. Biotin was found to be incorporated into different linear oligomers $(\text{CU})_x(\text{B})_y$ ($x = 1 \dots 8$, $y = 1 \dots 4$), as well as into a number of mono-, di-, tri-, and tetra-biotinylated mixHC[n]s ($n = 6 \dots 8$). Homomeric CU oligomers dominate at the initial phase of the polycondensation reaction (milling time: 5 min) and are kinetically favored products. Consequently, the milling time must be sufficient (60 min; Tables S14 and S15) to enable the accumulation of the slowly generated mixed biotin-containing chains. The content of the mixed oligomers ($n = 6–8$), which are essential for mixHC[n] formation, significantly increased after 45–60 min milling. This difference in the contents of the short- and long-milled mixtures emphasizes the dynamic shuffling of the monomers, which resulted in an increased random distribution of biotin upon prolonged milling. The low content of macrocycles in DCL

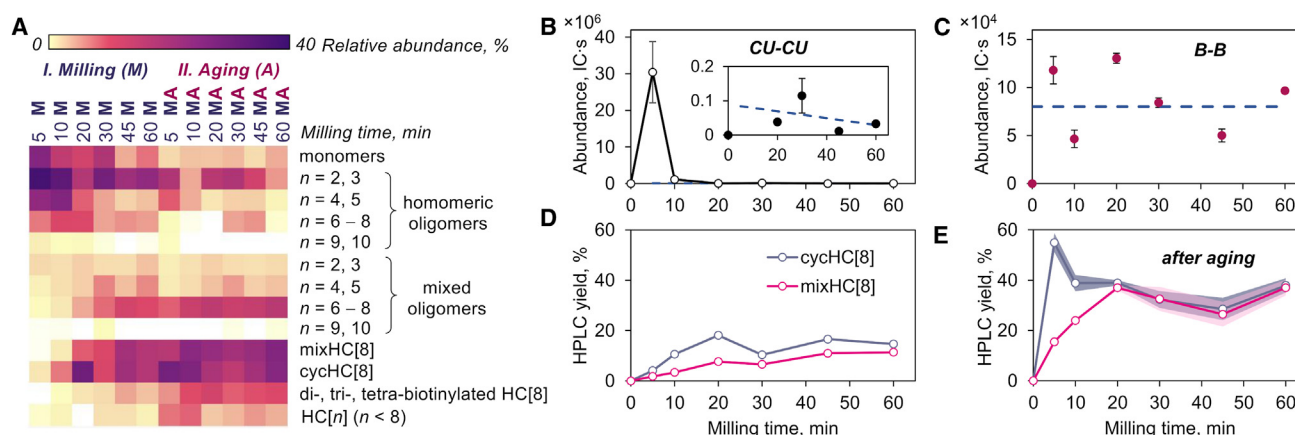


Figure 3. Dynamic covalent library composition and changes in the content of dimers and HC[8]s during mechanosynthesis

DCL composition summarized in a heatmap (A) based on MS abundance of the detected species (Tables S29 and S16; Figure S10); content of homomeric dimers CU-CU (B) and B-B (C) and HPLC yields of macrocycles (D and E) during milling and after aging. The content of the dimers is reported as the MS abundance for triplicate measurements ($n = 3$) \pm standard deviation, and the linear fit is expressed as dashed lines. The yields of macrocycles are presented as mean values obtained in a series of replicated experiments ($2 \leq n \leq 4$) with confidence intervals. More details are provided in Figures S11–S15 and Table S19.

directly after milling can be attributed to the unfavorable complexation with the template,^{11,17} most likely due to increased entropy during mechanical agitation. The macrocyclic products predominantly ripened at the aging stage, at which point the mixed and homomeric oligomers underwent additional, although less intense, crossover unit exchange. Moreover, crossover between monomers from macrocycles was observed under similar conditions using cycHC[n]s and biotin as the starting materials for mixHC[8] synthesis (Table S17), which confirms the dynamic character of the covalent self-assembly.

Further understanding of the dynamic processes and interconversion of intermediates occurring at the milling stage was obtained by tracking the fate of selected short oligomers (Figures 3B and 3C; Table S18). The changes in the content of characteristic dimers and trimers prior to and after the aging stage were determined by HPLC-MS analyses. The collected data confirmed that coupling between the CU monomers is kinetically preferred and occurs at the initial phase of the polycondensation reaction. Thus, the quantity of the CU-CU dimer drastically increased after 5 min of milling and subsequently underwent rapid decay (Figure 3B). Such fast dynamics and decay were absent for the biotin units, reflecting a major difference in the condensation between biotin and CU. In contrast to CU, the condensation of the biotin units to the respective dimer, B-B, reached its maximum at the beginning of the reaction and probably acts as a transient intermediate (Figures 3B and 3C). Similar behavior was observed for the respective trimers (Table S18). The yields of the macrocycles generated at the milling stage did not exceed 20% but greatly increased during aging (Figures 3D and 3E). Notably, the macrocyclic content in the aged mixtures is significantly affected by milling duration, when monomer shuffling occurs. Thus, aging of the short-milled (5 min) reaction mixture, which contained mainly homomeric CU oligomers, resulted in the ripening of cycHC[8] as the dominant product (55% yield), along with a minor quantity of mixHC[8] (16% yield). However, fast reversible C–N bond formation and cleavage during milling caused rapid dynamic changes in the oligomeric profile with a random distribution of the biotin units. Upon prolonged milling (60 min; Tables S14 and S15), the yield of mixHC[8] notably increased from 16% to 37%, with a concurrent decrease in the yield of cycHC[8] to 38%, resulting

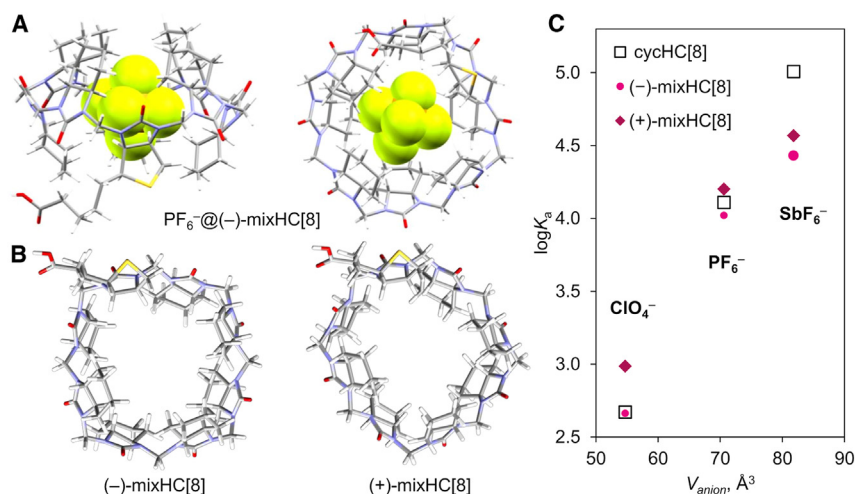


Figure 4. Structures of mixHC[8]s and data on anion binding

PF_6^- @(-)-mixHC[8] inclusion complex from SC-XRD (A) (CCDC: 2251913). DFT low-energy structures of (-)- and (+)-mixHC[8] diastereomers (B) (see the computational study in the supplemental experimental procedures; Data S2). Correlation between anion volumes (V_{anion}) and association constants ($\log K_a$) was determined by ITC for complexes with (TBA) ClO_4 , (TBA) PF_6 (TBA = tetrabutylammonium), and NaSbF_6 salts in methanol using one-to-one binding model (C) (Table S6.1).

in a 1:1 product ratio. Finally, a close examination of the aging duration (Table S15) revealed that the maximum content of mixHC[8] was achieved in 3 h, when the templated self-assembly process was essentially complete.

The developed mechanochemical procedure significantly surpassed mixHC[8] synthesis in solution, yielding superior selectivity and conversion rates (Table S30). Solution-state processes are affected by diffusion, with diffusion constants varying for monomers, aggregates, and oligomeric intermediates due to size differences. In mechanochemistry, reaction rates do not directly depend on the molecular size of the intermediates but rather on the number of molecular collisions.⁴⁷ In addition to the chemical advantages, solvent-free synthesis produces less waste (PMI = 4) compared to the reaction in solution (PMI = 306) and is more sustainable based on the respective green metrics (Table S30).³²

Diastereoisomeric (-)- and (+)-mixHC[8]s were synthesized via condensation of either (R,R)-CU or (S,S)-CU with (S,S,R)-B, isolated in 16% and 11% yields with high purity (88% and 90%, respectively), and characterized by nuclear magnetic resonance (NMR) and infrared spectroscopy (Figures S16–S32).

Anion binding properties

The encapsulation of suitably sized anionic guests by HC[n]s is likely governed by electrostatic and orbital interactions.⁴⁸ In addition, the anions form weak interactions with C-H groups of HC[n]s pointing inside the cavity.⁴⁹ Efficient anion recognition has been reported for bambusurils,^{22,50–53} heterobambusurils,⁵⁴ biotinurils,^{55,56} and cycHC[n]s.¹¹ We were fortunate to obtain single crystals of the PF_6^- inclusion complex with (-)-mixHC[8] (Figures 4A and S33–S39; Tables S19 and S20). A DFT modeling study of the mixHC[8] diastereomers (Figure S40; Tables S21–S24; Data S2) revealed clear differences in their conformations (Figure 4B; Data S2). The cavity, which is mainly surrounded by CU units, is mostly

distorted by the biotin position. Therefore, its influence on the anion binding properties was evaluated via comparison of the three HC[8] hosts.

Encapsulation of the selected anions by the mixHC[8]s was studied by ITC (Figures 4C and S51–S54; Table S25); the data for cycHC[8] were available from a previous work.¹¹ Complexation between the mono-biotinylated macrocycles and chaotropic anions (ClO_4^- , PF_6^- , and SbF_6^-) in methanol and a methanol-water mixture (1:1) occurred as an exothermic enthalpy-driven process. The association constants for PF_6^- were greater than that of ClO_4^- in both media, which explains the better templating properties of PF_6^- . Noticeably, the differences between the affinities of the three HC[8] derivatives are the smallest for the templating PF_6^- anion, while for ClO_4^- and SbF_6^- , either (+)-mixHC[8] or cycHC[8], respectively, exhibit stronger binding. The noted dissimilarities highlight distinctions in the cavities and point to the steric differences of these host compounds, which have potential in a diverse array of applications and unique guest-binding properties.

Selective capture of perchlorate by immobilized mixHC[8]

The mixHC[8] can be utilized to afford functional materials, which was showcased by the selective removal of perchlorates from contaminated soil samples. Perchlorate is a persistent pollutant that adversely affects human health by interfering with thyroid hormone production and occurs in soil, ground water, and food.^{40,41} The accumulation of perchlorate in fertilizers, soil, and irrigation water leads to increased plant uptake and subsequent food-chain transfer.^{57,58} This pollutant has been found in various environmental matrices and typically originates from human activities.

The carboxylate side chain of mixHC[8] enabled its facile covalent immobilization on the surface of 3-aminopropyl silica gel (APS; Figure 5A).⁵⁹ The resulting solid perchlorate-extracting material (mixHC[8]-APS) contained ca. 12% (w/w) of mixHC[8], based on infrared spectroscopic analysis (Figures 5B and S55). Once covalently attached to APS, the macrocycle remains in the solid phase even in the solvents where it is commonly soluble (i.e., dichloromethane, methanol) and can, therefore, be applied in solid-phase extraction. To prove the removal of perchlorate in the presence of other minerals, a regolith simulant⁶⁰ was employed as the matrix of the known composition and spiked with (TBA) ClO_4 , imitating contamination with perchlorate (1% w/w). The obtained model mixture contained cations (Ca^{2+} , Mg^{2+} , Fe^{2+} , Fe^{3+}), oxides, and kosmotropic anions (SO_4^{2-} , CO_3^{2-}) but was essentially free of the organic matter (Table S26). According to ion chromatography analysis (Tables S27 and S28; Figures S56–S59), the methanolic extract of the contaminated matrix contained primarily perchlorate and sulfate, the latter arising from the MgSO_4 component (Table S26). Treatment of the methanolic extract with solid mixHC[8]-APS resulted in the complete removal of ClO_4^- , in contrast to non-modified APS, which adsorbed ca. 15% ClO_4^- (Figures 5C and S59; Table S28).

The extraction of sulfate occurred with similar efficiency (ca. 85%–97%) using both APS and mixHC[8]-APS materials, demonstrating that mixHC[8] is not the main contributor responsible for the capture of SO_4^{2-} . The absence of mixHC[8] affinity toward sulfate was additionally confirmed by an ITC experiment (Table S25; Figures S47 and S54).

The captured perchlorate was easily removed by washing mixHC[8]-APS material with water, taking advantage of the weaker binding in the aqueous medium, which demonstrates the potential for the material's reusability.⁶¹

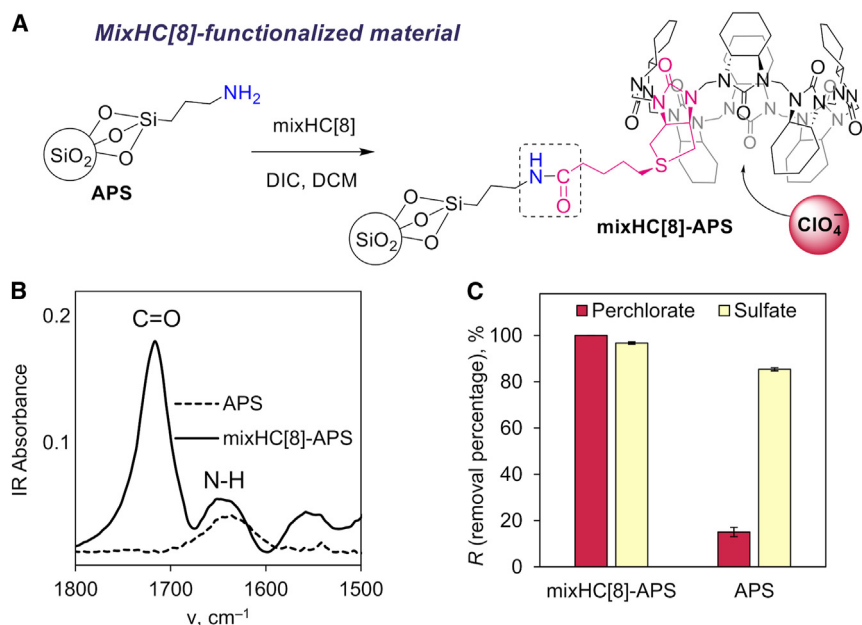


Figure 5. Derivatization of aminated silica by mixHC[8] and perchlorate removal efficiency of the obtained material

Immobilization of mixHC[8] on APS (A), DIC – *N,N'*-diisopropylcarbodiimide, and DCM (dichloromethane); characterization of material by infrared (IR) (B) and perchlorate removal from spiked mineral matrix using mixHC[8]-APS and non-modified APS, determined by ion chromatography (C). The error bars represent the standard deviation between the parallel experiments ($n \geq 2$) (isothermal calorimetric titration and immobilization of mixHC[8] on APS in the supplemental experimental procedures).

In conclusion, an efficient mechanochemical protocol for the synthesis of enantiopure mono-biotinylated HC[8]s was developed. The process involves two stages: (1) the mechanochemically assisted and acid-catalyzed polycondensation of D-biotin, (*R,R*)- or (*S,S*)-CU, and formaldehyde and (2) the aging step, in which the template-driven covalent self-assembly of oligomers into macrocycles takes place. Screening experiments uncovered the key process and chemical parameters affecting the assembly: the ratio of the monomers, the loading of the acid catalyst, and the nature of the templating anion. The present study offers insight into the complex mixture of oligomeric intermediates, including their interconversion and self-organization processes en route to the macrocyclic products. HPLC-MS analysis of short oligomers revealed differences in condensation kinetics of paraformaldehyde with biotin and CU into homomeric dimers and trimers under mechanochemical agitation. The faster condensation of CU led to amplification of the homomeric cycHC[8] during the aging of shortly agitated reaction mixtures. On the contrary, upon prolonged ball milling, which ensures sufficient shuffling of monomers, higher efficiency in the formation of the chimeric mixHC[8] in 38% yield was achieved. The mechanochemically driven solid-state approach allowed for the fine-tuning of the composition of the rich DCL and directing covalent self-assembly processes beyond statistical distribution. Diastereomeric (–)– and (+)–mixHC[8]s were isolated and their structures characterized by DFT, NMR, and SC-XRD methods. Furthermore, the comparison of their affinities toward chaotropic anions pointed at specific binding differences, which makes the chimeric family of HC[8] appealing for host-guest chemistry. The biotin carboxylate group of the mixHC[8] enabled its facile covalent immobilization on aminated silica. The functional material obtained was employed in the selective capture of anions, as

demonstrated by the complete removal of perchlorate from an extract of a mineral model mixture. Further applications of these chiral chimeric hemicucurbiturils are currently being studied.

EXPERIMENTAL PROCEDURES

Resource availability

Lead contact

Further information and requests for resources should be directed to and will be fulfilled by the lead contact, Riina Aav (riina.aav@taltech.ee).

Materials availability

All materials generated in this study are available from the [lead contact](#) without restrictions for research purposes.

Data and code availability

All data supporting this study's findings are included in the article and its [supplemental information](#) and are also available from the authors upon request. Crystallographic data for the structures reported in this paper have been deposited at the Cambridge Crystallographic Data Center under CCDC: 2251913. Copies of these data can be obtained free of charge via www.ccdc.cam.ac.uk/data_request/cif.

SUPPLEMENTAL INFORMATION

Supplemental information can be found online at <https://doi.org/10.1016/j.xcrp.2024.102161>.

ACKNOWLEDGMENTS

The authors would like to thank Jasper Adamson and Indrek Reile for input on the NMR analysis. The research by R.A., L.U., D.K., J.S.W., and K.R. was funded by the European Union's H2020- FETOPEN grant 828779 (INITIO). E.S.-T., T.J., K.-M.L., J.V.N., J.M., R.R., and M.O. were financed by Estonian Research Council grants PRG399 and PRG2169. R.A. was funded by the Ministry of Education and Research through Centre of Excellence in Circular Economy for Strategic Mineral and Carbon Resources (01.01.2024–31.12.2030, TK228). The authors also acknowledge COST Action CA18112 "Mechanochemistry for Sustainable Industry" for supporting research in mechanochemistry.

AUTHOR CONTRIBUTIONS

All authors contributed to the manuscript's preparation and have provided their approval for the final version of the manuscript. The authors' specific contributions are as follows: E.S.-T. was the main contributor for the development of the synthesis and mixHC[8] characterization and participated in binding studies; T.J. was the main contributor of the chemical analysis, binding, immobilization, and perchlorate removal studies; P.T. and S.P. contributed to perchlorate removal; K.-M.L., K.S., and J.V.N. contributed to the synthesis; J.M., J.S.W., and K.R. contributed to SC-XRD analysis; R.R. and M.Ö. contributed to computational studies; L.U. contributed to the script for MS data analysis and binding studies; M.V. contributed to the assessment of combinatorics; V.R. contributed to NMR analysis; D.K. contributed to conceptualization of the synthesis, perchlorate removal, and assessment of green metrics; and R.A. contributed to conceptualization of the overall research, data analysis, writing, and supervision.

DECLARATION OF INTERESTS

This research has been filed for patent application EP23181344.5 and PCT/IB2024/056236. Authors: R.A., E.S.-T., T.J., Tatsiana Nikonovich, D.K., and L.U. Title: "Method of preparation of chimeric HC[n]s, derivatives, and uses thereof," priority date: June 26, 2023.

Received: May 22, 2024

Revised: July 15, 2024

Accepted: July 29, 2024

Published: August 20, 2024

REFERENCES

- Schnitzer, T., Preuss, M.D., van Basten, J., Schoenmakers, S.M.C., Spiering, A.J.H., Vantomme, G., and Meijer, E.W. (2022). How subtle changes can make a difference: Reproducibility in complex supramolecular systems. *Angew. Chem.* 61, e202206738. <https://doi.org/10.1002/ange.202206738>.
- Yamaoki, Y., Nagata, T., Kondo, K., Sakamoto, T., Takami, S., and Katahira, M. (2022). Shedding light on the base-pair opening dynamics of nucleic acids in living human cells. *Nat. Commun.* 13, 7143. <https://doi.org/10.1038/s41467-022-34822-4>.
- Kwon, T.W., Song, B., Nam, K.W., and Stoddart, J.F. (2022). Mechanochemical enhancement of the structural stability of pseudorotaxane intermediates in the synthesis of rotaxanes. *J. Am. Chem. Soc.* 144, 12595–12601. <https://doi.org/10.1021/jacs.2c00515>.
- Dražinský, M., Hurtado, C.S., Masson, E., and Kaleta, J. (2021). Stuffed pumpkins: Mechanochemical synthesis of host–guest complexes with cucurbit[7]uril. *Chem. Commun.* 57, 2132–2135. <https://doi.org/10.1039/D1CC00240F>.
- Fršić, T., Mottillo, C., and Titi, H.M. (2020). Mechanochemistry for synthesis. *Angew. Chem.* 132, 1030–1041. <https://doi.org/10.1002/ange.201906755>.
- Cuccu, F., De Luca, L., Delogu, F., Colacino, E., Solin, N., Mocchi, R., and Porcheddu, A. (2022). Mechanochemistry: New tools to navigate the uncharted territory of "impossible" reactions. *ChemSusChem* 15, e202200362. <https://doi.org/10.1002/cssc.202200362>.
- Reynes, J.F., Isoni, V., and García, F. (2023). Tinkering with mechanochemical tools for scale-up. *Angew. Chem., Int. Ed. Engl.* 62, e202300819. <https://doi.org/10.1002/anie.202300819>.
- Kaabel, S., and Aav, R. (2018). Templating effects in the dynamic chemistry of cucurbiturils and hemicucurbiturils. *Isr. J. Chem.* 58, 296–313. <https://doi.org/10.1002/ijch.201700106>.
- Lehn, J.-M. (1999). Dynamic combinatorial chemistry and virtual combinatorial libraries. *Chem. Eur. J.* 5, 2455–2463. [https://doi.org/10.1002/\(SICI\)1521-3765\(19990903\)5:9<2455::AID-CHEM2455>3.0.CO;2-H](https://doi.org/10.1002/(SICI)1521-3765(19990903)5:9<2455::AID-CHEM2455>3.0.CO;2-H).
- Corbett, P.T., Leclaire, J., Vial, L., West, K.R., Wietor, J.-L., Sanders, J.K.M., and Otto, S. (2006). Dynamic combinatorial chemistry. *Chem. Rev.* 106, 3652–3711. <https://doi.org/10.1021/cr020452p>.
- Kaabel, S., Adamson, J., Topić, F., Kiesilä, A., Kalenius, E., Öeren, M., Reimund, M., Prigorchenko, E., Lökene, A., Reich, H.J., et al. (2017). Chiral hemicucurbit[8]uril as an anion receptor: Selectivity to size, shape and charge distribution. *Chem. Sci.* 8, 2184–2190. <https://doi.org/10.1039/C6SC05058A>.
- Andersen, N.N., Lisbjerg, M., Eriksen, K., and Pittelkow, M. (2018). Hemicucurbit[n]urils and their derivatives – Synthesis and applications. *Isr. J. Chem.* 58, 435–448. <https://doi.org/10.1002/ijch.201700129>.
- Lisbjerg, M., Jessen, B.M., Rasmussen, B., Nielsen, B.E., Madsen, A.Ø., and Pittelkow, M. (2014). Discovery of a cyclic 6 + 6 hexamer of D-biotin and formaldehyde. *Chem. Sci.* 5, 2647–2650. <https://doi.org/10.1039/C4SC00990H>.
- Havel, V., Yawer, M.A., and Sindelar, V. (2015). Real-time analysis of multiple anion mixtures in aqueous media using a single receptor. *Chem. Commun.* 51, 4666–4669. <https://doi.org/10.1039/C4CC10108A>.
- Yawer, M.A., Havel, V., and Sindelar, V. (2015). A bambusuril macrocycle that binds anions in water with high affinity and selectivity. *Angew. Chem., Int. Ed. Engl.* 54, 276–279. <https://doi.org/10.1002/anie.201409895>.
- Lizal, T., and Sindelar, V. (2018). Bambusuril anion receptors. *Isr. J. Chem.* 58, 326–333. <https://doi.org/10.1002/ijch.201700111>.
- Kaabel, S., Stein, R.S., Fomitšenko, M., Järving, I., Fršić, T., and Aav, R. (2019). Size-control by anion templating in mechanochemical synthesis of hemicucurbiturils in the solid state. *Angew. Chem., Int. Ed. Engl.* 58, 6230–6234. <https://doi.org/10.1002/anie.201813431>.
- Prigorchenko, E., Öeren, M., Kaabel, S., Fomitšenko, M., Reile, I., Järving, I., Tamm, T., Topić, F., Rissanen, K., and Aav, R. (2015). Template-controlled synthesis of chiral cyclohexylhemicucurbit[8]uril. *Chem. Commun.* 51, 10921–10924. <https://doi.org/10.1039/C5CC04101E>.
- Zeng, Q., Long, Q., Lu, J., Wang, L., You, Y., Yuan, X., Zhang, Q., Ge, Q., Cong, H., and Liu, M. (2021). Synthesis of a novel aminobenzene-containing hemicucurbituril and its fluorescence spectral properties with ions. *Beilstein J. Org. Chem.* 17, 2840–2847. <https://doi.org/10.3762/bjoc.17.195>.
- Wang, L., Han, J., Pan, R., Yuan, X., You, Y., Cen, X., Zhang, Q., Ge, Q., Cong, H., and Liu, M. (2022). Synthesis of hybrid thiohemicucurbiturils. *Tetrahedron Lett.* 101, 153918. <https://doi.org/10.1016/j.tetlet.2022.153918>.
- Maršálek, K., and Sindelar, V. (2020). Monofunctionalized bambus[6]urils and their conjugates with crown ethers for liquid–liquid extraction of inorganic salts. *Org. Lett.* 22, 1633–1637. <https://doi.org/10.1021/acs.orglett.0c00216>.
- De Simone, N.A., Chvojka, M., Lapešová, J., Martínez-Crespo, L., Slávik, P., Sokolov, J., Butler, S.J., Valkenier, H., and Sindelar, V. (2022). Monofunctionalized fluorinated bambusurils and their conjugates for anion transport and extraction. *J. Org. Chem.* 87, 9829–9838. <https://doi.org/10.1021/acs.joc.2c00870>.
- Del Mauro, A., Lapešová, J., Rando, C., and Sindelar, V. (2024). Merging bambus[6]uril and biotin[6]uril into an enantiomerically pure monofunctionalized hybrid macrocycle. *Org. Lett.* 26, 106–109. <https://doi.org/10.1021/acs.orglett.3c03715>.
- Langerreiter, D., Kostianen, M.A., Kaabel, S., and Anaya-Plaza, E. (2022). A greener route to blue: Solid-state synthesis of phthalocyanines. *Angew. Chem., Int. Ed. Engl.* 61, e202209033. <https://doi.org/10.1002/anie.202209033>.
- Pascu, M., Ruggi, A., Scopelliti, R., and Severin, K. (2013). Synthesis of borasiloxane-based macrocycles by multicomponent condensation reactions in solution or in a ball mill. *Chem. Commun.* 49, 45–47. <https://doi.org/10.1039/C2CC37538A>.
- Sim, Y., Shi, Y.X., Ganguly, R., Li, Y., and García, F. (2017). Mechanochemical synthesis of phosphazane-based frameworks. *Chem. Eur. J.* 23, 11279–11285. <https://doi.org/10.1002/chem.201701619>.
- Xi, H.-T., Zhao, T., Sun, X.-Q., Miao, C.-B., Zong, T., and Meng, Q. (2013). Rapid and efficient solvent-free synthesis of cyclophanes based on bipyridinium under mechanical ball milling. *RSC Adv.* 3, 691–694. <https://doi.org/10.1039/C2RA22802E>.
- Kunde, T., Pausch, T., Guńka, P.A., Krzyżanowski, M., Kasprzak, A., and Schmidt,

- B.M. (2022). Fast, solvent-free synthesis of ferrocene-containing organic cages via dynamic covalent chemistry in the solid state. *Chem. Sci.* 13, 2877–2883. <https://doi.org/10.1039/D1SC06372C>.
29. Shy, H., Mackin, P., Orvieto, A.S., Gharbharan, D., Peterson, G.R., Bamos, N., and Hamilton, T.D. (2014). The two-step mechanochemical synthesis of porphyrins. *Faraday Discuss* 170, 59–69. <https://doi.org/10.1039/C3FD00140G>.
30. Su, Q., and Hamilton, T.D. (2019). Extending mechanochemical porphyrin synthesis to bulkier aromatics: Tetramesitylporphyrin. *Beilstein J. Org. Chem.* 15, 1149–1153. <https://doi.org/10.3762/bjoc.15.111>.
31. MathWorld—A Wolfram Web Resource. Weisstein, E. W. Necklace. <https://mathworld.wolfram.com/Necklace.html>.
32. McElroy, C.R., Constantinou, A., Jones, L.C., Summerton, L., and Clark, J.H. (2015). Towards a holistic approach to metrics for the 21st century pharmaceutical industry. *Green Chem.* 17, 3111–3121. <https://doi.org/10.1039/C5CG00340G>.
33. Friščić, T., Childs, S.L., Rizvi, S.A.A., and Jones, W. (2009). The role of solvent in mechanochemical and sonochemical cocrystal formation: A solubility-based approach for predicting cocrystallization outcome. *CrystEngComm* 11, 418–426. <https://doi.org/10.1039/B815174A>.
34. Do, J.-L., and Friščić, T. (2017). Chemistry 2.0: Developing a new, solvent-free system of chemical synthesis based on mechanochemistry. *Synlett* 28, 2066–2092. <https://doi.org/10.1055/s-0036-1590854>.
35. Belenguer, A.M., Lampronti, G.I., De Mitri, N., Driver, M., Hunter, C.A., and Sanders, J.K.M. (2018). Understanding the influence of surface solvation and structure on polymorph stability: A combined mechanochemical and theoretical approach. *J. Am. Chem. Soc.* 140, 17051–17059. <https://doi.org/10.1021/jacs.8b08549>.
36. Prigorchenko, E., Kaabel, S., Narva, T., Baškir, A., Fomitsenko, M., Adamson, J., Järving, I., Rissanen, K., Tamm, T., and Aav, R. (2019). Formation and trapping of the thermodynamically unfavoured inverted-hemicucurbit[6]uril. *Chem. Commun.* 55, 9307–9310. <https://doi.org/10.1039/C9CC04990H>.
37. Myers, R.H., Montgomery, D.C., and Anderson-Cook, C.M. (2016). *Response Surface Methodology: Process and Product Optimization Using Designed Experiments* (John Wiley & Sons).
38. Czapla, M., and Skurski, P. (2015). Strength of the Lewis–Brønsted superacids containing In, Sn, and Sb and the electron binding energies of their corresponding superhalogen anions. *J. Phys. Chem. A* 119, 12868–12875. <https://doi.org/10.1021/acs.jpca.5b10205>.
39. Bour, C., Guillot, R., and Gandon, V. (2015). First evidence for the existence of hexafluoroantimonic(V) acid. *Chem. Eur J.* 21, 6066–6069. <https://doi.org/10.1002/chem.201500334>.
40. Urbansky, E.T. (2002). Perchlorate as an environmental contaminant. *Environ. Sci. Pollut. Res. Int.* 9, 187–192. <https://doi.org/10.1007/BF02987487>.
41. Kumarathilaka, P., Oze, C., Indraratne, S.P., and Vithanage, M. (2016). Perchlorate as an emerging contaminant in soil, water and food. *Chemosphere* 150, 667–677. <https://doi.org/10.1016/j.chemosphere.2016.01.109>.
42. Sigel, H., and Scheller, K.H. (1982). Metal ion complexes of D-biotin in solution. Stability of the stereoselective thioether coordination. *J. Inorg. Biochem.* 16, 297–310. [https://doi.org/10.1016/S0162-0134\(00\)80266-4](https://doi.org/10.1016/S0162-0134(00)80266-4).
43. Aoki, K., and Saenger, W. (1983). Interactions of biotin with metal ions. X-ray crystal structure of the polymeric biotin-silver(I) nitrate complex: metal bonding to thioether and ureido carbonyl groups. *J. Inorg. Biochem.* 19, 269–273. [https://doi.org/10.1016/0162-0134\(83\)85031-4](https://doi.org/10.1016/0162-0134(83)85031-4).
44. Altaf, M., and Stoeckli-Evans, H. (2013). Chiral one- and two-dimensional silver(I)–biotin coordination polymers. *Acta Crystallogr. C* 69, 127–137. <https://doi.org/10.1107/S0108270113000322>.
45. Lehn, J.-M. (2013). Perspectives in chemistry—steps towards complex matter. *Angew. Chem., Int. Ed. Engl.* 52, 2836–2850. <https://doi.org/10.1002/anie.201208397>.
46. Ustrnul, L., Jarg, T., Jantson, M., Osadchuk, I., Anton, L., and Aav, R. (2024). MatchMass: A web-based tool for efficient mass spectrometry data analysis. Preprint at ChemRxiv. <https://doi.org/10.26434/chemrxiv-2024-9j8n7>.
47. Ma, X., Yuan, W., Bell, S.E.J., and James, S.L. (2014). Better understanding of mechanochemical reactions: Raman monitoring reveals surprisingly simple ‘pseudo-fluid’ model for a ball milling reaction. *Chem. Commun.* 50, 1585–1587. <https://doi.org/10.1039/C3CC47898J>.
48. Ortolan, A.O., Madureira, L., Rodríguez-Kessler, P.L., Maturana, R.G., Olea Ulloa, C., Caramori, G.F., Parreira, R.L., and Muñoz-Castro, A. (2023). The nature of the central halide encapsulation in bambusuril hosts (BU[6]). Structural and interaction energy insights in BU[6]-X (X = Cl, Br, I) from relativistic DFT calculations. *Inorg. Chim. Acta.* 555, 121596. <https://doi.org/10.1016/j.ica.2023.121596>.
49. Ören, M., Shmatova, E., Tamm, T., and Aav, R. (2014). Computational and ion mobility MS study of (All-S)-Cyclohexylhemicucurbit[6]uril structure and complexes. *Phys. Chem. Chem. Phys.* 16, 19198–19205. <https://doi.org/10.1039/C4CP02202E>.
50. Jašiková, L., Rodrigues, M., Lapešová, J., Lízal, T., Šindelář, V., and Roithová, J. (2019). Bambusurils as a mechanistic tool for probing anion effects. *Faraday Discuss* 220, 58–70. <https://doi.org/10.1039/C9FD00038K>.
51. Sokolov, J., Štefek, A., and Šindelář, V. (2020). Functionalized chiral bambusurils: Synthesis and host-guest interactions with chiral carboxylates. *ChemPlusChem* 85, 1307–1314. <https://doi.org/10.1002/cplu.202000261>.
52. Itterheimová, P., Bobacka, J., Šindelář, V., and Lubal, P. (2022). Perchlorate solid-contact ion-selective electrode based on dodecabenzyrbambus[6]uril. *Chemosensors* 10, 115. <https://doi.org/10.3390/chemosensors10030115>.
53. Rando, C., Vázquez, J., Sokolov, J., Kokan, Z., Nečas, M., and Šindelář, V. (2022). Highly efficient and selective recognition of dicyanoaurate(I) by a bambusuril macrocycle in water. *Angew. Chem., Int. Ed. Engl.* 61, e202210184. <https://doi.org/10.1002/anie.202210184>.
54. Reany, O., Mohite, A., and Keinan, E. (2018). Hetero-bambusurils. *Isr. J. Chem.* 58, 449–460. <https://doi.org/10.1002/ijch.201700138>.
55. Lisbjerg, M., Nielsen, B.E., Milhøj, B.O., Sauer, S.P.A., and Pittelkow, M. (2015). Anion binding by biotin[6]uril in water. *Org. Biomol. Chem.* 13, 369–373. <https://doi.org/10.1039/C4OB02211D>.
56. Andersen, N.N., Eriksen, K., Lisbjerg, M., Ottesen, M.E., Milhøj, B.O., Sauer, S.P.A., and Pittelkow, M. (2019). Entropy/enthalpy compensation in anion binding: Biotin[6]uril and biotin-l-sulfoxide[6]uril reveal strong solvent dependency. *J. Org. Chem.* 84, 2577–2584. <https://doi.org/10.1021/acs.joc.8b02797>.
57. Calderón, R., Palma, P., Arancibia-Miranda, N., Kim, U.-J., Silva-Moreno, E., and Kannan, K. (2022). Occurrence, distribution and dynamics of perchlorate in soil, water, fertilizers, vegetables and fruits and associated human exposure in Chile. *Environ. Geochem. Health* 44, 527–535. <https://doi.org/10.1007/s10653-020-00680-6>.
58. Chen, Y., Zhu, Z., Wu, X., Zhang, D., Tong, J., Lin, Y., Yin, L., Li, X., Zheng, Q., and Lu, S. (2022). A nationwide investigation of perchlorate levels in staple foods from China: Implications for human exposure and risk assessment. *J. Hazard Mater.* 439, 129629. <https://doi.org/10.1016/j.jhazmat.2022.129629>.
59. Tabakci, M. (2008). Immobilization of calix[6]arene bearing carboxylic acid and amide groups on aminopropyl silica gel and its sorption properties for Cr(VI). *J. Inclusion Phenom. Macrocycl. Chem.* 61, 53–60. <https://doi.org/10.1007/s10847-007-9392-2>.
60. Cannon, K.M., Britt, D.T., Smith, T.M., Fritsche, R.F., and Batchelder, D. (2019). Mars global simulant MGS-1: A rocknest-based open standard for basaltic Martian regolith simulants. *Icarus* 317, 470–478. <https://doi.org/10.1016/j.icarus.2018.08.019>.
61. Shalima, T., Mishra, K.A., Kaabel, S., Ustrnul, L., Bartkova, S., Tõnsuaadu, K., Heinmaa, I., and Aav, R. (2021). Cyclohexanohemicucurbit[8]uril inclusion complexes with heterocycles and selective extraction of sulfur compounds from water. *Front. Chem.* 9, 786746. <https://doi.org/10.3389/fchem.2021.786746>.

Supplemental information

Mechanochemically driven covalent self-assembly of a chiral mono-biotinylated hemicucurbit[8]uril

Elina Suut-Tuule, Tatsiana Jarg, Priit Tikker, Ketren-Marlein Lootus, Jevgenija Martõnova, Rauno Reitalu, Lukas Ustrnul, Jas S. Ward, Vitalijs Rjabovs, Kirill Shubin, Jagadeesh V. Nallaparaju, Marko Vendelin, Sergei Preis, Mario Öeren, Kari Rissanen, Dzmitry Kananovich, and Riina Aav

Supplemental Experimental Procedures

Table of contents

General Information.....	S2
1. Theoretical Number of Linear and Cyclic Oligomers	S3
2. Screening and Optimization of Reaction Conditions	S4
2.1 Synthesis in Solution.....	S5
2.2 Synthesis in Solid State	S6
2.3 Analysis of Oligomers and Side-Products	S17
3. Preparative Synthesis, Purification, and Characterization of mixHC[8]	S28
3.1 NMR spectra	S31
3.2 IR spectra.....	S46
4. Single Crystal X-ray Diffraction Analysis.....	S48
5. The Computational Study	S55
5.1 Methods.....	S55
5.2 Results	S55
5.3 Comparing the Calculated Structure to the Crystal Structure	S57
5.4 The Cartesian Coordinates of the Found Conformers.....	S60
6. Anion Binding Studies.....	S68
6.1 Isothermal Calorimetric Titration.....	S68
6.2 Immobilization of mixHC[8] on APS	S83
6.3 Removal of Perchlorate from Methanol Solutions.....	S84
References.....	S88

General Information

Unless otherwise stated, all reagents were purchased from commercial suppliers and used without further purification. (*R,R*)- and (*S,S*)-*N,N'*-cyclohexa-1,2-diylurea (CU) monomers, and (*R,R*)-cycHC[8] were synthesised in our laboratory following the procedures described in literature.¹⁻³

Mechanochemical experiments were carried out in FTS-1000 ball mill, at a frequency of 30 Hz in 14 mL ZrO₂-coated grinding jars charged with two 10 mm ZrO₂ milling balls. For aging reaction mixtures at elevated temperatures VWR Incu-line Digital Incubator was used.

¹H, ¹³C and 2D NMR spectra were acquired using a Triple Resonance Probe (TXI) on a Bruker AVANCE III 800 MHz spectrometer at 298.15 K. The samples were dissolved in CDCl₃ and the chemical shifts were referenced to CDCl₃ residual peak. Optical rotation was measured with an Anton Paar MCP 500 polarimeter. IR spectra were recorded on a Bruker Tensor 27 FT spectrometer. HRMS data was collected on Agilent 6540 Accurate-Mass Q-TOF mass spectrometer. Thermodynamic measurements by ITC were performed on MicroCal PEAQ-ITC calorimeter using a 200 μ L calorimetric cell and a 40 μ L syringe.

Silica gel 40-63 μ m was used for column chromatography, silica gel 60 F₂₅₄ plates were used for TLC. Visualization of TLC plates was performed using phosphomolybdic acid (PMA) stain. To perform automatic column chromatography Biotage Isolera Prime machine was used. HPLC-UV-MS analysis was performed on Agilent 1200 Series System equipped with multiple wavelength detector (MWD) and single quadrupole mass detector (MSD), using Phenomenex Kinetex XB-C18 column (150 mm \times 4.6 mm, 2.6 μ m). Ion chromatographic analysis was carried out on Metrohm Ltd 761 Compact IC with chemical suppression of eluent conductivity.

1. Theoretical Number of Linear and Cyclic Oligomers

All combinations

Number of all possible oligomers was calculated assuming that up to 10-membered oligomers are formed. Three different monomers were considered, CU and D-biotin (B) in its two orientations (See Figure 1 in main text for clarity). Oligomers could form either in linear or cyclic forms, latter would be HC[*n*]s. By considering all non-superimposable combinations with the length from 2 to 10, we found that up to 5293 different cyclic and 44646 linear oligomers can form, leading to total 49939 possible combinations.

Combinations were found by a Python script using SymPy iterables module (bracelets combinations) and Python Itertools module for finding the possible linear oligomers. Corresponding script is attached as a Data S1 (alloligos.py) and requires SymPy module in addition to the standard Python installation.

HC[8] combinations

To predict theoretical distribution of cyclic 8-membered oligomers (HC[8]s), we considered CU and biotin in its two orientations (See Figure 1 in main text for clarity). It was assumed that the formation of a specific HC[8] is directly proportional to the product of the initial concentrations of the constituent monomers. For biotin, the concentration of the both orientations were considered to be equal to each other and the half of the total biotin concentration. Based on these assumptions, we found the list of all possible cyclic oligomers and their relative concentration in the mixture of all 8-membered HC[*n*]s. Combinations and concentrations were found by a Python script attached as Data S1 (necgen.py) using SymPy iterables module.

Table S1. Theoretical distribution of 8-membered macrocycles (HC[8]s) resulting from various molar ratios of starting monomers B and CU.

Monomer* ratio B:CU	HC[8]s distribution		
	mixHC[8]	cycHC[8]	other HC[8]
1:5	0.15	0.73	0.12
1:7	0.12	0.82	0.06
1:15	0.062	0.925	0.014

*biotin unit can be incorporated into macrocycles in 2 different orientations with equal probabilities

2. Screening and Optimization of Reaction Conditions

General procedure for screening reaction conditions

D-biotin (46 mg, 0.19 mmol, 1 eq.), (*R,R*)- or (*S,S*)-*N,N'*-cyclohexa-1,2-diylurea (183 mg, 1.30 mmol, 7 eq.), paraformaldehyde (45 mg, 1.50 mmol, 8 eq.) and triphenylmethane (10 mg, internal standard for HPLC yield estimation) were placed into a 14 mL ZrO₂-coated jar charged with two 10 mm ZrO₂ balls (3.5 g). The template consisting of aqueous acid or acid and corresponding salt (0.56 mmol, 3 eq.) was added to the mixture, which was then set to mill at 30 Hz for 60 minutes. After milling the jar was sealed with parafilm and the reaction mixture was aged at 60 °C for 24 hours. The resulting crude mixture was further washed on a glass filter with distilled water until neutral pH, which was determined by test strips. The quenched mixture was dried in open air at room temperature.

General conditions for HPLC analysis

System A (estimation of HPLC yield). Eluents A (water / 0.1% formic acid) and B (acetonitrile / 0.1% formic acid) were used in a gradient mode from A:B 50:50 (v/v) to A:B 10:90 (v/v) with the flow rate of 0.75 mL/min. The column temperature was set at 30 °C, injection volume at 2 μ L and detection wavelength at 210 nm. The peaks of the macrocycles were identified by ESI-MS.

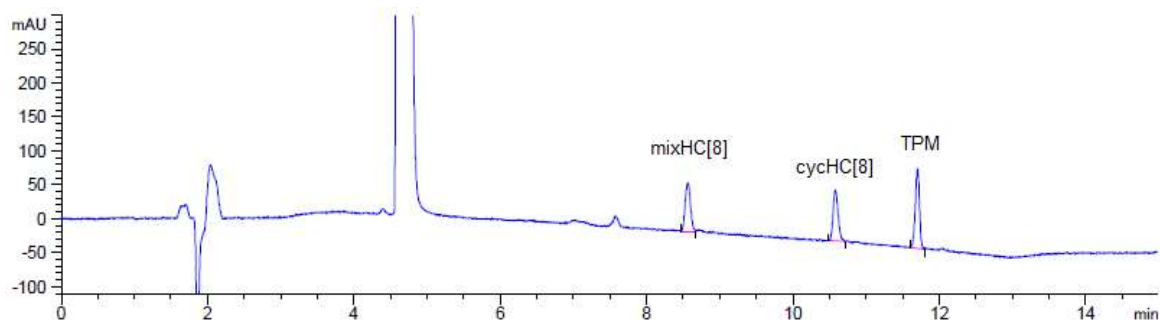


Figure S1. Typical HPLC-UV chromatogram at 210 nm used for yield determination.

HPLC yields were calculated based on calibration graphs for isolated macrocycles and internal standard (triphenylmethane) introduced into reaction mixture before milling. The sampling was performed in triplicate, ~1 mg of crude mixture after aging was dissolved in chloroform: isopropanol 1:1 (v/v) and filtered through 0.2 μ m PTFE syringe filter.

System B (MS analysis of oligomers). Eluents A (water / 0.1% formic acid) and B (acetonitrile / 0.1% formic acid) were used in a gradient mode from A:B 90:10 (v/v) to A:B 0:100 (v/v), followed by the isocratic stage at A:B 0:100 (v/v). The flow rate was set at 0.5 mL/min, column temperature at 30 °C and injection volume at 2 or 5 μ L. The general oligomeric profile was studied by ESI-HRMS in scan mode with positive polarity. The quantitative analysis was carried out using selected ion monitoring (SIM).

2.1 Synthesis in Solution

HPF₆ as template

D-biotin (10 mg, 0.041 mmol, 1 eq.), (*R,R*)-*N,N'*-cyclohexa-1,2-diyliurea (40 mg, 0.29 mmol, 7 eq.), paraformaldehyde (10 mg, 0.33 mmol, 8 eq.) were placed in a vial, followed by addition of 55% aq. HPF₆ (20 μ L) and ACN (0.6 mL). The heterogeneous mixture was stirred for 2 hours at room temperature. The heterogeneous solution mixture was analysed by HPLC-UV-MS. Complex mixture formed and only trace amounts of products were detected (0.03 ± 0.01 % of mixHC[8] and 0.24 ± 0.07 % of cycHC[8]).

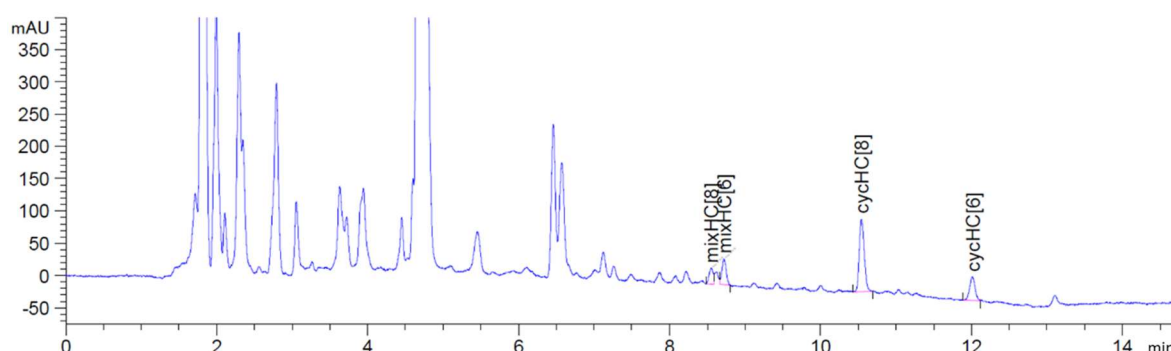
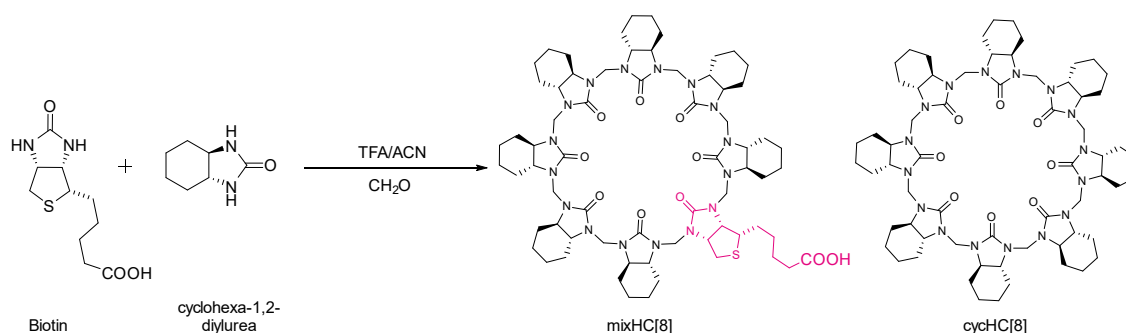


Figure S2. HPLC chromatogram (210 nm) of crude mixture with HPF₆ used as template.

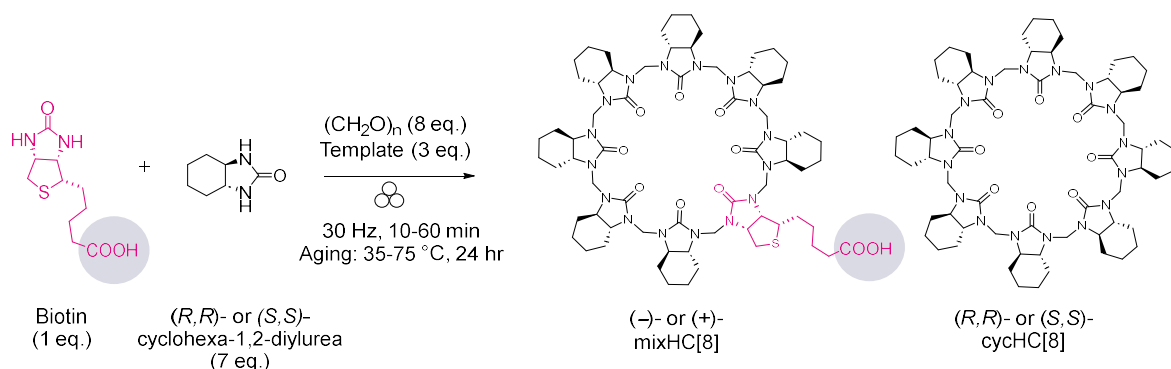
TFA as template

The reaction was performed following the standard procedure for cycHC[8] synthesis with TFA in acetonitrile², using 1:7 ratio of biotin to cyclohexa-1,2-diylurea monomer.



D-biotin (73 mg, 0.30 mmol, 1 eq.), (*R,R*)-*N,N'*-cyclohexa-1,2-diylurea (293 mg, 2.09 mmol, 7 eq.), paraformaldehyde (72 mg, 2.40 mmol, 8 eq.) were placed in a round bottom flask, followed by addition of TFA (4.5 mL) and ACN (4.5 mL). The heterogeneous mixture was stirred for 2 hours at room temperature. Reaction progress was monitored by TLC. To the resulting clear solution water (13 mL) was added, and the mixture was stirred on ice bath for 30 min. Then the solid mixture was filtered out, washed with 3×10 mL of water and dried in open air. HPLC-UV-MS analysis of the dried solid confirmed the formation of mixHC[8] and cycHC[8] in $(9.48 \pm 0.04)\%$ and $(38 \pm 1)\%$ yields, respectively.

2.2 Synthesis in Solid State



Screening of conditions using RSM

Reaction conditions: D-biotin (26–65 mg, 0.11–0.27 mmol, 1 eq.), (R,R)-N,N'-cyclohexa-1,2-diylurea (187–225 mg, 1.33–1.60 mmol, 5–15 eq.), paraformaldehyde (48–52 mg, 1.6–1.7 mmol, 8 eq.) and 70% aq. HClO_4 (8.6–75 μl , 0.10–0.87 mmol, 0.5–4 eq.) were milled for 10–60 minutes and aged at 35–75 °C for 24 hours. The HPLC yields were determined in triplicate, standard deviation between measurements did not exceed 2%.

Table S2. Simultaneous screening of monomer ratio, acid amount, milling time and aging temperature using HClO_4 as the catalyst and template.

Entry	Monomer molar ratio (B:CU)	HClO_4 , eq.	Milling time, min	Aging T, °C	HPLC yield, %	
					mixHC[8]	cycHC[8]
1	1.0 : 5.0	4.0	60.0	35	9	16
2	1.0 : 15.0	0.5	50.0	75	4	12
3	1.0 : 11.0	1.9	36.0	35	10	18
4	1.0 : 7.6	3.1	60.0	75	7	17
5	1.0 : 5.0	4.0	10.0	75	2	2
6	1.0 : 15.0	3.0	12.8	75	15	50
7	1.0 : 8.0	0.5	12.3	75	5	9
8	1.0 : 11.1	4.0	34.0	59	9	33
9	1.0 : 15.0	0.5	12.5	47	2	6
10	1.0 : 5.0	1.9	36.8	59	16	24
11	1.0 : 6.6	0.5	60.0	75	5	6
12	1.0 : 11.4	1.8	48.3	59	20	44
13	1.0 : 5.0	0.5	10.0	35	2	4
14	1.0 : 15.0	3.0	60.0	45	20	72
15	1.0 : 5.0	1.9	36.8	59	17	28
16	1.0 : 7.9	0.5	60.0	45	2	3
17	1.0 : 11.0	1.9	36.0	35	8	17
18	1.0 : 8.5	2.7	10.0	49	17	44
19	1.0 : 15.0	4.0	10.0	35	9	51
20	1.0 : 5.0	4.0	25.7	35	11	17
21	1.0 : 11.1	4.0	37.0	59	7	36
22	1.0 : 8.5	2.7	10.0	49	14	39
23	1.0 : 7.0	3.0	60.0	60	19	40

The experiments were planned in Design-Expert 13 using Optimal (Custom) Design for 4 numeric factors and polynomial model with quadratic process order. The total 23 runs included 15 required model points, 3 lack-of-fit points, 4 replicate points and 1 additional model point. The collected data were processed using polynomial analysis.

Table S3. Optimal (Custom) Design: the choice of variable factors.

Factor	Name	Units	Minimum value	Maximum value
A	Monomer ratio (CU:B)	eq	5	15
B	Acid amount	eq	0.5	4
C	Milling time	min	10	60
D	Aging temperature	°C	35	75

The factors **A–D** were chosen based on our previous experience in the solid-state synthesis of cycHC[*n*].⁵ **A** determines the tolerance and selectivity of the self-assembly process with respect to the content of the non-*C*₂-symmetric biotin. Additionally, the ratio of monomers might affect the number of biotin units incorporated into the macrocyclic scaffold. Compared to the stoichiometric 7:1 monomer ratio, the excess of biotin would be beneficial in case it reacts slower than CU. The excess of CU was meant to suppress the formation of polybiotinylated side-products. **B** characterizes the number of template anions and protons mediating the cyclization and condensation reactions, as well as the quantity of water acting as a liquid grinding additive. The maximal loading was chosen to confine the system within liquid-assisted grinding conditions. The minimal amount of acid modelled the conditions close to neat grinding. **C** reflects the duration of the polycondensation and monomer crossover reaction, as well as the amount of mechanical force transferred. In general, ball-milling accelerates chemical reactions, and our previous study on cycHC[*n*] showed that 30–60 min milling provided quantitative yields after aging. We wondered if the milling time can be decreased, bearing in mind that it must be sufficient to ensure proper mixing of the reagents and transfer of mechanical energy. **D** impacts the self-assembly step in the conversion of the oligomers into macrocycles via dynamic exchange between reactive acyliminium intermediates and templating. Our previous study on solid-state synthesis of cycHC[*n*] demonstrated that elevated temperatures accelerate the aging; the preliminary experiments in the current work resulted in poor yields at 80 °C, pointing to optimal range for the studied molecular system.

Table S4. Fit summary.

Response	Sequential p-value	Lack of Fit p-value	Adjusted R ²	Predicted R ²
mixHC[8] HPLC yield	0.0002	0.0281	0.8215	0.0802
cycHC[8] HPLC yield	< 0.0001	0.0690	0.9487	0.6575

The analysis of variance (ANOVA) for mixHC[8] quadratic model identified acid amount as significant factor, and to some extent temperature. For cycHC[8], monomer ratio and acid amount were found significant, and to a lesser extent milling time and temperature.

Table S5. Analysis of variance for mixHC[8] quadratic model.

Source	Sum of Squares	df	Mean Square	F-value	p-value ^b	
Model	774.32	14	55.31	8.23 ^a	0.0027	significant
A (monomer ratio)	0.3676	1	0.3676	0.0547	0.8209	
B (acid)	64.97	1	64.97	9.67	0.0144	
C (milling time)	1.76	1	1.79	0.2667	0.6195	
D (T)	1.26	1	1.26	0.1880	0.6761	
AB (monomer ratio, acid)	20.04	1	20.04	2.98	0.1224	
AC (monomer ratio, milling time)	5.70	1	5.70	0.8493	0.3837	
AD (monomer ratio, T)	9.86	1	9.86	1.47	0.2602	
BC (acid, milling time)	1.54	1	1.54	0.2297	0.6446	
BD (acid, T)	101.87	1	101.87	15.17	0.0046	
CD (milling time, T)	1.42	1	1.42	0.2111	0.6581	
A ² (monomer ratio)	24.26	1	24.26	3.61	0.0939	
B ² (acid)	378.87	1	378.87	56.40	< 0.0001	
C ² (milling time)	4.32	1	4.32	0.6432	0.4457	
D ² (T)	103.23	1	103.23	15.37	0.0044	
Residual	53.74	8	6.72			
Lack of Fit	48.35	4	12.09	8.98 ^c	0.0281	significant
Pure Error	5.39	4	1.35			
Cor Total	828.05	22				

[a] The **Model F-value** of 8.23 implies the model is significant. [b] **P-values** less than 0.0500 indicate model terms are significant. In this case B, BD, B², D² are significant model terms (highlighted in blue). [c] The **Lack of Fit F-value** of 8.98 implies the Lack of Fit is significant, which can be attributed to smaller variance between mixHC[8] yields in replicate points compared to cycHC[8].⁴

Table S6. Analysis of variance for cycHC[8] quadratic model.

Source	Sum of Squares	df	Mean Square	F-value	p-value ^b	
Model	7639.89	14	545.71	30.06 ^a	< 0.0001	significant
A (monomer ratio)	1549.10	1	1549.10	85.34	< 0.0001	
B (acid)	2037.44	1	2037.44	112.24	< 0.0001	
C (milling time)	7.88	1	7.88	0.4339	0.5286	
D (T)	7.14	1	7.14	0.3932	0.5481	
AB (monomer ratio, acid)	866.62	1	866.62	47.74	0.0001	
AC (monomer ratio, milling time)	185.00	1	185.00	10.19	0.0128	
AD (monomer ratio, T)	87.12	1	87.12	4.80	0.0599	
BC (acid, milling time)	9.67	1	9.67	0.5330	0.4862	
BD (acid, T)	536.39	1	536.39	29.55	0.0006	
CD (milling time, T)	4.03	1	4.03	0.2220	0.6501	
A ² (monomer ratio)	95.75	1	95.75	5.28	0.0507	
B ² (acid)	1241.57	1	1241.57	68.40	< 0.0001	
C ² (milling time)	284.19	1	284.19	15.66	0.0042	
D ² (T)	776.69	1	776.69	42.79	0.0002	

Residual	145.22	8	18.15			
Lack of Fit	121.91	4	30.48	5.23 ^c	0.0690	not significant
Pure Error	23.31	4	5.83			
Cor Total	7785.10	22				

[a] The **Model F-value** of 30.06 implies the model is significant. [b] **P-values** less than 0.0500 indicate model terms are significant. In this case A, B, AB, AC, BD, B², C², D² are significant model terms (highlighted in yellow). [c] The **Lack of Fit F-value** of 5.23 implies there is a 6.90% chance that a Lack of Fit F-value this large could occur due to noise.

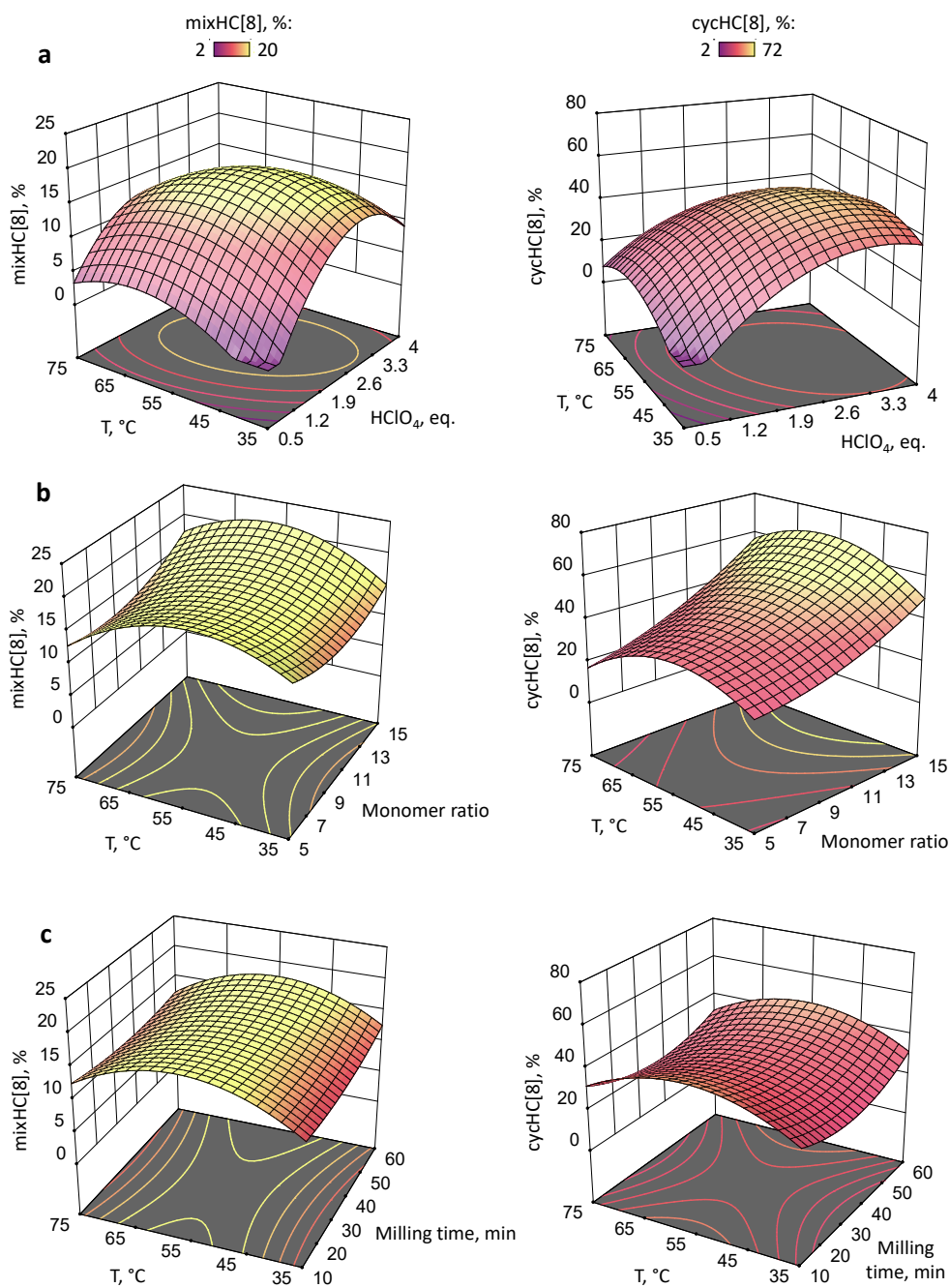


Figure S3. 3D response surfaces describing the trends upon varying the aging temperature and acid amount (a), temperature and monomer ratio (b), temperature and milling time (c).

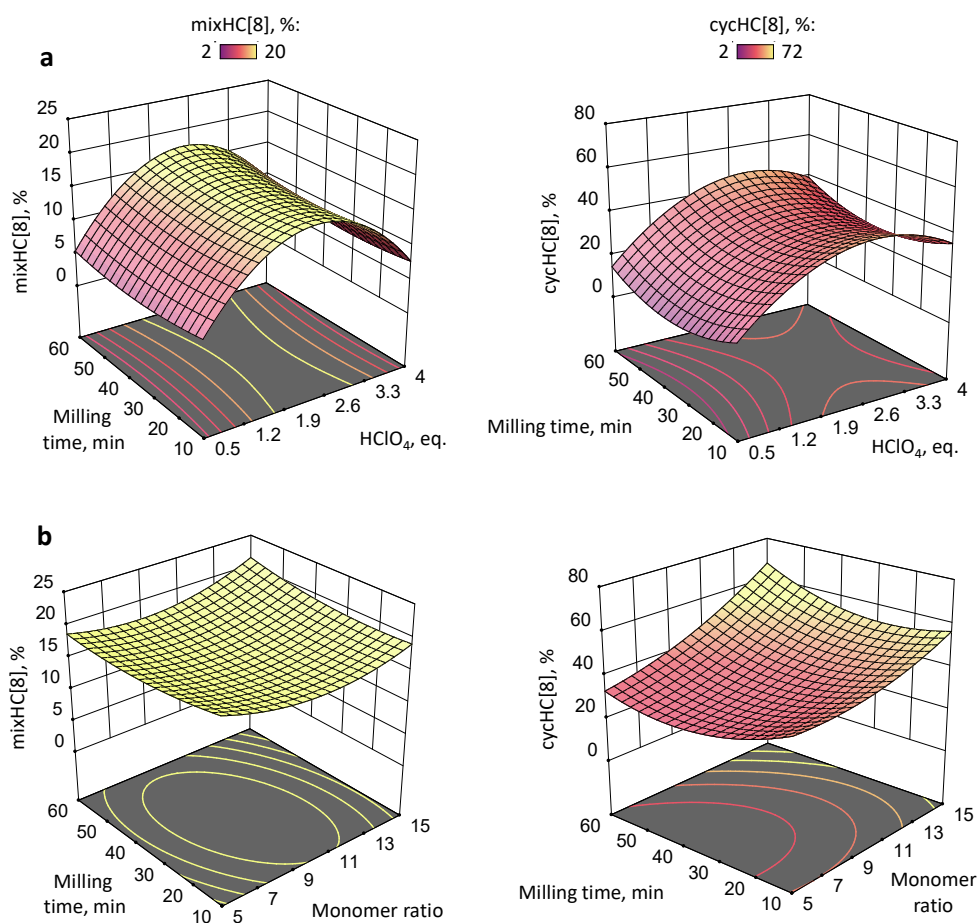


Figure S4. 3D response surfaces describing the trends upon varying the milling time and acid amount (a), milling time and monomer ratio (b).

Screening different templates

Reaction conditions: D-biotin (38–52 mg, 0.15–0.21 mmol, 1 eq.), (*R,R*)-*N,N'*-cyclohexa-1,2-diylurea (151–208 mg, 1.08–1.48 mmol, 7 eq.), paraformaldehyde (38–52 mg, 1.3–1.7 mmol, 8 eq.) and template (3 eq.) were milled for 60 minutes and aged at 60 °C for 24 hours.

Individual HPLC yields were determined from triplicate measurements, the deviation between parallel measurements did not exceed 1.1%; Average HPLC yields expressed as the mean value \pm standard deviation between reactions reproduced *n* times. See results in Table S7.

Table S7. Comparison of various acids and salt additives. (see experimental details in previous page)

Entry	Acid (eq.)	Salt (eq.)	Template anion	LAG (η , $\mu\text{l}/\text{mg}$)	mixHC[8] HPLC yield, %		cycHC[8] HPLC yield, %	
					Individual	Average	Individual	Average
1	70% aq HClO_4 (3)	—	ClO_4^-	0.18	17.7	19 \pm 2	38.2	40 \pm 3
					19.2		41.1	
					19.9		40.0	
					19.7		39.8	
					18.1		40.1	
					16.6		35.8	
					20.6		41.8	
					23.3		44.3	
2	55% aq. HPF_6 (2.4)	—	PF_6^-	0.26	27.5	27.6 \pm 0.1	36.0	34 \pm 2
	55% aq. HPF_6 (3)			0.33	27.7		32.8	
3	50% aq. H_2SO_4 (3)	KPF_6 (3)	PF_6^-	0.21	14.7	15.0 \pm 0.3	19.5	22 \pm 4
		KPF_6 (1.5)		0.24	15.2		24.5	
4	55% aq. HPF_6 (2)	KPF_6 (1)	PF_6^-	0.20	40.5	37 \pm 2	38.1	38 \pm 2
					36.5		41.0	
					36.3		36.4	
					34.9		36.3	
5	55% aq. HPF_6 (2)	AgPF_6 (1)	PF_6^-	0.19	27.3	29 \pm 2	47.9	42 \pm 8
					29.8		36.4	
6	55% aq. HPF_6 (2)	$[\text{Cu}(\text{CH}_3\text{CN})_4]\text{PF}_6$ (1)	PF_6^-	0.18	31.3	31.1 \pm 0.4	43.2	44 \pm 2
					30.8		45.4	

Optimization of KPF₆/HPF₆ amount

Reaction conditions: D-biotin (44.3–45.8 mg, 0.181–0.188 mmol, 1 equiv.), (*R,R*)-*N,N'*-cyclohexa-1,2-diylurea (178.4–188.7 mg, 1.273–1.346 mmol, 7 equiv.), paraformaldehyde (43.8–52.1 mg, 1.46–1.54 mmol, 8 equiv.), KPF₆ (2.0–104.5 mg, 0.011–0.568 mmol, 0–3 eq.), 55% aq. HPF₆ (3–234 μ l, 0.019–1.455 mmol, 0.1–8 equiv.) and water (0–233 mg, LAG additive η =0.2–0.85 μ l/mg) were milled for 60 min and aged at 60 °C for 24 h. The HPLC yields were determined in triplicate, standard deviation did not exceed 2%.

Table S8. Screening of KPF₆/HPF₆ added as the template.

Entry	KPF ₆ , eq.	HPF ₆ , eq.	mixHC[8] yield, %	cycHC[8] yield, %
1	2.1	4.5	22	49
2	3.0	4.0	25	43
3	0	3.8	29	30
4	0.1	6.1	10	32
5	0	2.0	27	33
6	1.7	2.7	29	43
7	0.3	2.6	25	33
8	0	8.0	11	34
9	2.6	8.0	20	37
10	3.0	5.6	25	39
11	0	2.0	28	36
12	0.8	7.9	6	32
13	1.8	6.8	11	46
14	0	1.0	25	47
15	1.2	4.9	21	50
16	0.0	3.8	29	38
17	0	5.0	30	35
18	2.0	0.1	4	10
19	1.0	2.0	37	41
20	1.0	2.0	36	46

The experiments were planned in Design-Expert 13 using Optimal (Custom) Design for 2 numeric factors and polynomial model with quadratic process order. The total 20 runs included 8 required model points, 3 lack-of-fit points, 3 replicate points and 6 additional model points. The collected data were processed using polynomial analysis.

Table S9. Optimal (Custom) Design: the choice of variable factors.

Factor	Name	Units	Minimum value	Maximum value
A	Salt (KPF ₆)	eq	0	3.0
B	Acid (HPF ₆)	eq	0.1	8.0

Table S10. Fit summary.

Response	Sequential p-value	Lack of Fit p-value	Adjusted R ²	Predicted R ²
mixHC[8] HPLC yield	0.0128	0.0020	0.7834	0.1043
cycHC[8] HPLC yield	0.0116	0.4193	0.7242	-1.7409

The software suggested cubic model for processing the collected data. The analysis of variance (ANOVA) for mixHC[8] and cycHC[8] cubic models identified components attributed to both salt and acid amount as significant. The amount of acid, however, was more crucial for mixHC[8] formation.

Table S11. Analysis of variance for mixHC[8] cubic model.

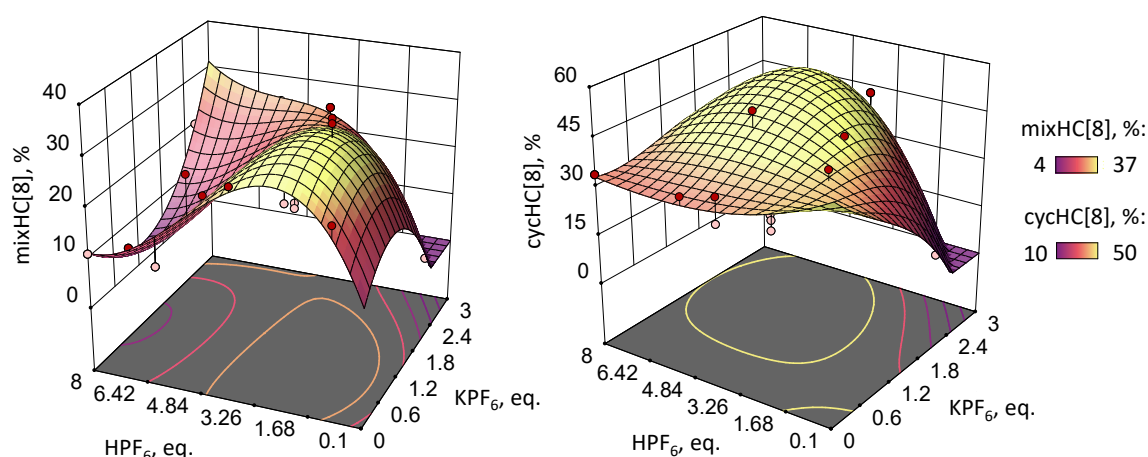
Source	Sum of Squares	df	Mean Square	F-value	p-value ^b	
Model	1501.76	9	166.86	8.63 ^a	0.0012	significant
A (salt)	9.24	1	9.24	0.4780	0.5050	
B (acid)	318.28	1	318.28	16.47	0.0023	
AB (salt, acid)	134.79	1	134.79	6.98	0.0247	
A ² (salt)	3.40	1	3.40	0.1758	0.6838	
B ² (acid)	551.59	1	551.59	28.54	0.0003	
A ² B (salt, acid)	140.23	1	140.23	7.26	0.0226	
AB ² (salt, acid)	2.03	1	2.03	0.1049	0.7527	
A ³ (salt)	3.57	1	3.57	0.1846	0.6766	
B ³ (acid)	124.72	1	124.72	6.45	0.0293	
Residual	193.24	10	19.32			
Lack of Fit	192.24	7	27.46	82.39 ^c	0.0020	significant
Pure Error	1.0000	3	0.3333			
Cor Total	1695.00	19				

[a] The **Model F-value** of 8.63 implies the model is significant. [b] **P-values** less than 0.0500 indicate model terms are significant. In this case B, AB, B², A²B, B³ are significant model terms (highlighted in yellow). [c] The **Lack of Fit F-value** of 82.39 implies the Lack of Fit is significant, which can be related to a smaller variance of mixHC[8] yields compared to cycHC[8].

Table S12. Analysis of variance for cycHC[8] cubic model.

Source	Sum of Squares	df	Mean Square	F-value	p-value ^b	
Model	1249.10	9	138.79	6.54 ^a	0.0035	significant
A (salt)	89.81	1	89.81	4.23	0.0666	
B (acid)	57.07	1	57.07	2.69	0.1320	
AB (salt, acid)	222.44	1	222.44	10.49	0.0089	
A ² (salt)	242.30	1	242.30	11.42	0.0070	
B ² (acid)	521.37	1	521.37	24.58	0.0006	
A ² B (salt, acid)	3.53	1	3.53	0.1667	0.6917	
AB ² (salt, acid)	405.68	1	405.68	19.13	0.0014	
A ³ (salt)	54.10	1	54.10	2.55	0.1413	
B ³ (acid)	0.7610	1	0.7610	0.0359	0.8536	
Residual	212.10	10	21.21			
Lack of Fit	163.10	7	23.30	1.43 ^c	0.4193	not significant
Pure Error	49.00	3	16.33			
Cor Total	1461.20	19				

[a] The **Model F-value** of 6.54 implies the model is significant. [b] **P-values** less than 0.0500 indicate model terms are significant. In this case AB, A², B², AB² are significant model terms (highlighted in yellow). [c] The **Lack of Fit F-value** of 1.43 implies the Lack of Fit is not significant relative to the pure error.

**Figure S5.** 3D response surfaces describing the trends upon varying the amounts of KPF₆ and HPF₆ used as the template.

Screening monomer ratios

Ratio 1:5: D-biotin (60 mg, 0.25 mmol, 1 eq.), (*R,R*)-*N,N'*-cyclohexa-1,2-diylurea (172 mg, 1.23 mmol, 5 eq.), paraformaldehyde (44 mg, 1.5 mmol, 6 eq.), KPF₆ (34 mg, 0.19 mmol, 1 eq.) and 55% aq. HPF₆ (59 μ l, 0.37 mmol, 2 eq.) as LAG additive (η =0.19 μ l/mg);

Ratio 1:7: D-biotin (45–46 mg, 0.19 mmol, 1 eq.), (*R,R*)-*N,N'*-cyclohexa-1,2-diylurea (182–184 mg, 1.30–1.31 mmol, 7 eq.), paraformaldehyde (44–45 mg, 1.5 mmol, 8 eq.), KPF₆ (35 mg, 0.19 mmol, 1 eq.) and 55% aq. HPF₆ (60 μ l, 0.37 mmol, 2 eq.) as LAG additive (η =0.20 μ l/mg);

Ratio 1:15: D-biotin (23 mg, 0.094 mmol, 1 eq.), (*R,R*)-*N,N'*-cyclohexa-1,2-diylurea (198 mg, 1.41 mmol, 15 eq.), paraformaldehyde (45 mg, 1.19 mmol, 16 eq.), KPF₆ (35 mg, 0.19 mmol, 1 eq.) and 55% aq. HPF₆ (61 µl, 0.34 mmol, 2 eq.) as LAG additive ($\eta=0.20$ µl/mg) were milled at 30 Hz for 60 minutes and aged at 60 °C for 24 hours.

Table S13. Effect of ratios of starting monomers

Entry	Monomer molar ratio	HPLC yield, %	
		mixHC[8]	cycHC[8]
1 ^a	1:5	34	30
2 ^b	1:7	37±2	38±2
3 ^c	1:15	27	62

The HPLC yields are provided as the ^bmean value ± standard deviation for the reaction reproduced ^b 4 times (see Table S3) or ^{a, c} once. The deviation between triplicate measurements did not exceed 0.7%.

Screening milling duration

Reaction conditions: D-biotin (45–46 mg, 0.19 mmol, 1 eq.), (*R,R*)-*N,N'*-cyclohexa-1,2-diylurea (182–184 mg, 1.30–1.31 mmol, 7 eq.), paraformaldehyde (44–46 mg, 1.5–1.5 mmol, 8 eq.) and KPF₆ (34–35 mg, 0.19 mmol, 1 eq.) and 55% aq. HPF₆ (60 µl, 0.37 mmol, 2 eq.; $\eta=0.20$ µl/mg) were milled for 5–90 minutes and aged at 60 °C for 24 hours.

Table S14. Screening milling time.

Entry	Milling time, min	mixHC[8] HPLC yield, %		cycHC[8] HPLC yield, %	
		Individual ^a	Average ^b	Individual ^a	Average ^b
1	5	15.1	15.5±0.4	55.4	55±3
		15.6		51.8	
		15.8		57.6	
2	10	24.1	23.9±0.2	36.7	39±3
		23.9		38.1	
		23.7		41.6	
3	20	37.4	37±1	39.2	39±1
		37.3		39.6	
		36.1		38.0	
4	30	28.2	33±4	29.2	32±3
		29.6		30.4	
		36.3		34.1	
		36.2		35.5	
5	45	23.3	26±4	25.2	29±4
		23.8		26.1	
		32.8		33.9	
		25.9		28.9	
6	60	40.5	37±2	38.1	38±2
		36.5		41.0	
		36.3		36.4	
		34.9		36.3	
7	90	34.5	34±1	32.5	32±1
		33.1		31.0	

^a HPLC yields from triplicate measurements, the deviation between parallel measurements did not exceed 3.1%; ^b HPLC yields expressed as the mean value ± standard deviation between reactions reproduced *n* times.

60 min is the optimal milling time, which ensures efficient shuffling of the intermediates. Increasing milling time to 90 min did not improve the yields. Shorter milling times required long aging time, see Table S15.

Screening aging duration

Reaction conditions: D-biotin (45–46 mg, 0.19 mmol, 1 eq.), (*R,R*)-*N,N'*-cyclohexa-1,2-diylurea (183– mg, 1.31 mmol, 7 eq.), paraformaldehyde (45 mg, 1.5 mmol, 8 eq.), KPF₆ (34–35 mg, 0.19 mmol, 1 eq.) and 55% aq. HPF₆ (60 µl, 0.37 mmol, 2 eq., $\eta=0.20$ µl/mg) were milled for 60 minutes and aged at 60 °C for 0, 3, 6, 12 or 24 hours.

Table S15. Screening aging time.

Entry	Aging time, h	mixHC[8] HPLC yield, %		cycHC[8] HPLC yield, %	
		Individual ^a	Average ^b	Individual ^a	Average ^b
1	0	14.8	13±3	20.7	18±4
		11.4		14.7	
2	3	38.6	38±1	33.3	34±2
		37.7		35.6	
3	6	36.9	38±1	35.4	35.3±0.1
		38.0		35.2	
4	12	31.6	31.2±0.5	33.9	33±2
		30.9		31.6	
5	24	40.5	37±2	38.1	38±2
		36.5		41.0	
		36.3		36.4	
		34.9		36.3	
6	3 ^c	30.4	30.1±0.3	31.8	31.7±0.2
		29.9		31.6	

^a HPLC yields from triplicate measurements, the deviation between parallel measurements did not exceed 1.5%;

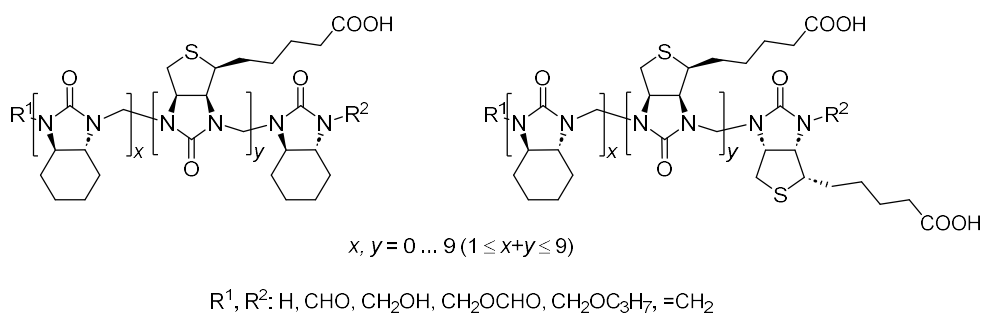
^b HPLC yields expressed as the mean value ± standard deviation between reactions reproduced n times.

^c Reaction mixture was milled for 20 min and it resulted in lower yields compared to 60 min milling.

Optimal aging time is 3 hours for 60 min milled reactions.

2.3 Analysis of Oligomers and Side-Products

2.3.1. General oligomeric and macrocyclic profile



The iminium intermediates can react with isopropanol used in sample preparation (1:1 chloroform : isopropanol solvent mixture), which results in $-CH_2OC_3H_7$ terminal groups.

General oligomeric and macrocyclic profile of crude reaction mixtures was studied on Agilent 6540 Accurate-Mass Q-TOF mass-spectrometer, using the HPLC setup from system B. The mass spectra were acquired in positive polarity, mass range m/z 50 – 3200 and fragmentor voltage 175 V. The AJS-ESI source parameters were set as follows: gas temperature 200 °C, drying gas flow 6 L/min, nebulizer pressure 30 psi, sheath gas temperature 200 °C, sheath gas flow 8 L/min, capillary voltage 3500 V, nozzle voltage 1000 V, skimmer voltage 65 V, octopole peak-peak voltage 750 V. Prior to analysis the instrument was tuned in m/z 50–3200 mass range.

The collected data was processed with the aid of MatchMass Tool.⁶

Composition of the crude mixtures after different milling duration (HPLC-HRMS)

A	5 min milling	G	5 min milling + 24 h aging
B	10 min milling	H	10 min milling + 24 h aging
C	20 min milling	I	20 min milling + 24 h aging
D	30 min milling	J	30 min milling + 24 h aging
E	45 min milling	K	45 min milling + 24 h aging
F	60 min milling	L	60 min milling + 24 h aging

Reaction conditions: D-biotin (45–46 mg, 0.19 mmol, 1 eq.), (*R,R*)-*N,N'*-cyclohexa-1,2-diylurea (183 mg, 1.31 mmol, 7 eq.), paraformaldehyde (45 mg, 1.50 mmol, 8 eq.) and KPF_6 (34–35 mg, 0.19 mmol, 1 eq.) and 55% aq. HPF_6 (60 μ l, 0.37 mmol, 2 eq.) were milled for 5–60 minutes and aged 60 °C for 24 hours. The samples for analysis were collected after milling and after aging.

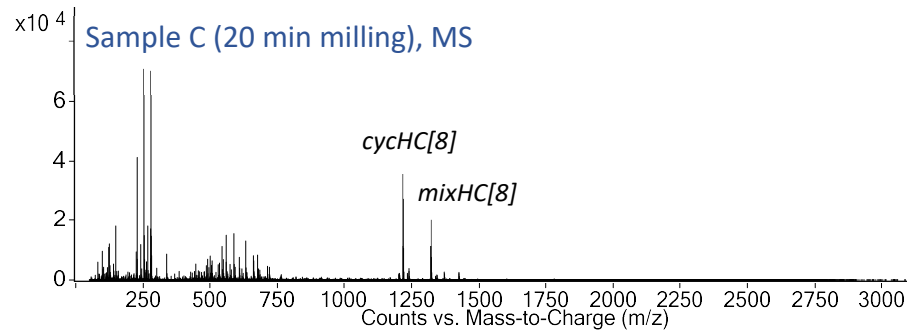
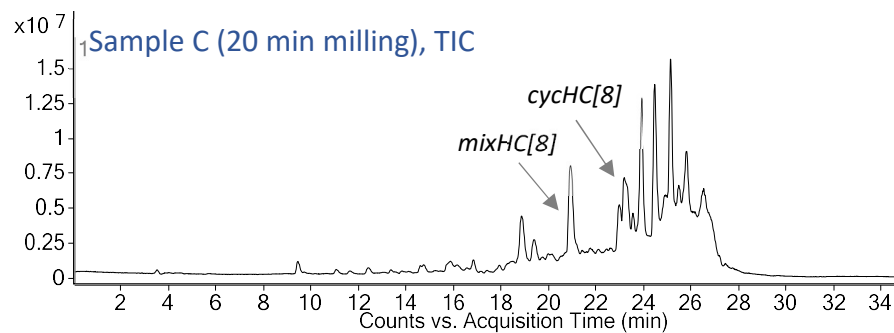
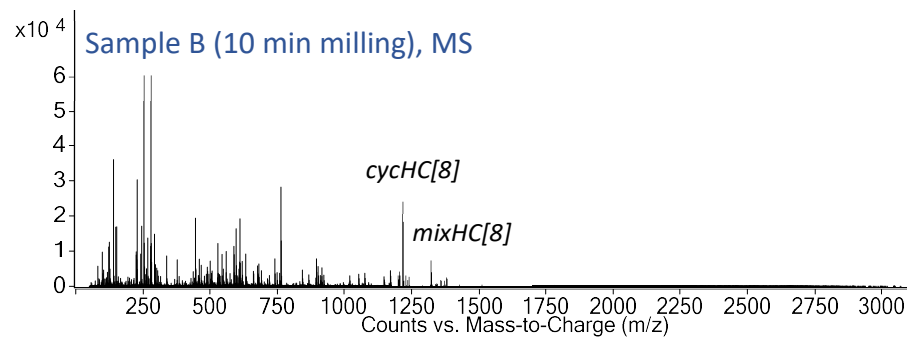
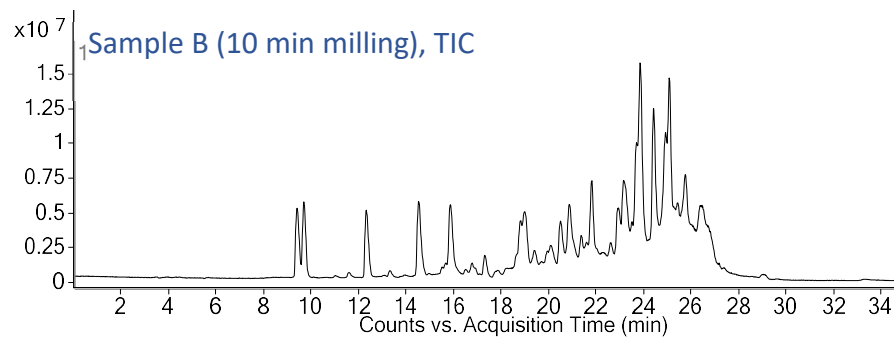
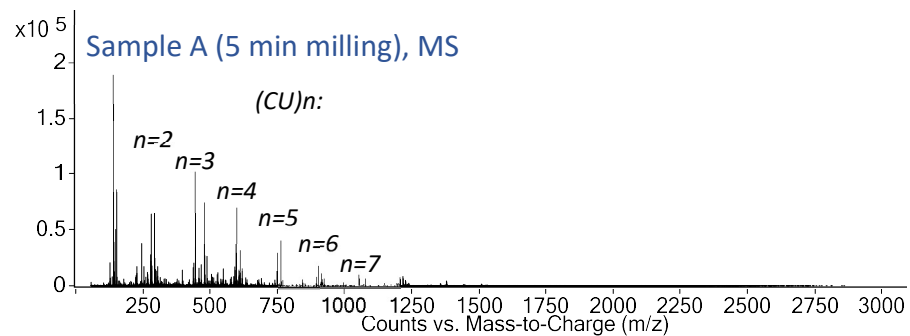
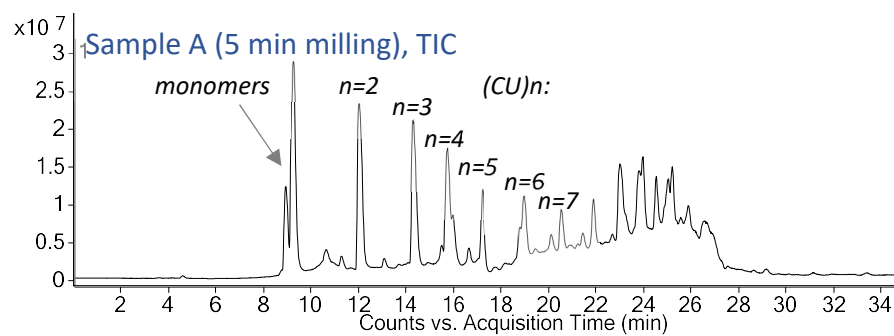


Figure S6. Total ion chromatograms and mass spectra of samples A–C.

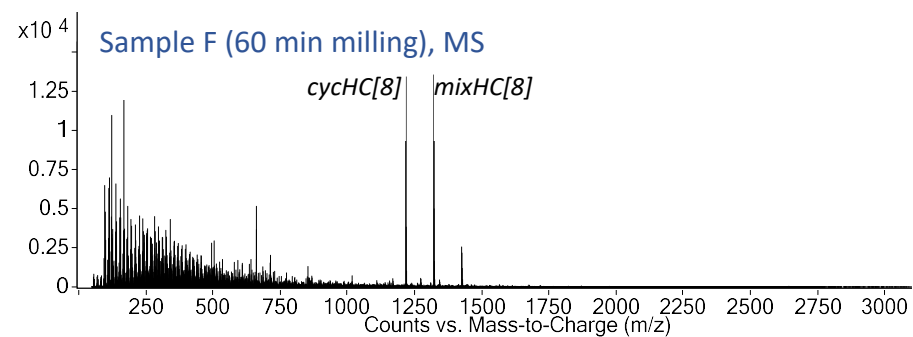
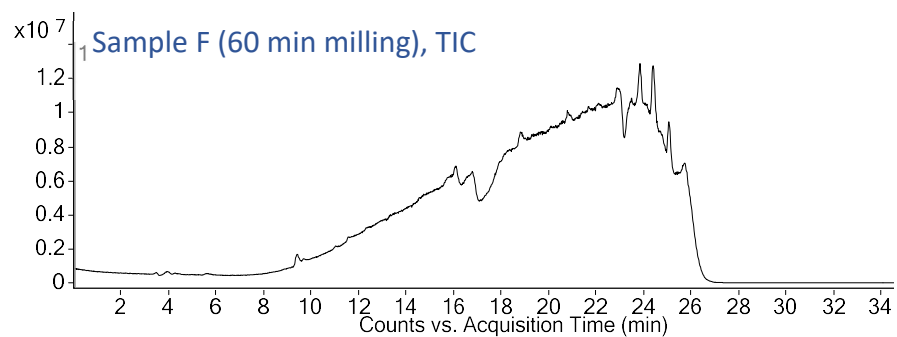
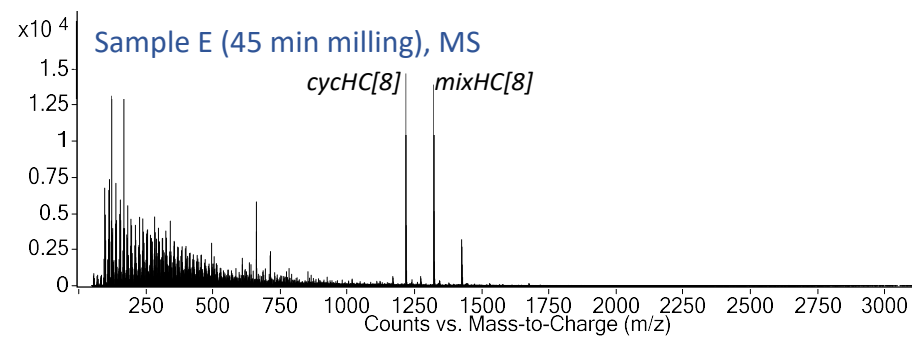
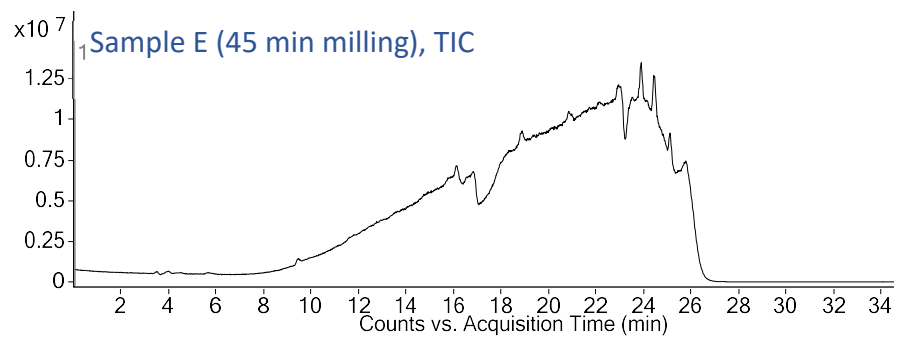
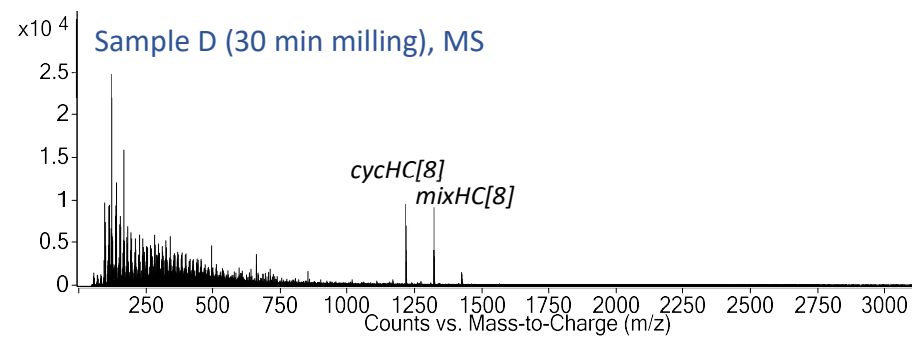
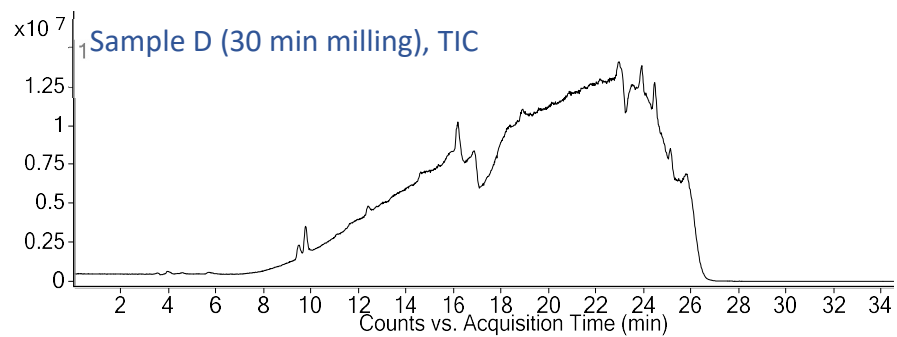


Figure S7. Total ion chromatograms and mass spectra of samples D–F.

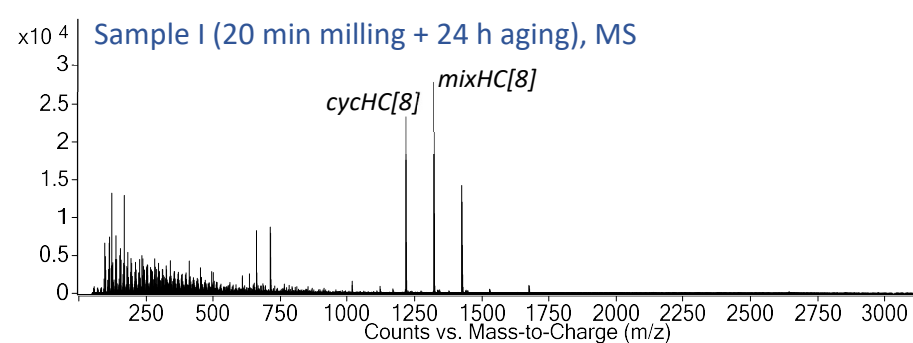
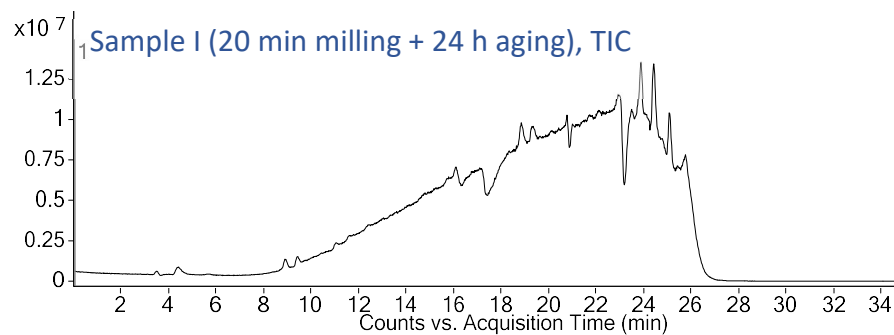
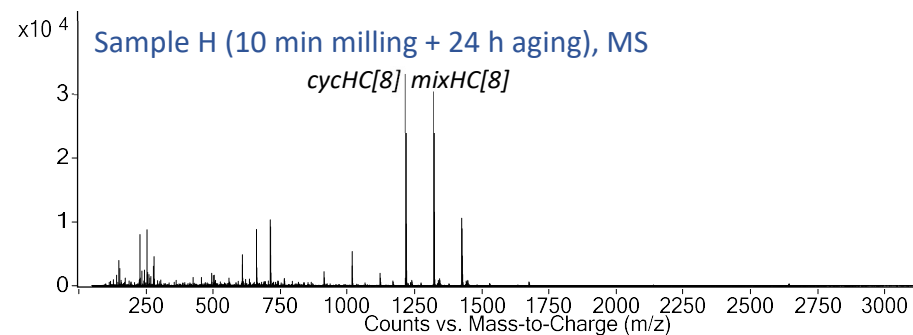
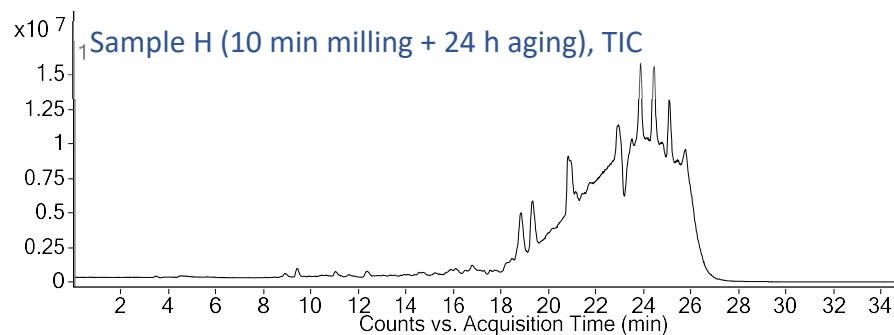
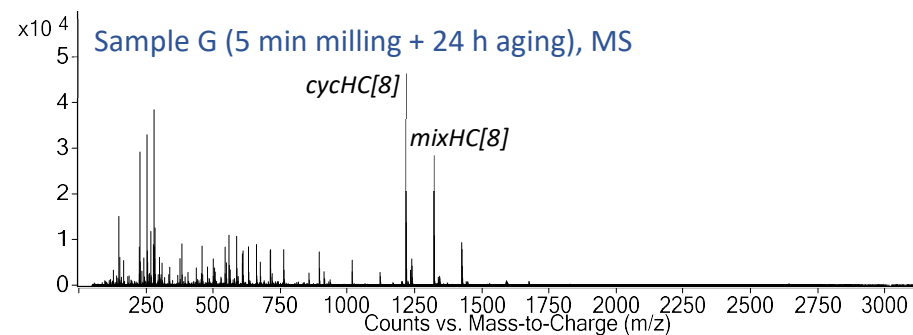
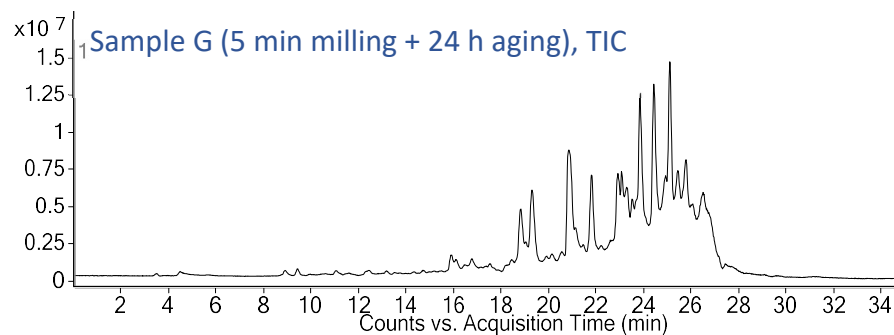


Figure S8. Total ion chromatograms and mass spectra of samples G–I.

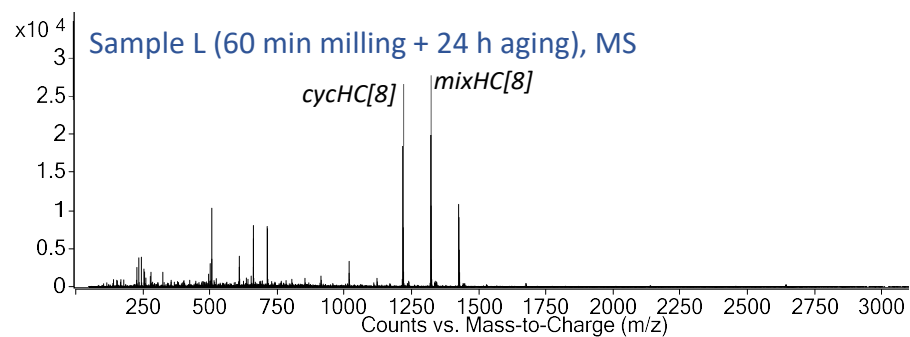
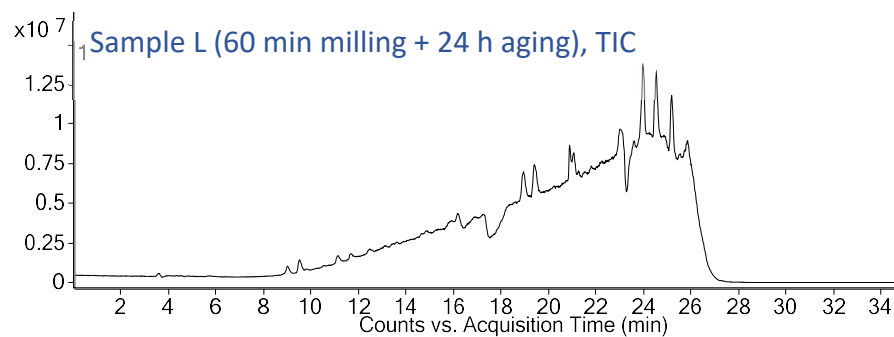
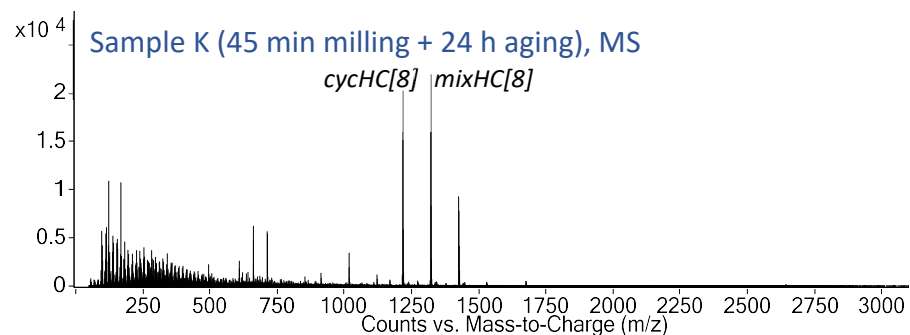
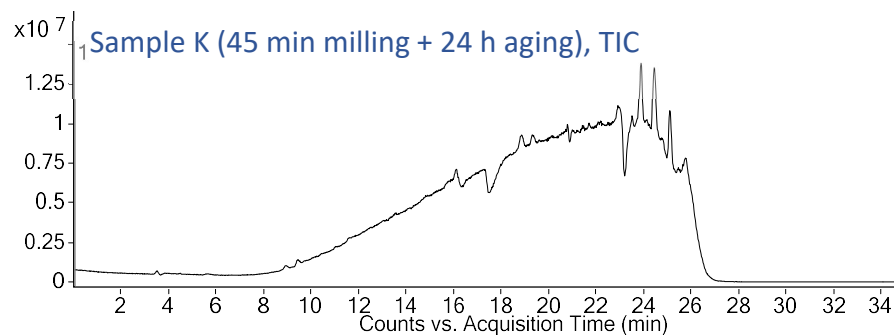
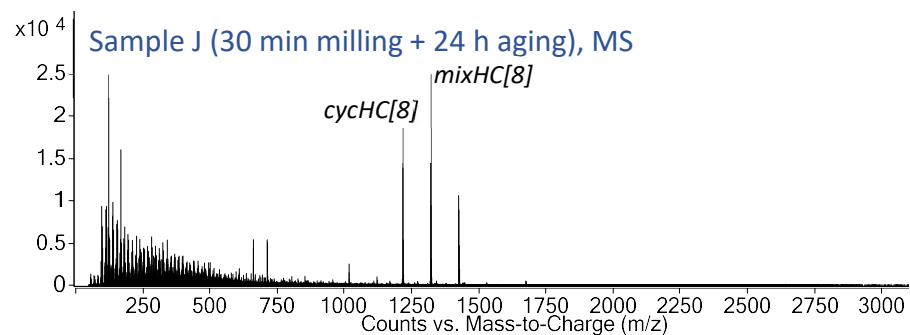
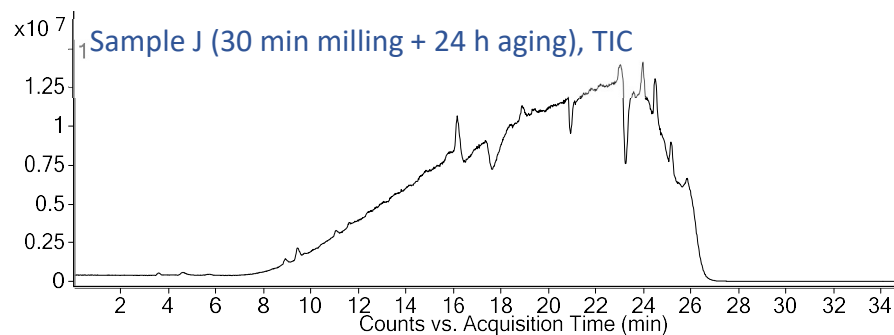


Figure S9. Total ion chromatograms and mass spectra of samples J–L.

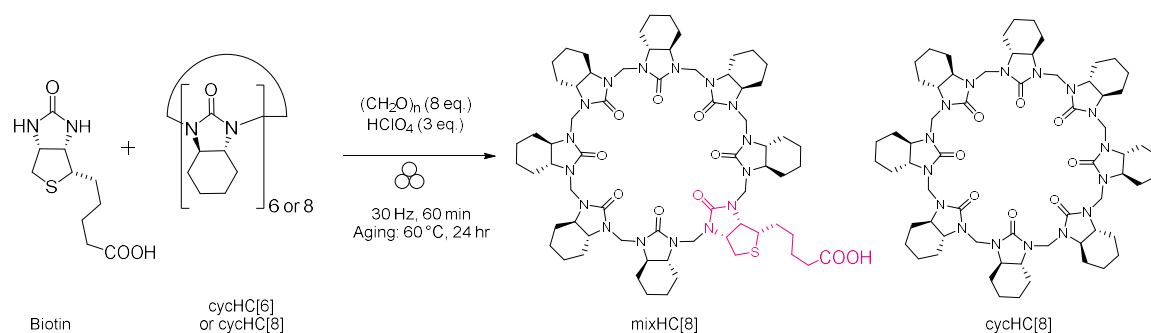


Figure S10. Relative abundance of the observed monomers, oligomers and macrocycles⁶, visualized as a heat map⁷. See details in separate file with Table S29 .

Table S16. Relative abundance (%) of detected species used in the heat map in the main text.

Oligomers	<i>n</i>	A	B	C	D	E	F	G	H	I	J	K	L
Monomers	1	25.92	15.51	12.27	18.48	4.51	7.77	2.01	3.27	3.19	3.84	1.89	4.54
Homomeric oligomers	2-3	37.69	33.24	17.96	29.16	21.54	23.67	18.24	4.65	16.69	18.66	12.70	5.63
	4-5	23.65	26.32	8.72	4.89	2.48	3.38	9.05	4.54	1.34	2.55	2.59	0.62
	6-8	7.30	10.76	10.40	4.99	5.96	5.35	0.28	0.03	-	4.97	5.87	0.08
	9-10	0.92	0.18	0.30	0.05	0.00	0.03	0.14	-	-	-	-	-
Mixed oligomers	2-3	2.03	1.74	2.64	1.84	1.81	3.34	0.92	1.67	2.56	1.88	1.68	1.97
	4-5	0.80	1.75	2.62	6.76	3.49	6.42	1.11	1.94	3.42	5.45	2.62	3.33
	6-8	0.26	1.28	4.67	8.08	11.95	10.47	8.73	13.50	15.83	13.47	14.31	16.63
	9-10	0.02	0.03	0.00	0.20	0.00	0.00	0.00	0.00	0.00	0.04	0.00	0.05
mixHC[8]	8	0.02	1.11	8.95	10.79	20.40	17.74	16.89	24.77	22.68	20.64	22.38	26.51
cycHC[8]	8	1.31	7.32	30.06	11.07	21.21	17.73	29.04	27.10	19.05	15.74	20.61	25.89
other HC[8]	8	-	0.14	1.42	1.97	4.94	3.32	5.93	9.96	12.24	8.80	9.67	10.44
other HC	6-7	0.08	0.62	-	1.72	1.70	0.77	7.66	8.56	3.00	3.96	5.67	4.31

2.3.2 Crossover of monomer units between cycHC[*n*] and biotin



General synthesis procedure for screening reaction with cycHC[6] as starting material: D-biotin (56 mg, 0.23 mmol, 1 eq.) and (*R,R*)-cyclohexanohemicucurbit[6]uril (249 mg, 0.270 mmol, 1.2 eq.) and 70% aq. HClO₄ (60 μl, 0.69 mmol, 3 eq.) were milled for 60 minutes and aged at 60 °C for 24 hours.

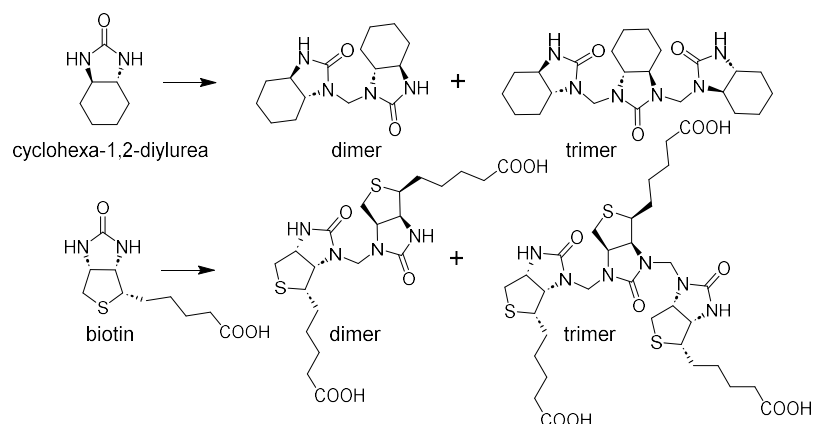
General synthesis procedure for screening reaction with cycHC[8] as starting material: D-biotin (55 mg, 0.23 mmol, 1 eq.) and (*R,R*)-cyclohexanohemicucurbit[8]uril (240 mg, 0.196 mmol, 0.9 eq.) and 70% aq. HClO₄ (58 μl, 0.68 mmol, 3 eq.) were milled for 60 minutes and aged at 60 °C for 24 hours.

Table S17. MixHC[8] synthesis using cycHC[*n*] macrocycles as starting material

Entry	Biotin:cycHC[<i>n</i>] molar ratio ^a	HClO ₄ , eq.	HPLC yield, %	
			mixHC[8]	cycHC[8]
1	1:1.2 (cycHC[6])	3	10	47
2	1:0.9 (cycHC[8])	3	9	51

^a Ratio of starting materials was chosen to satisfy 1:7 ratio of monomers in mixHC[8], each reaction was performed once. The deviation between triplicate HPLC measurements did not exceed 1%.

2.3.3 Quantitative analysis of dimers and trimers



The quantitative determination of uniformly composed $\text{CU}[n]$ and $\text{B}[n]$ ($n = 2$ or 3) in crude reaction mixtures was performed for the samples A–L (see 1.3.1) and additional sample T0 for 0 min reaction time. The sampling was performed in triplicate, as outlined in page S3. If necessary, the solutions were diluted to ensure the peak areas were within the linear range of the method.

Quantification of the oligomers was performed using the HPLC setup from system B, following the target m/z values corresponding to the chosen oligomeric species $[\text{M}+\text{H}]^+$ and $[\text{M}+\text{Na}]^+$. The chromatograms were acquired in positive polarity with the following ESI source parameters: drying gas temperature 300 °C, drying gas flow 5 L/min, nebulizer pressure 60 psig, vaporizer temperature 150 °C, capillary voltage 2000 V, charging voltage 2000 V, fragmentor voltage 140 V.

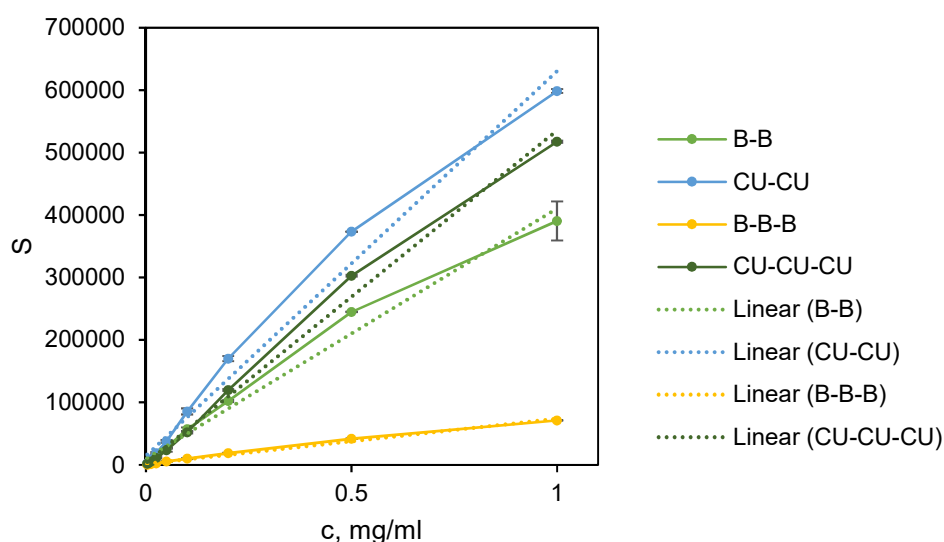


Figure S11. Full studied range for determination of the method linearity. The error bars express deviation between two parallel measurements. Note: the concentration units are not related to the real concentrations of the oligomers, as the latter have not been isolated.

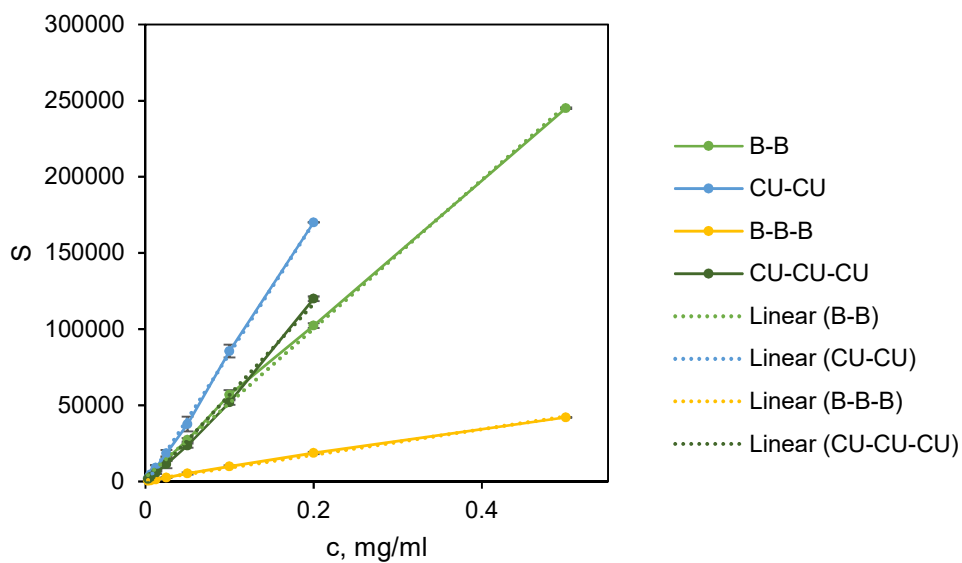


Figure S12. Established linear range of the method. The error bars express deviation between two parallel measurements. Note: the concentration units are not related to the real concentrations of the oligomers, as the latter have not been isolated.

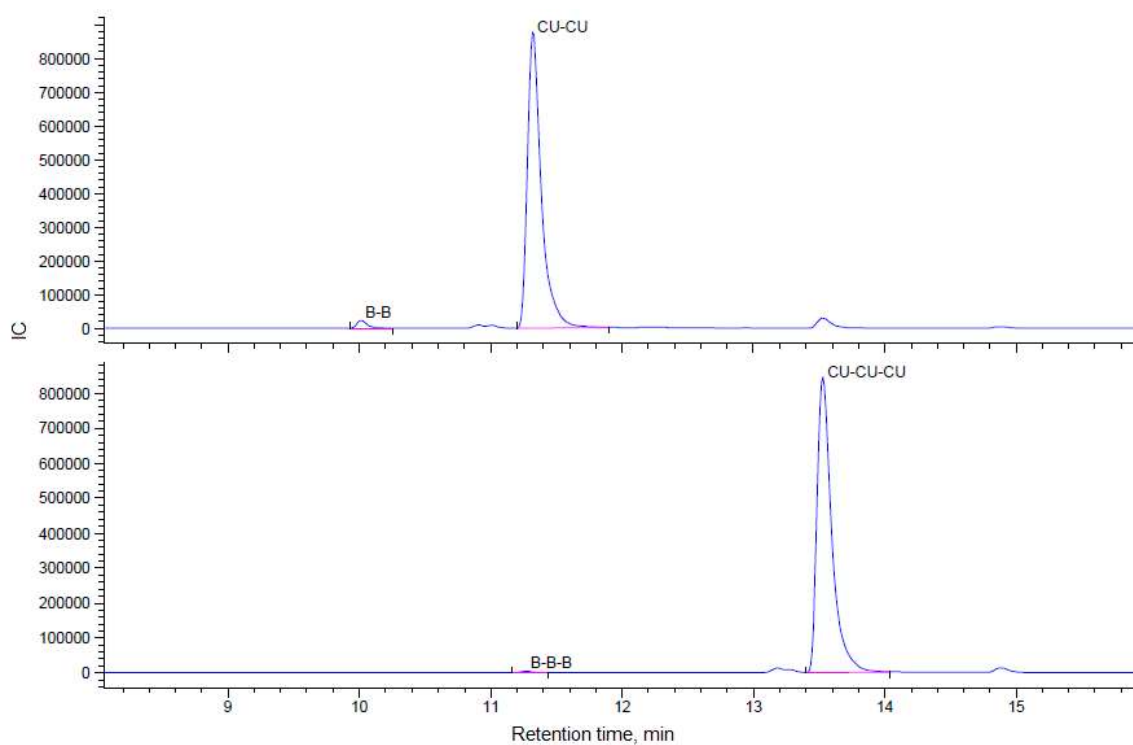


Figure S13. SIM chromatograms of dimers and trimers in sample A.

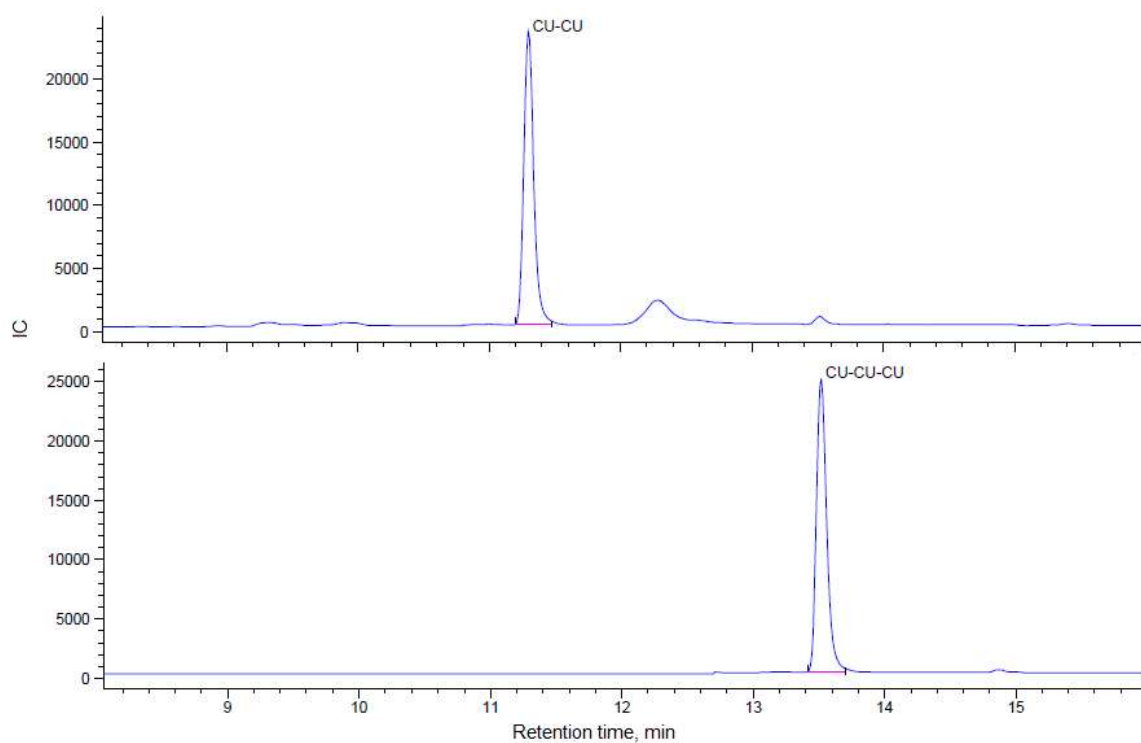


Figure S14. SIM chromatograms of dimers and trimers in sample A diluted 200 times.

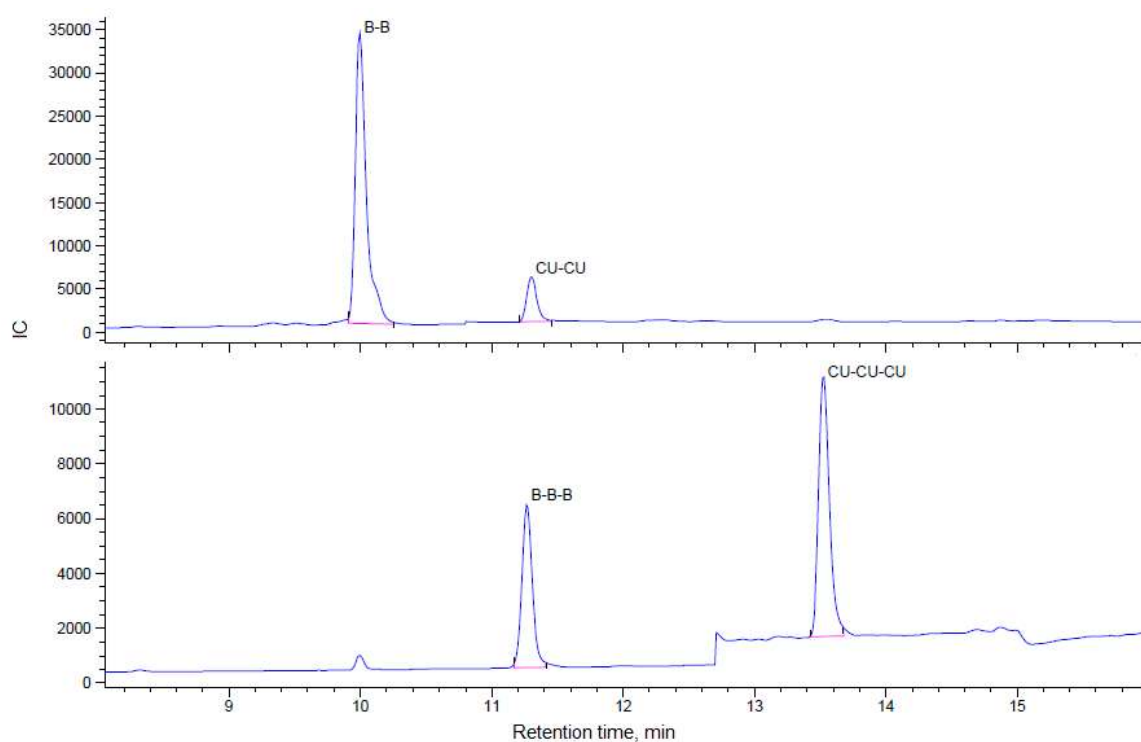


Figure S15. SIM chromatograms of dimers and trimers in sample L.

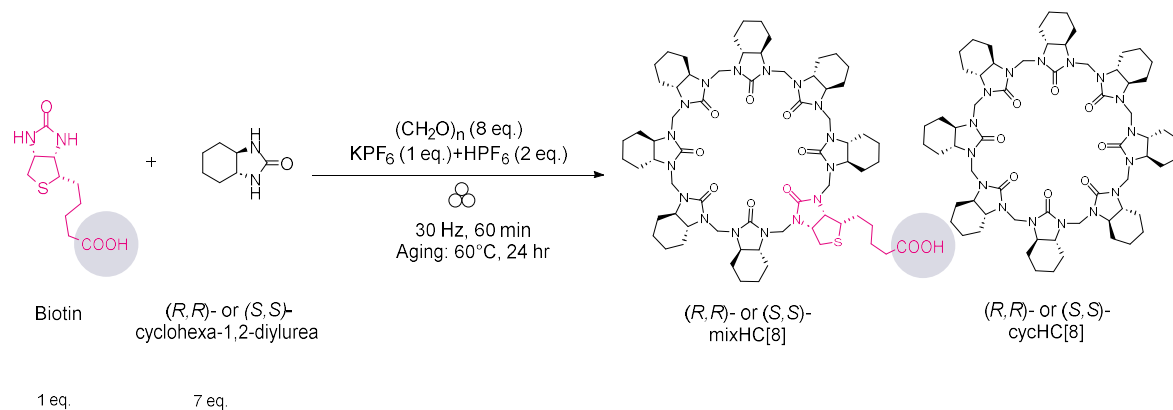
Table S18. Distribution of short homomeric oligomers after milling and aging.

Sample	Milling time, min	Aging time, h	Peak area, IC's				HPLC yield, %	
			B-B	CU-CU	B-B-B	CU-CU-CU	mixHC[8]	cycHC[8]
T0	0	0	0	0	0	0	0	0
A	5	0	118000±14000	30400000±8400000 ^a	25100±3100	29700000±4300000 ^a	1.9±0.3	4±2
B	10	0	46500±9200	1100000±310000 ^b	13200±2200	1620000±460000 ^b	3.4±0.2	11±1
C	20	0	130300±5200	38000±1900	22300±1200	73000±2900	7.7±0.3	18.13±0.01
D	30	0	84100±4900	115000±50000	10490±490	160000±56000	6.6±0.2	10±1
E	45	0	50100±6700	11165±940	5770±180	26100±2400	11.0±0.3	17±1
F	60	0	96600±2200	33000±3000	10200±120	75500±5800	11.4±0.3	15±1
G	5	60	57200±8200	32800±1300	7570±340	2470±560	15.8±0.3	57.6±0.1
H	10	60	94000±12000	31500±6200	19900±1800	28600±2100	24±1	41.6±0.3
I	20	60	175500±3600	25130±710	32100±1100	38990±960	36±1	38±1
J	30	60	185900±6500	33400±1800	31390±930	60500±370	36±1	36±1
K	45	60	74100±1100	17430±540	9850±240	35300±470	26±1	29±1
L	60	60	206000±5800	28300±910	34200±1500	52800±2200	34.9±0.2	36±1

The peak areas are reported as the mean value ± standard deviation of triplicates. [a] The sample was diluted 200 times. [b] The sample was diluted 50 times. For the diluted samples, the peak area was divided by corresponding dilution factor

3. Preparative Synthesis, Purification, and Characterization of mixHC[8]

Best reaction conditions from the screening was selected for the synthesis of mixHC[8] in gram-scale.



General synthesis procedure: D-Biotin (45 mg, 0.19 mmol, 1 eq.), (R,R) -or (S,S) - N,N' -cyclohexa-1,2-diylurea (183 mg, 1.30 mmol, 7 eq.) and paraformaldehyde (45 mg, 1.49 mmol, 8 eq.) were placed into a 14 mL ZrO_2 -coated jar charged with two 10 mm ZrO_2 balls (3.5 g). After addition of 55% aq. HPF_6 (60 μL , 0.37 mmol, 2 eq.) and KPF_6 (34 mg, 0.19 mmol, 1 eq.) the mixture was milled at 30 Hz for 60 minutes. The jar was then sealed with parafilm and reaction mixture was aged at 60 °C for 24 hours. The crude mixture was further washed on a glass filter with distilled water until neutral pH, which was determined by test strips. The quenched mixture was dried in open air at room temperature. The procedure was repeated 8 times with both diastereoisomers, resulting in 2.6 g of crude product with each diastereoisomer for further purification.

Purification procedure: To convert mixHC[8] into potassium salt 350 mL of 5% KOH/MeOH solution was added to the dry quenched reaction mixture, followed by stirring for 45 min and resulting in white heterogeneous mixture. MeOH and water were evaporated via azeotropic removal with toluene (50 mL \times 3) until light yellow dry mixture was obtained. Solid-liquid toluene extraction was performed three times with 70 mL of toluene and allowed to remove cycHC[8]. The remaining mixture in the flask and on the filter was dissolved in 350 mL of distilled water, providing white milky suspension. The aqueous mixture was then acidified with conc. HCl till pH 2–3. The precipitated solid was then filtered and left to dry. The dried solid was purified by flash column chromatography (gradient 0–50% $i\text{PrOH}$ (1% acetic acid)/ CH_2Cl_2). This procedure afforded pure mixHC[8] and cycHC[8] with oligomers which were not separated in pure form.

225 mg of (+)-mixHC[8] (isolated yield 11%, NMR purity 90%), and 320 mg (–)-mixHC[8] (isolated yield 16%, NMR purity 88%) was obtained. NMR purity was assessed using internal standard.⁸

Both diastereoisomers were characterized with HRMS, 1D and 2D (COSY, TOCSY, HSQC, TOCSY-HSQC, HMBC, NOESY) NMR, IR and optical rotation.

(-)-((S,S,R)(R,R)₇)-mixHC[8]:

¹H NMR (800 MHz, CDCl₃) δ 4.93 (d, *J* = 14.5 Hz, 1H, CH[h8(1)]), 4.83 (d, *J* = 14.4 Hz, 1H, CH[h8(2)]), 4.83–4.80 (m, 1H, CH[a11(1)]), 4.83–4.76 (m, 6H, CH₂[b8, d8, f8]), 4.67–4.64 (m, 1H, CH[a11(2)]), 4.67–4.58 (m, 6H, CH₂[c8, e8, g8]), 4.25 (dt, *J* = 9.9, 6.2 Hz, 1H, CH(a2)), 3.86 (dd, *J* = 9.9, 6.0 Hz, 1H, CH(a3)), 3.46 (ddd, *J* = 12.6, 6.1, 2.5 Hz, 1H, CH(a4)), 3.09 (dd, *J* = 12.8, 5.6 Hz, 1H, CH[a5(1)]), 2.94–2.89 (m, 1H, CH[a5(2)]), 2.90–2.79 (m, 7H), 2.70–2.61 (m, 7H), 2.59 (tt, *J* = 11.2, 3.2 Hz, 2H), 2.51 (tt, *J* = 11.1, 2.6 Hz, 2H), 2.49 – 2.45 (m, 2H), 2.41 – 2.35 (m, 2H), 2.37 (t, *J* = 7.2 Hz, 2H, CH₂(a9)), 2.35–2.28 (m, 3H), 2.28–2.24 (m, 1H), 2.18–2.14 (m, 1H), 1.94–1.64 (m, 12H), 1.82–1.63 (m, 6H, CH₂(a8)+4H), 1.49–1.39 (m, 7H, CH₂(a7)+5H), 1.38–1.30 (m, 6H, CH₂(a6)+4H), 1.29–1.23 (m, 8H), 1.21–1.07 (m, 10H).

¹³C NMR (201 MHz, CDCl₃) δ 177.33(a10), 162.62, 162.60(h1), 162.07(b1), 162.01, 161.89, 161.80, 161.79, 157.99(a1), 65.31, 65.06, 64.93, 64.68, 64.62, 64.50, 62.07(a3), 59.82, 59.79, 59.74(4C), 59.67, 58.99(h2), 58.54(a2), 56.59, 56.00, 55.48, 52.52(a4), 51.96(a11), 48.34(h8), 46.80, 46.79, 46.59, 33.93(a9), 33.81(a5), 28.90(2C), 28.89(2C), 28.82, 28.57, 28.44, 28.18(a8), 27.72, 27.66(2C), 27.64, 27.62, 27.51, 27.49(a6), 27.35, 25.45, 24.72, 24.58, 24.54, 24.48(a7+C), 24.44, 24.43, 24.39(2C), 24.26(2C), 24.23, 24.15(3C).

HRMS (AJS-ESI) calcd. for C₆₇H₉₉N₁₆O₁₀S⁻ [M-H]⁻ 1319.7456, found *m/z* 1319.7469.

IR (KBr pellet): ν = 3484, 2936, 2858, 1710, 1436, 1358, 1332, 1309, 1231, 1133, 1057, 1013, 986, 918, 830, 772, 627, 531, 515 cm⁻¹.

Optical rotation [α]_D²⁰ = -76.0 (*c* 0.132, CHCl₃)

Melting point 238-242 °C

(+)-((S,S,R)(S,S)₇)-mixHC[8]:

¹H NMR (800 MHz, CDCl₃) δ 4.83–4.74 (m, 8H, CH₂[c8, e8, g8, a11]), 4.75 (d, *J* = 7.0 Hz, 1H, CH[h8(1)]), 4.69 (d, *J* = 14.4 Hz, 1H, CH[h8(2)]), 4.60 (dd, *J* = 10.0, 3.7 Hz, 6H, CH₂[b8, d8, f8]), 4.10 (dd, *J* = 9.7, 5.8 Hz, 1H, CH(a3)), 3.88 (dt, *J* = 10.5, 6.0 Hz, 1H, CH(a2)), 3.36 (ddd, *J* = 12.6, 5.9, 2.9 Hz, 1H, CH(a4)), 3.11 (dd, *J* = 13.0, 5.2 Hz, 1H, CH[a5(1)]), 3.04 (dd, *J* = 13.0, 6.6 Hz, 1H, CH[a5(2)]), 2.89 – 2.77 (m, 8H), 2.66 – 2.55 (m, 10H), 2.47 (qd, *J* = 10.9, 3.0 Hz, 2H), 2.46 – 2.42 (m, 2H), 2.40–2.24 (m, 10H), 2.15 (d, *J* = 11.4 Hz, 1H), 1.91–1.75 (m, 12H), 1.72–1.71 (m, 1H, CH[a6(1)]), 1.75–1.63 (m, 7H), 1.49 (q, *J* = 6.6 Hz, 1H), 1.46–1.35 (m, 7H), 1.33 (d, *J* = 4.2 Hz, 1H, CH[a6(2)]), 1.32–1.28 (m, 4H), 1.27–1.04 (m, 14H).

¹³C NMR (201 MHz, CDCl₃) δ 177.10(a10), 163.11(h1), 162.37(b1), 162.17, 161.95, 161.84, 161.74, 161.71, 158.19(a1), 65.20, 65.20, 65.08, 65.06, 64.97, 64.93, 64.87, 64.55, 64.49, 61.54(a3), 59.87, 59.75, 59.73, 59.71, 59.59(a2), 59.23, 56.55, 56.38, 55.32, 53.88(h8),

53.35(a4), 46.82, 46.78, 46.68(a11), 46.63, 34.42(a5), 33.97, 28.98, 28.92, 28.92, 28.89, 28.86, 28.64, 28.63, 28.48, 28.21, 27.74, 27.69, 27.66, 27.63, 27.59, 27.58, 27.47, 27.38, 24.59, 24.57, 24.54, 24.49, 24.47, 24.46, 24.41, 24.41, 24.24, 24.22, 24.17, 24.16, 24.06, 24.05.

HRMS (AJS-ESI) calcd. for $C_{67}H_{99}N_{16}O_{10}S^-$ $[M-H]^-$ 1319.7456, found m/z 1319.7436.

IR (KBr pellet): $\nu = 3502, 2936, 2859, 1710, 1437, 1357, 1332, 1309, 1259, 1132, 1057, 1013, 986, 918, 831, 773, 627, 531, 515\text{ cm}^{-1}$.

Optical rotation $[\alpha]_D^{20} = +31.6$ (c 0.121, $CHCl_3$)

Melting point 245-250 °C

3.1 NMR spectra

(-)-mixHC[8] (left) and (+)-mixHC[8] (right):

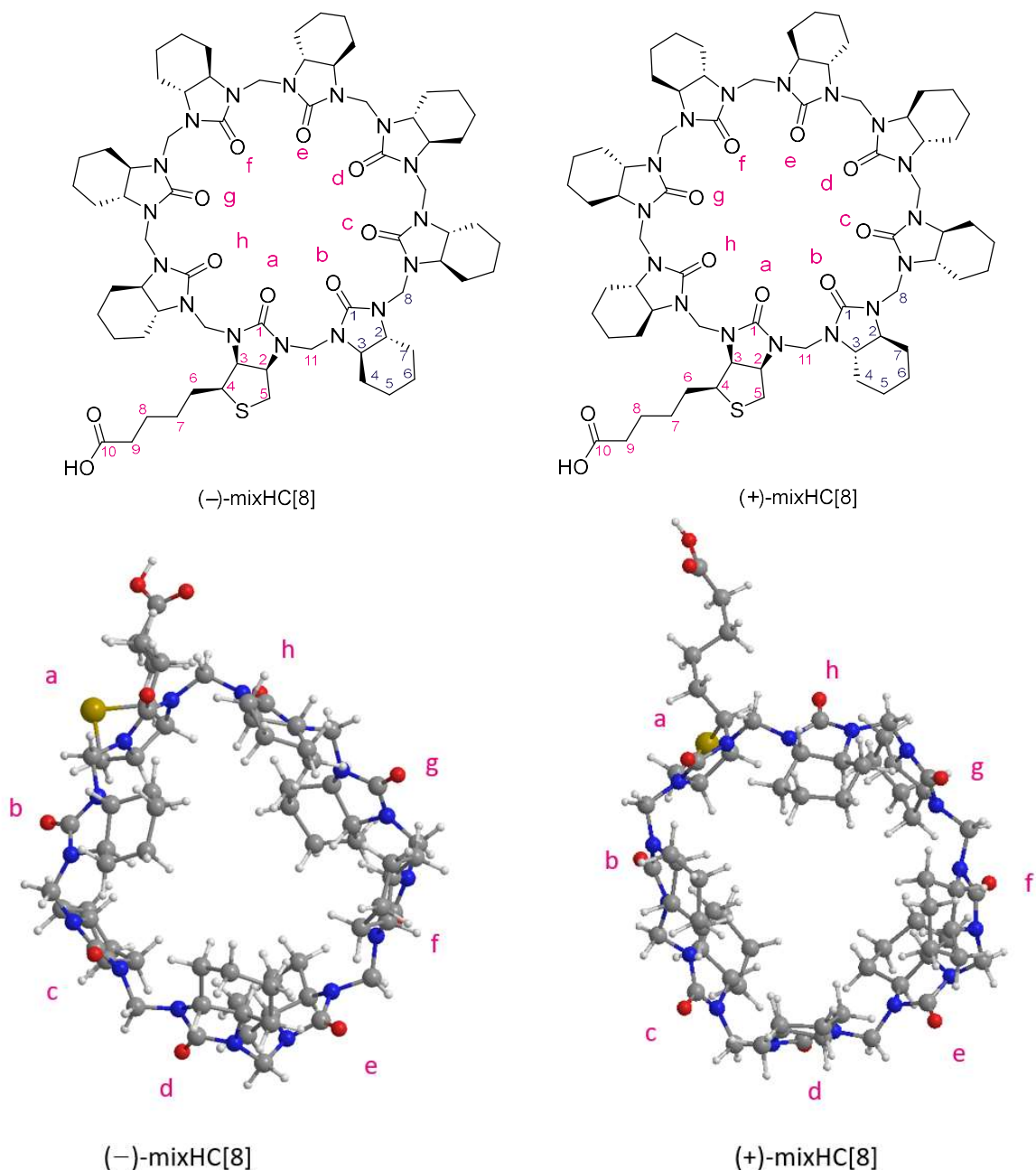


Figure S16. Structures of mixHC[8] diastereoisomers for NMR assignment. 3D structures were obtained from DFT calculations.

MixHC[8] macrocycle is not symmetrical, therefore the NMR analysis is complex. Determining the bridge protons of the diastereoisomers were analogous to cycHC[8]. From 3D structure viewed from above it is seen that there are 90 degree angles and the protons which are on that angle are coupled by each other (geminal coupling) and those protons have bigger chemical shift.

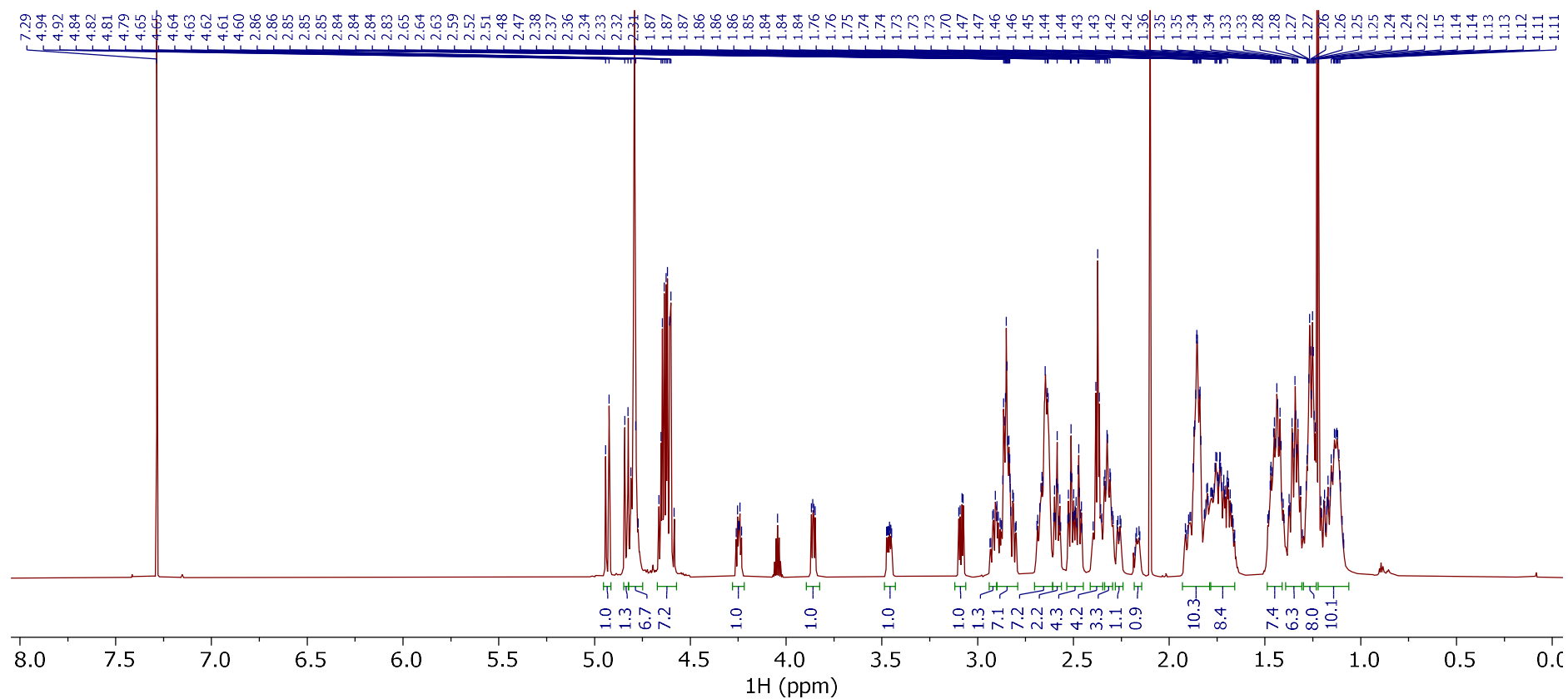


Figure S17. The full ^1H NMR spectra from (-)-mixHC[8]

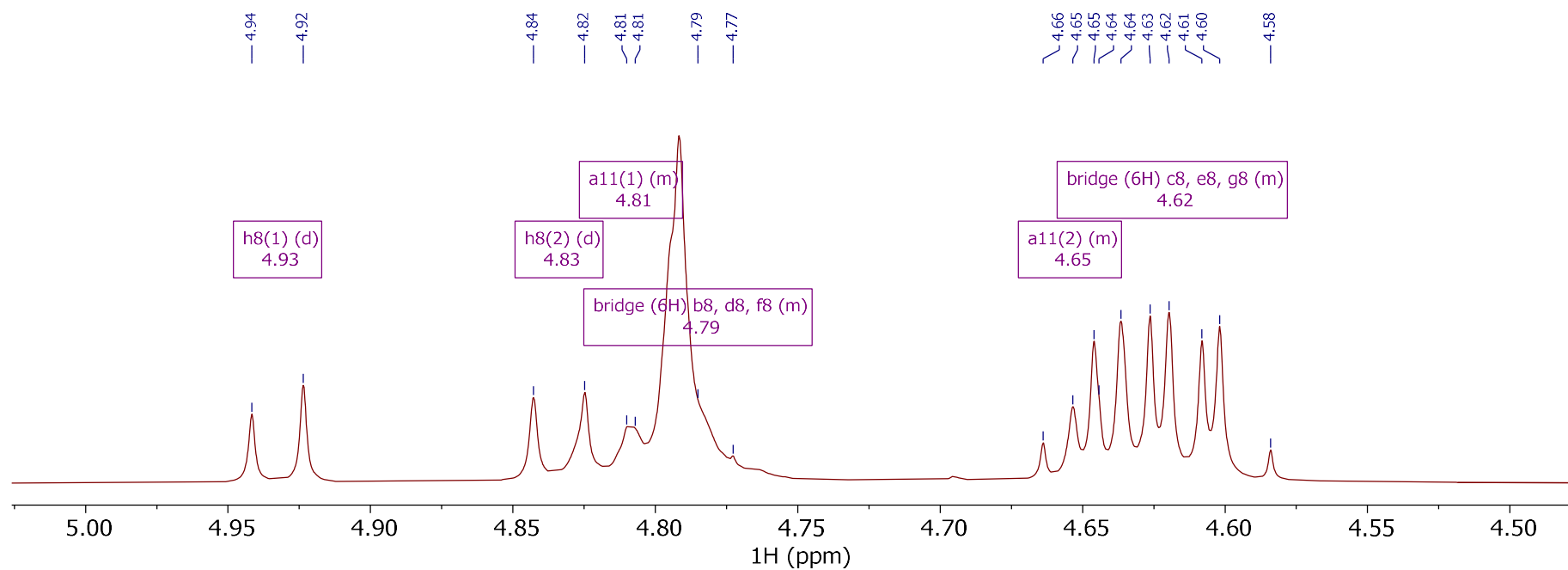


Figure S18. Fragment of ^1H NMR spectra showing bridge protons of $(-)\text{-mixHC[8]}$ in range of 4.58-4.94 ppm.

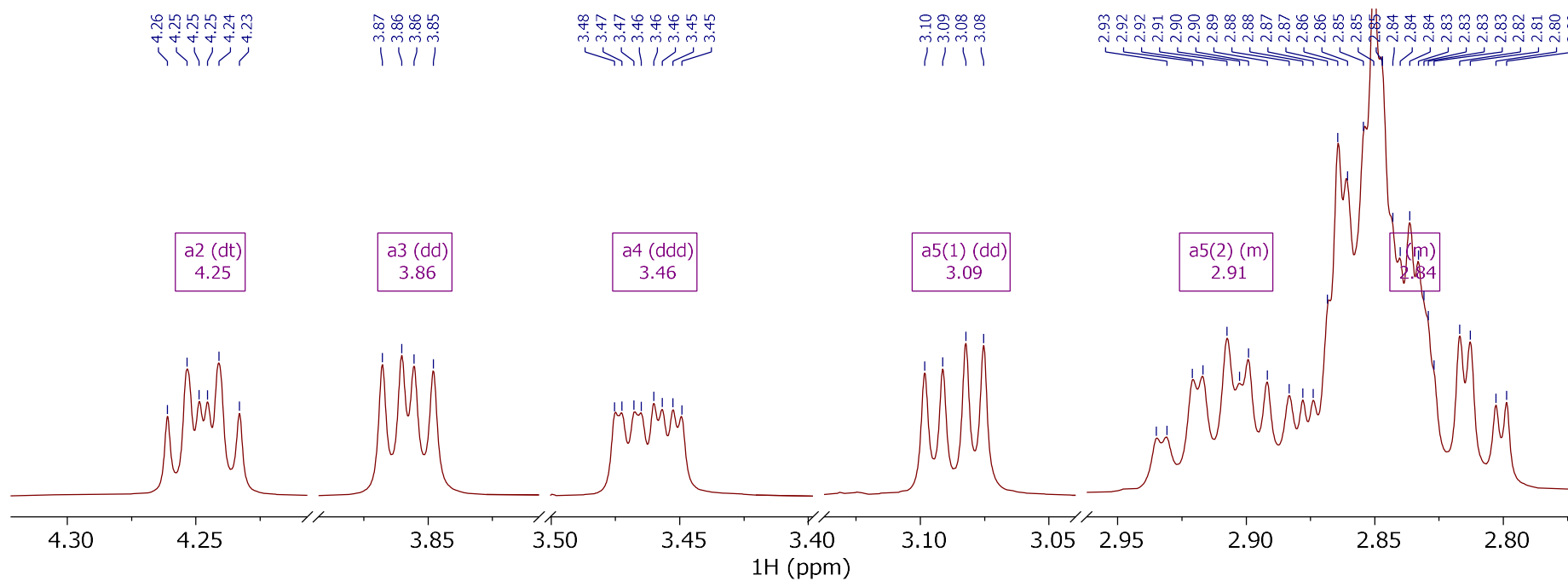


Figure S19. Fragment of ^1H NMR spectra showing biotin monomer's thiolane motif protons of (-)-mixHC[8] in range of 2.87-4.26 ppm.

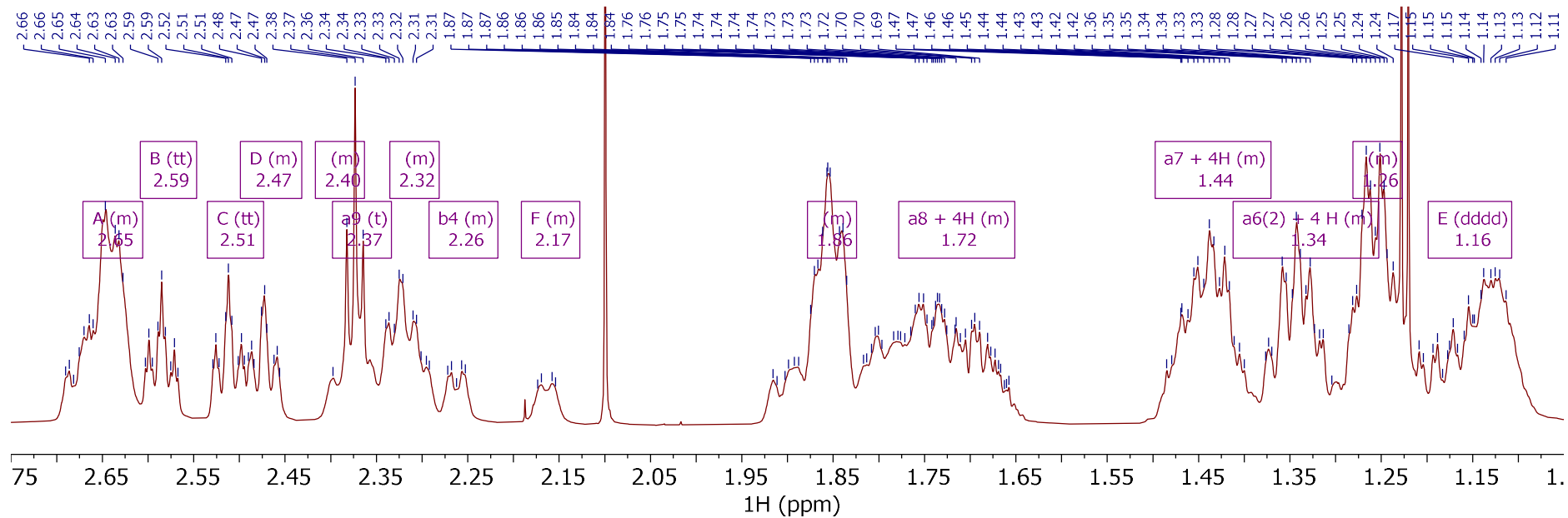


Figure S20. Fragment of the ^1H NMR spectra of $(-)\text{-mixHC[8]}$ including cyclohexane unit and biotin aliphatic chain protons in range of 1.11-2.66 ppm.

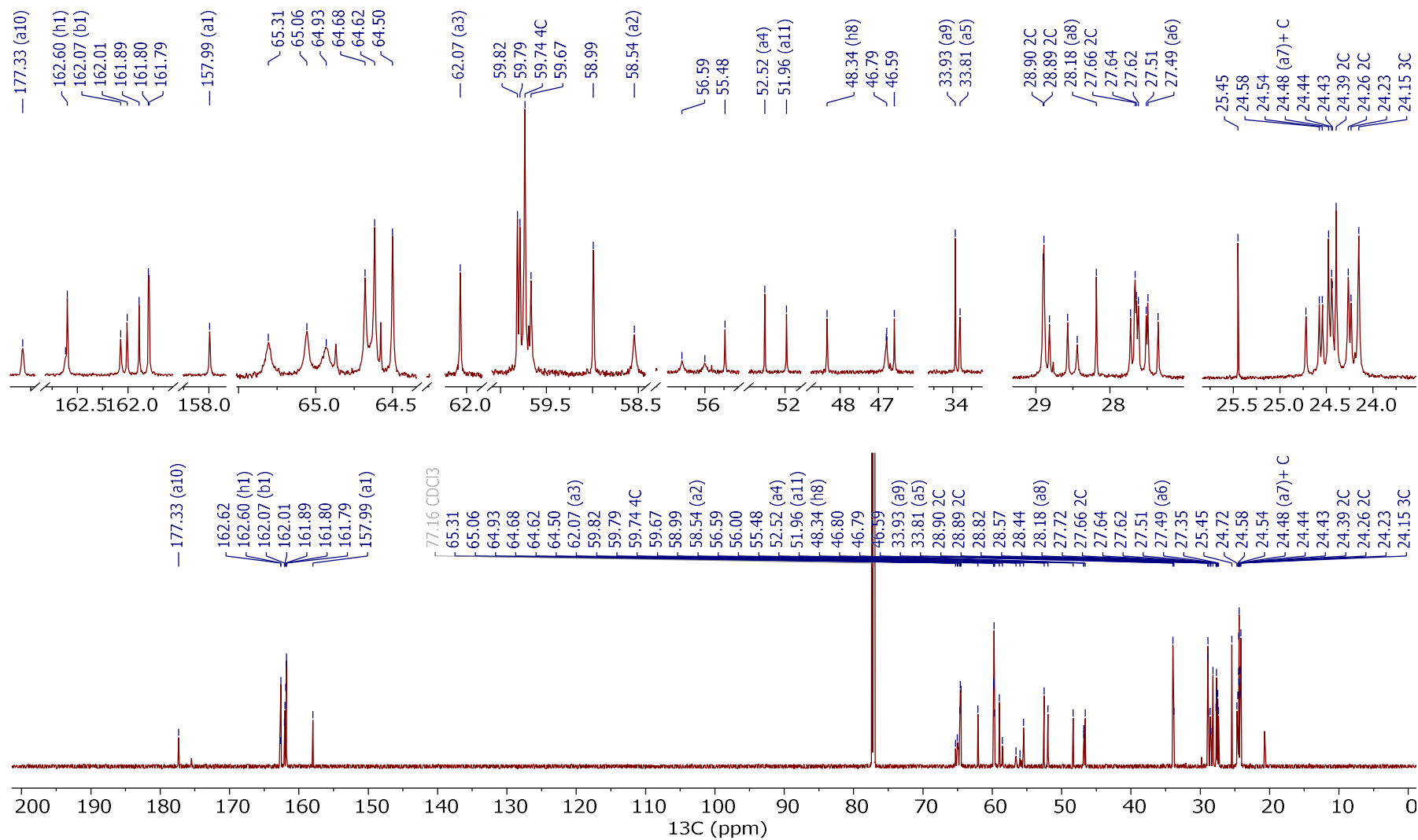


Figure S21. The ^{13}C NMR spectra from (-)-mixHC[8], the full spectra is at the bottom and zoomed in regions are at the top.

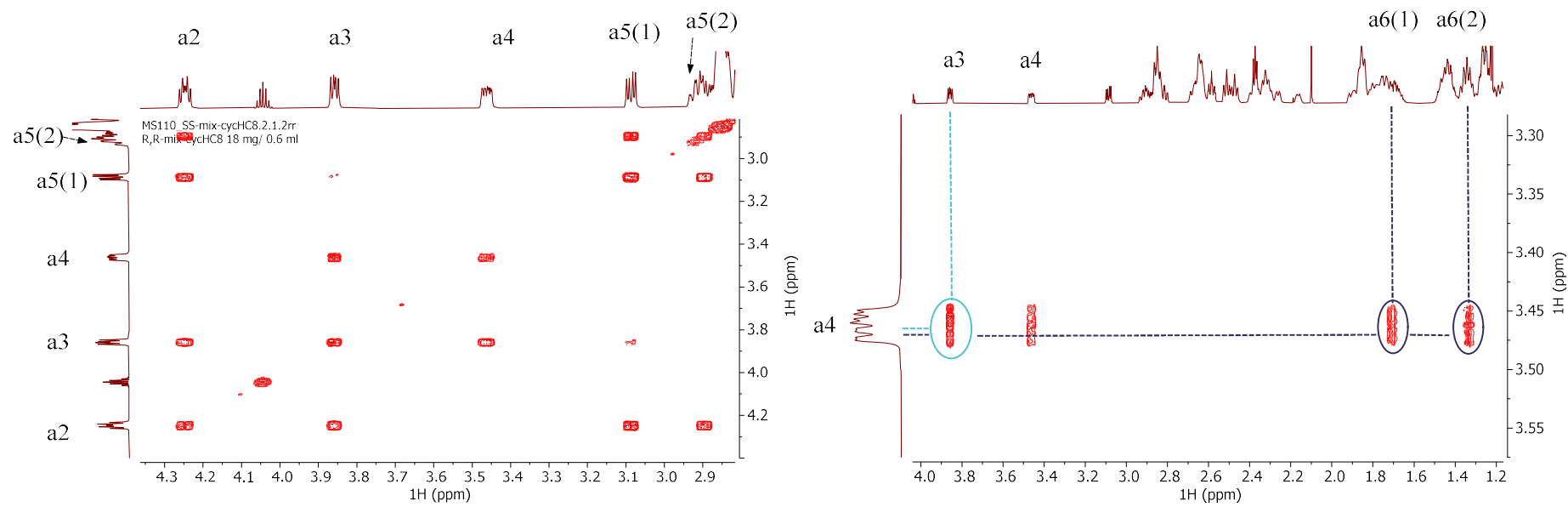


Figure S22. On the left: part of COSY spectrum, indicating neighbouring hydrogens in biotin monomer thiolane structure in (–)-mixHC[8]. On the right: part of COSY spectrum, showing the correlation between a proton in biotin thiolane motif (a4) with protons in biotin side chain (a6) in (–)-mixHC[8].

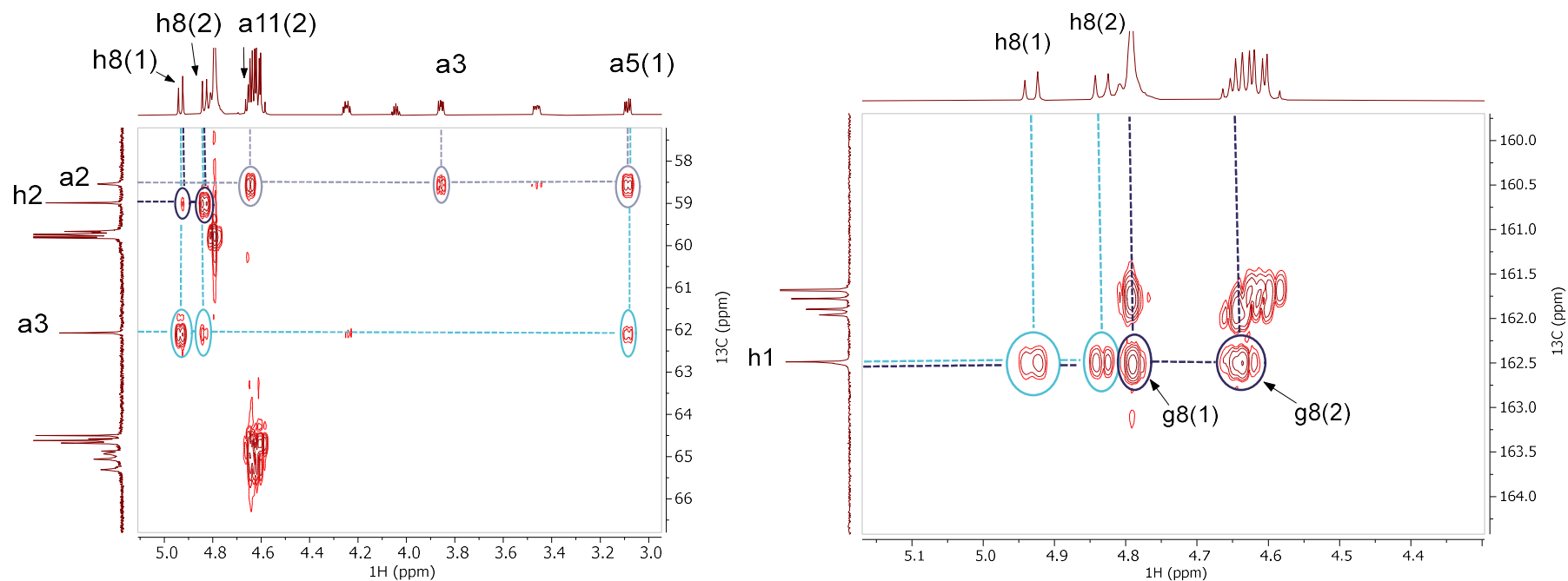


Figure S23. On the left: part of HMBC spectra, indicating the correlations between h8 bridge protons to a3 and h2 carbon, and a2 carbon correlation to a11(2) bridge proton, a3 proton and a5(1) proton in biotin monomer in (–)-mixHC[8], also it is seen a3 carbon correlation to a5(1) proton. On the right: part of HMBC spectra showing the correlation between h1 carbonyl carbon to h8 bridge protons and the correlation with g8 bridge protons in (–)-mixHC[8].

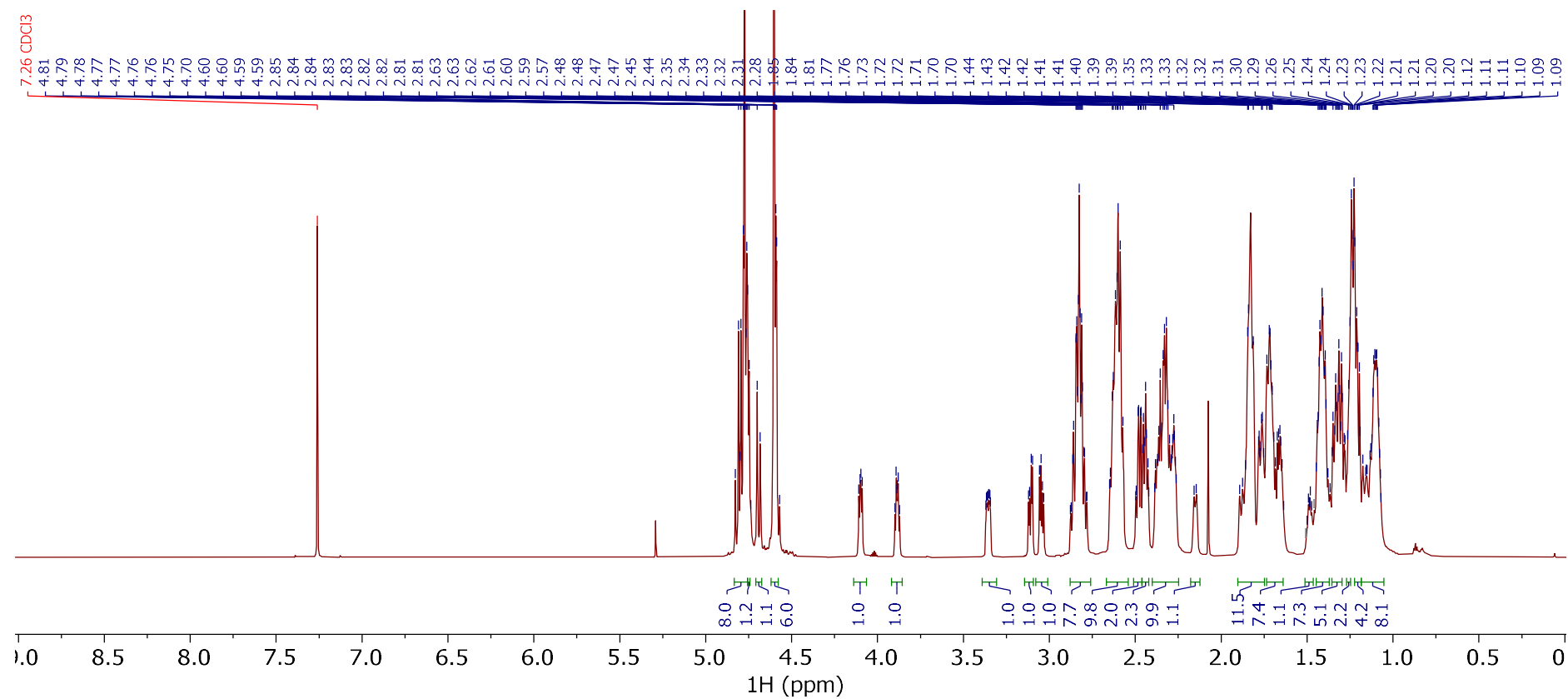


Figure S24. The full ^1H NMR spectra from (+)-mixHC[8].

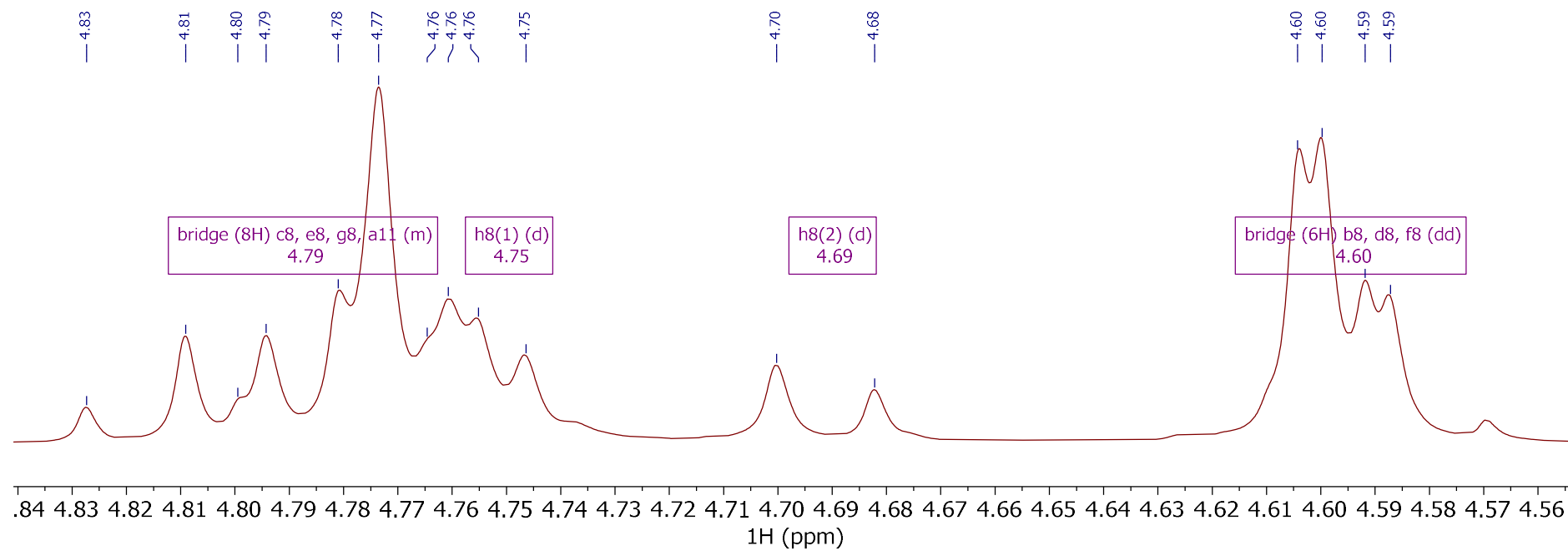


Figure S25. Fragment of ^1H NMR spectra showing bridge protons of (+)-mixHC[8] in range of 4.59-4.83 ppm.

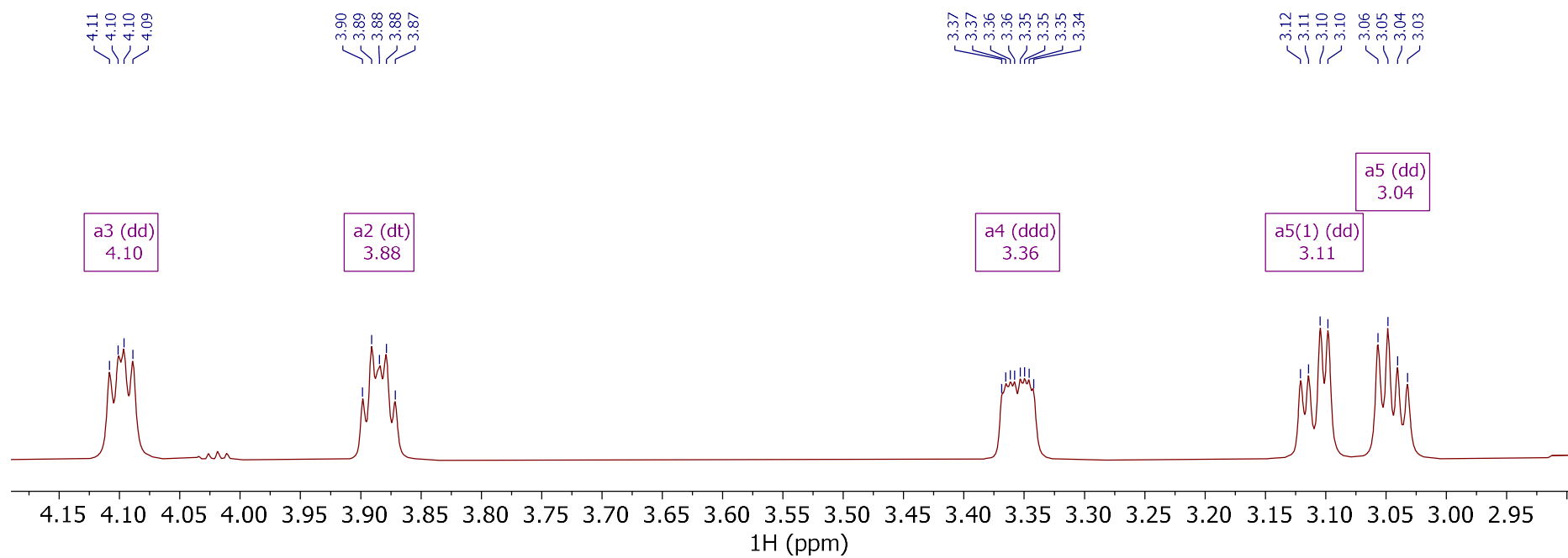


Figure S26. Fragment of ^1H NMR spectra showing biotin monomer's thiolane motif protons of (+)-mixHC[8] in range of 3.03-4.11 ppm.

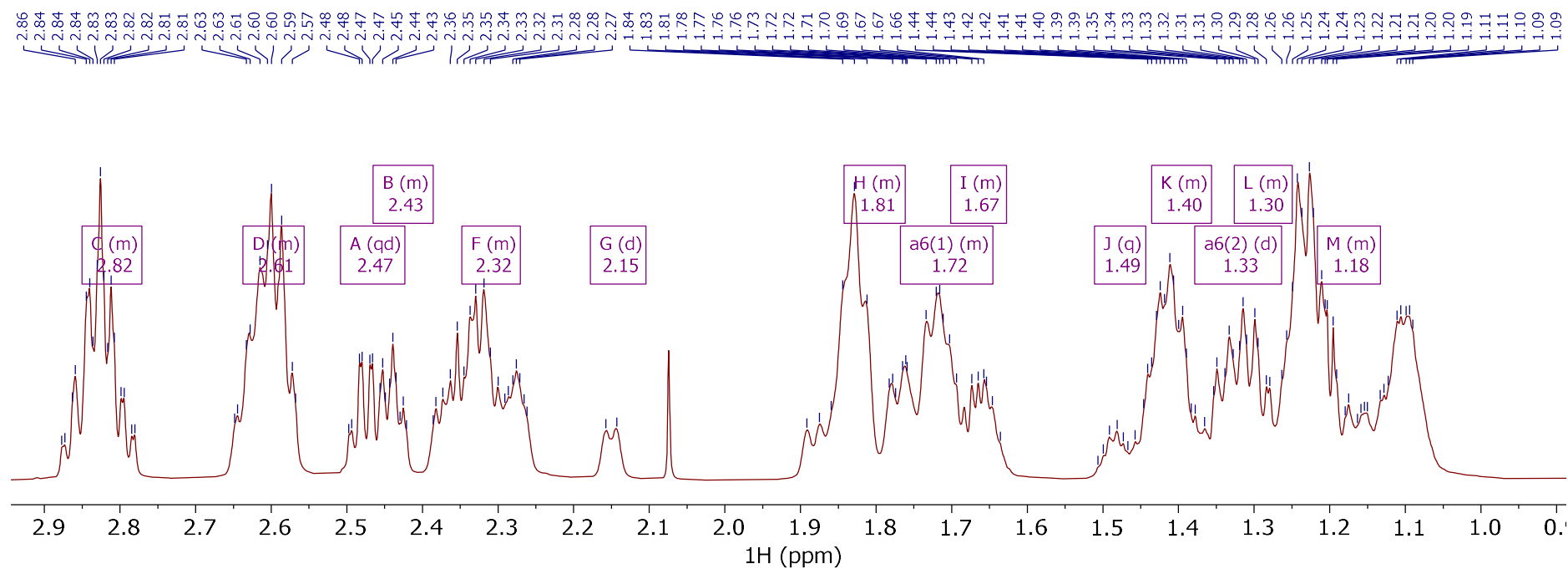


Figure S27. Fragment of ^1H NMR spectra of (+)-mixHC[8] including cyclohexane unit and biotin aliphatic chain protons in range of 1.09-2.86 ppm.

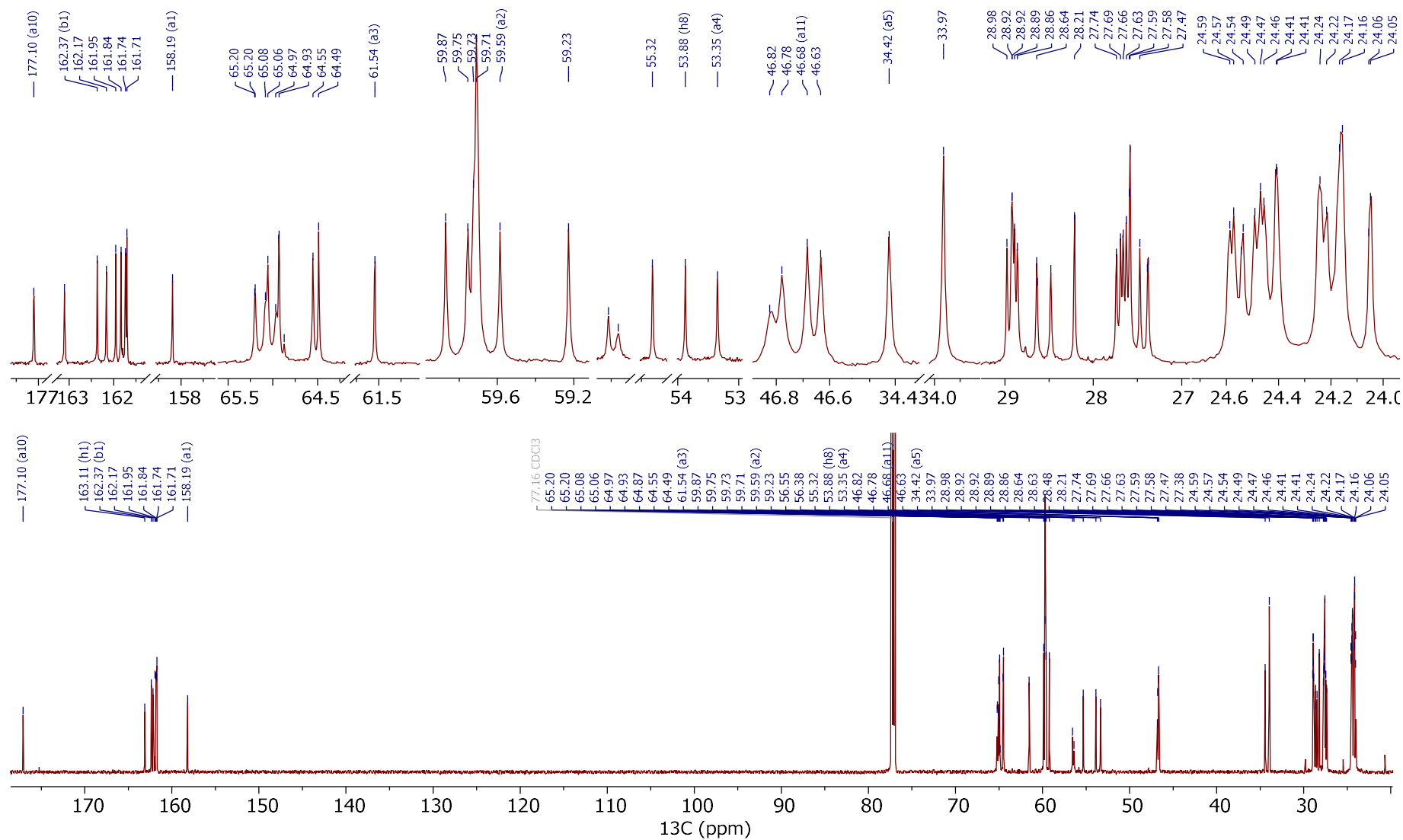


Figure S28. The ^{13}C NMR spectra from (+)-mixHC[8], the full spectra is at the bottom and zoomed in regions are at the top.

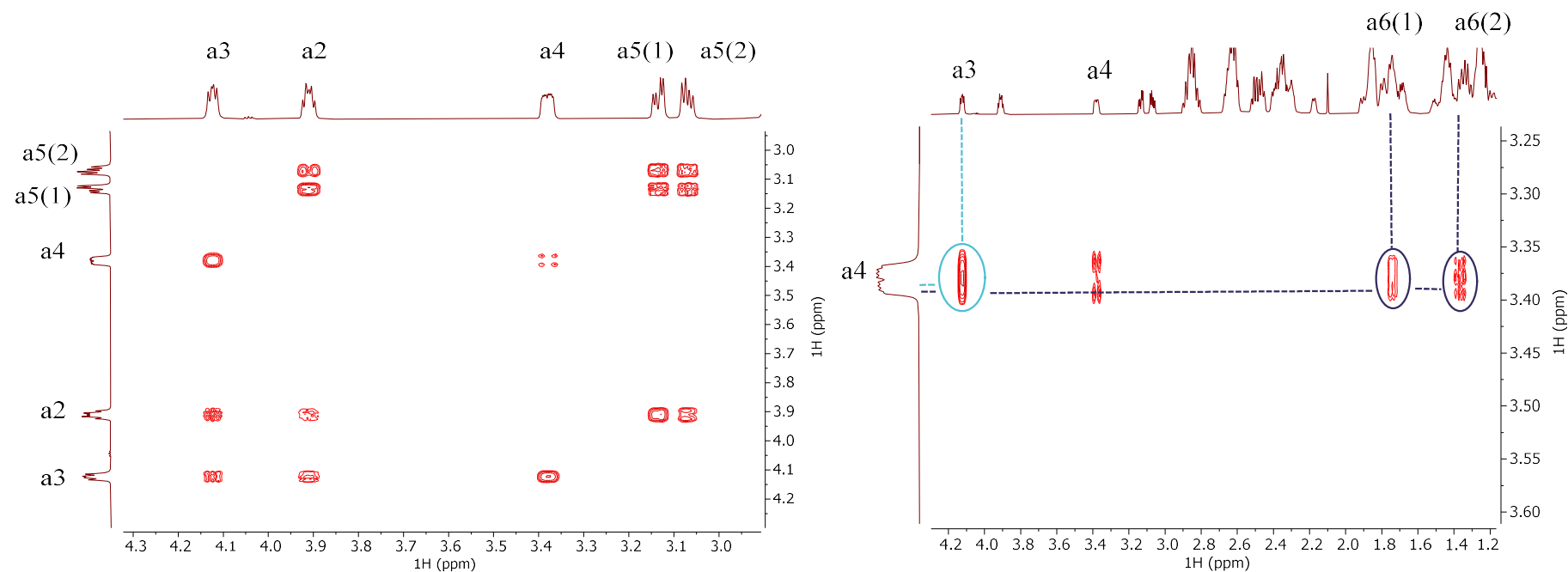


Figure S29. On the left: part of COSY spectrum, indicating neighbouring hydrogens in biotin monomer thiolane structure in (+)-mixHC[8]. On the right: part of COSY spectrum, showing the correlation between a proton in biotin thiolane motif (a4) with protons in biotin side chain (a6) in (+)-mixHC[8].

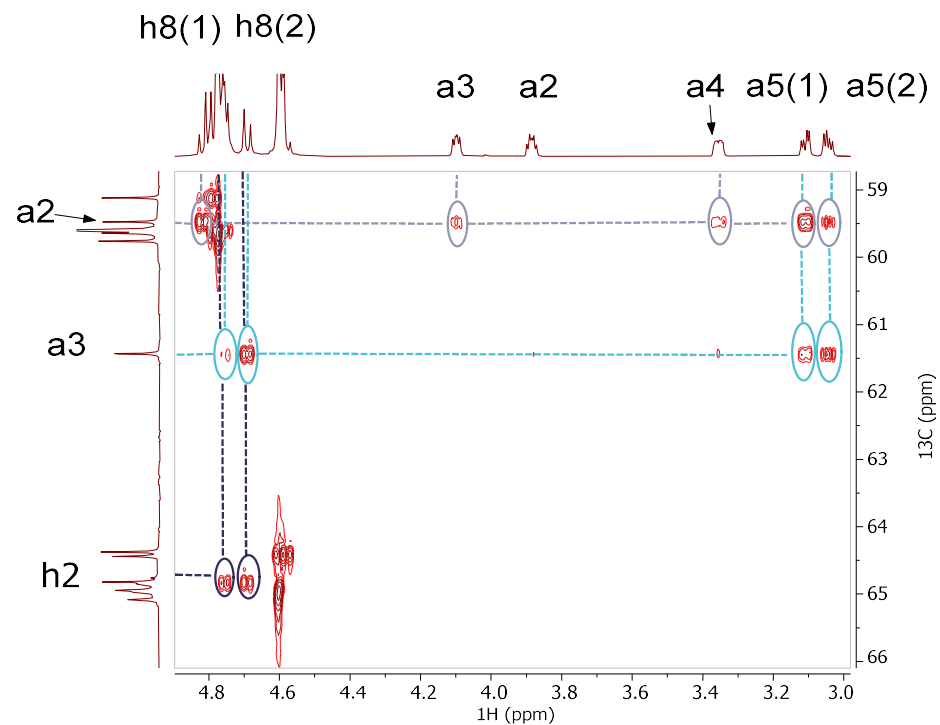


Figure S30. Part of HMBC spectra, indicating the correlations between a3 carbon to h8 bridge protons, a2 , a4 and to both a5 protons in biotin monomer in (+)-mixHC[8]; here it is also shown the correlation between h8 bridge protons and h2 carbon and finally a2 carbon correlation to a3 , a4 and to both a5 protons.

3.2 IR spectra

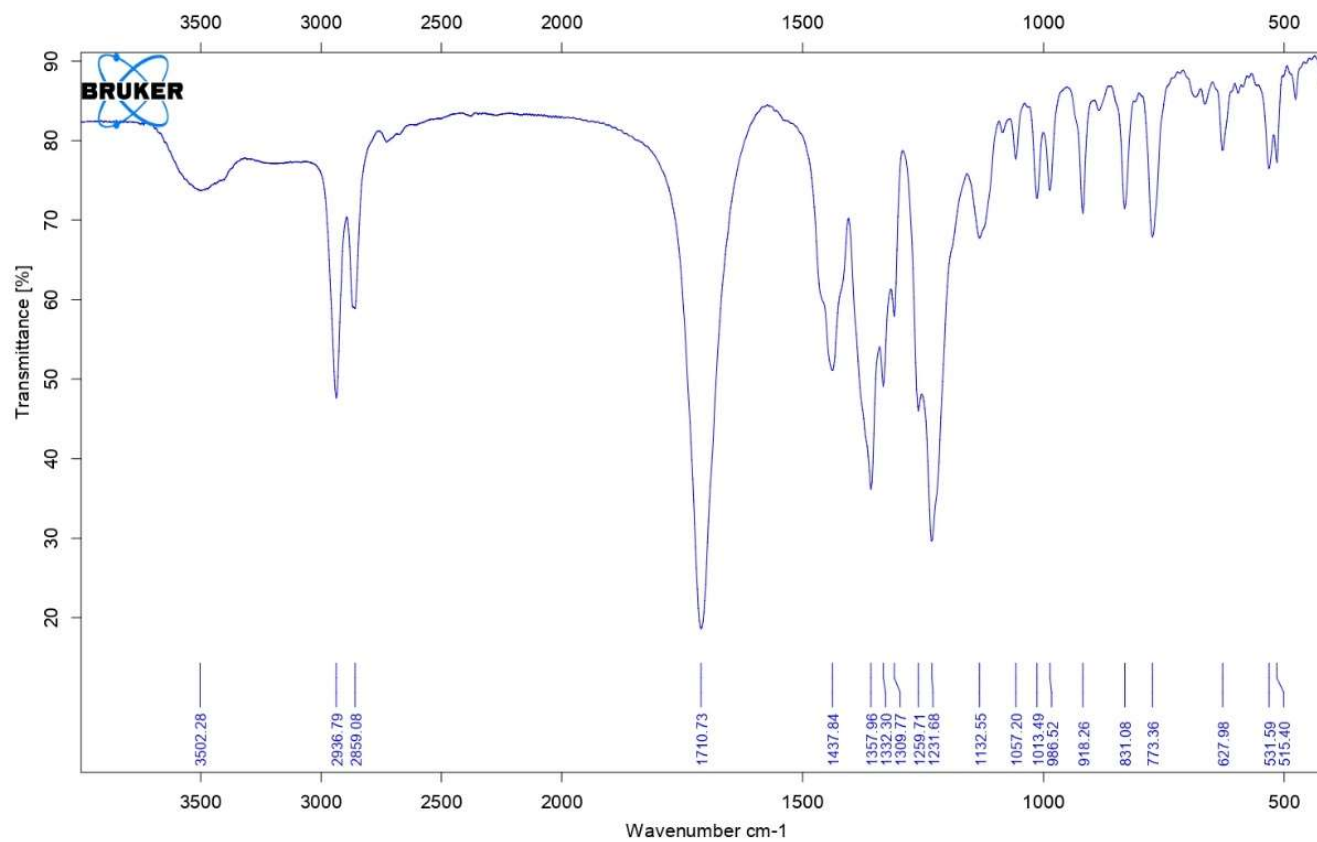


Figure S31. IR spectrum of (+)-mixHC[8].

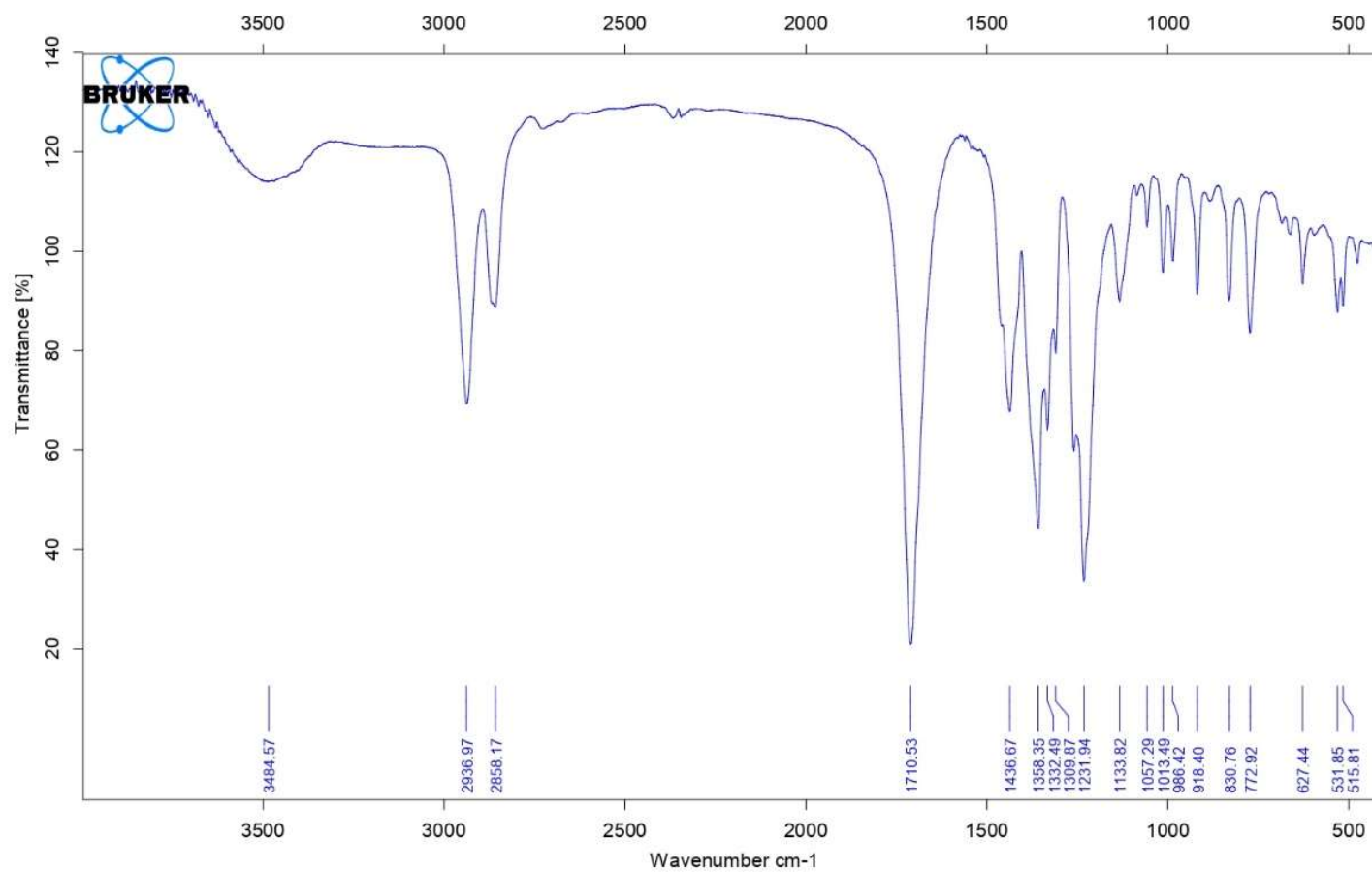


Figure S32. IR spectrum of (-)-mixHC[8].

4. Single Crystal X-ray Diffraction Analysis

General remarks

Single crystal X-ray diffraction data was collected at 120 K using a Rigaku XtaLAB Synergy-R diffractometer with a HyPix-Arc 100 detector using mirror-monochromated Cu-K α ($\lambda = 1.54184$ Å) radiation. The data was solved by intrinsic phasing (SHELXT)⁹ and refined by full-matrix least squares on F^2 using Olex2¹⁰, utilising the SHELXL module⁹. Anisotropic displacement parameters were assigned to non-H atoms and isotropic displacement parameters for all H atoms were constrained to multiples of the equivalent displacement parameters of their parent atoms with $U_{\text{iso}}(\text{H}) = 1.2 U_{\text{eq}}(\text{methylene, methine})$ or $U_{\text{iso}}(\text{H}) = 1.5 U_{\text{eq}}(\text{methyl, hydroxy})$ of their respective parent atoms. The crystallographic data is deposited with the Cambridge Crystallographic Data Centre (CCDC 2251913) and can be obtained free of charge from The Cambridge Crystallographic Data Centre via www.ccdc.cam.ac.uk/data_request/cif.

Crystallographic details for TBA(PF₆⁻@(-)-((S,S,R)(R,R)7)-mixHC[8]) as a 1:1 co-crystal with TBA(PF₆⁻@cycHC[8])

[C₁₆H₃₆N][C₆₇H₁₀₀N₁₆O₁₀S][PF₆] \cdot [C₁₆H₃₆N][C₆₄H₉₆N₁₆O₈][PF₆]: Single crystals of the complex were obtained from a methanol solution of (-)-((S,S,R)(R,R)7)-mixHC[8] with twofold excess of TBAPF₆ by slow evaporation of the solvent. The resulting crystals were found to be of an inclusion complex of the PF₆⁻ in a 1:1 co-crystal of (-)-((S,S,R)(R,R)7)-mixHC[8] and cycHC[8].

C₁₆₃H₂₆₈F₁₂N₃₄O₁₈P₂S, $M = 3314.10 \text{ g mol}^{-1}$, colorless plates, $0.06 \times 0.09 \times 0.14$, orthorhombic, $P2_12_12_1$, $a = 20.2233(2) \text{ Å}$, $b = 20.5002(2) \text{ Å}$, $c = 20.7796(2) \text{ Å}$, $V = 8614.84(15) \text{ Å}^3$, $Z = 2$, Cu-K α radiation ($\lambda = 1.54184 \text{ Å}$), $T = 120.0(1) \text{ K}$, $\mu(\text{Cu-K}\alpha) = 1.04 \text{ mm}^{-1}$, 17604 reflections measured ($6.032^\circ \leq 2\theta \leq 148.476^\circ$), $R_{\text{int}} = 0.098$, 1273 parameters, 394 restraints, $S = 1.00$, $0.58 < d\rho < -0.29 \text{ e Å}^{-3}$, $R_1[F^2 > 2\sigma(F^2)] = 0.083$, $wR_2(\text{all data}) = 0.238$, Flack = 0.015(10).

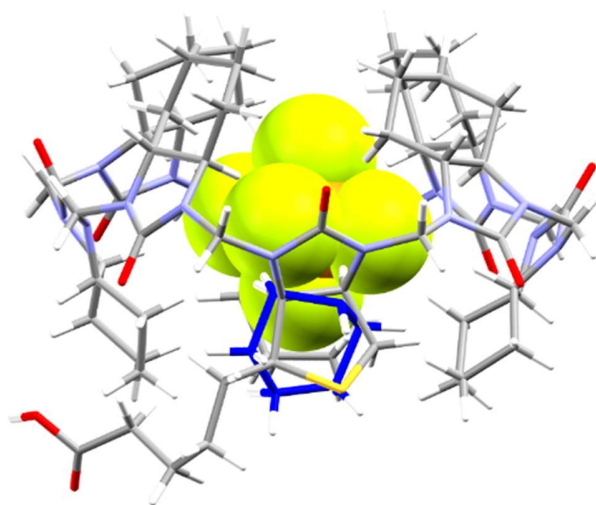


Figure S33. Crystal structure of a co-crystal with the cycHC[8] and $(-)-((S,S,R)(R,R)_7)$ -mixHC[8] with the 50:50 disorder of the cyclohexyl and biotin 5-membered ring (cyclohexyl unit is coloured blue for clarity)

Additionally, the TBA salt of ClO_4^- , as well as Ag^+ , K^+ , and Na^+ salts of PF_6^- were screened; however, only the TBA salt of PF_6^- yielded single crystals. Crystallizations were also set up with $(+)-((S,S,R)(S,S)_7)$ -mixHC[8], yet, crystals did not form under any of the conditions used.

Single-crystal XRD analysis unambiguously revealed that we obtained a crystal structure of a 1:1 co-crystal of $(-)-((S,S,R)(R,R)_7)$ -mixHC[8] and cycHC[8], modelled with overlapping hosts of the co-crystal with 50:50 disorder of the biotin 5-membered ring and one of the cyclohexyl groups (and shared TBA/ PF_6 positions). The identity of the co-crystal was established through examination of the electron density with respect to the biotin sulfur atom, which was only observed in the exo conformation. The occupancies of the disordered biotin 5-membered ring and a cyclohexyl group were refined as a group using a single free variable (with total occupancy of 100%), then manually rounded to the nearest integer for ease of reporting. No other significant residual electron density in a feasible position to be the sulfur atom of further disordered biotin groups (in either exo or endo conformations) was identified in the final model. Although the crystallisations were set using 88% (by NMR) pure $(-)-((S,S,R)(R,R)_7)$ -mixHC[8], cycHC[8] happened to be present as a minor additive. The composition of the SC-XRD model was confirmed by HPLC analysis (Figure S57), which showed that a dissolved crystal contains 96.7% of $(-)-((S,S,R)(R,R)_7)$ -mixHC[8] and 2% of cycHC[8]. The latter was sufficient for spontaneous co-crystallisation to occur.

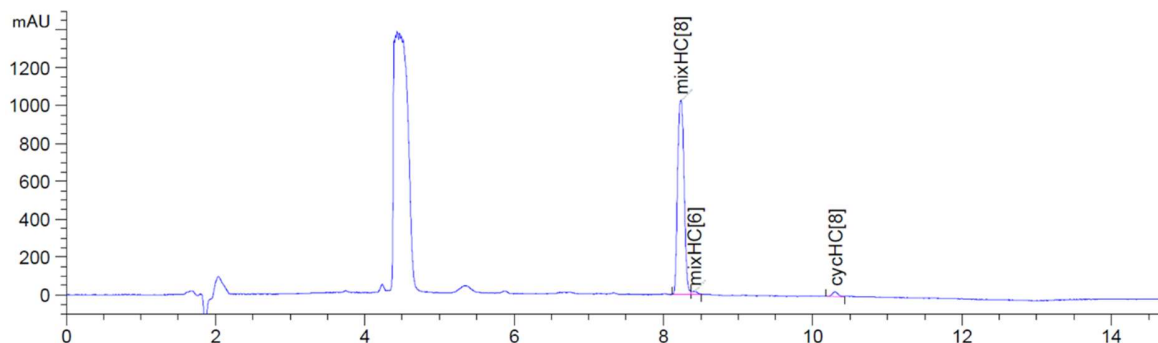


Figure S34. HPLC-UV chromatogram (210 nm) of the sample used for crystallization.

Measured crystal structure was compared to DFT calculated one by overlaying two structures using Mercury program (Figure S58). Molecular overlay verifies the thiolane envelope to be pointing outwards from the cavity with only minor differences in spatial arrangement.

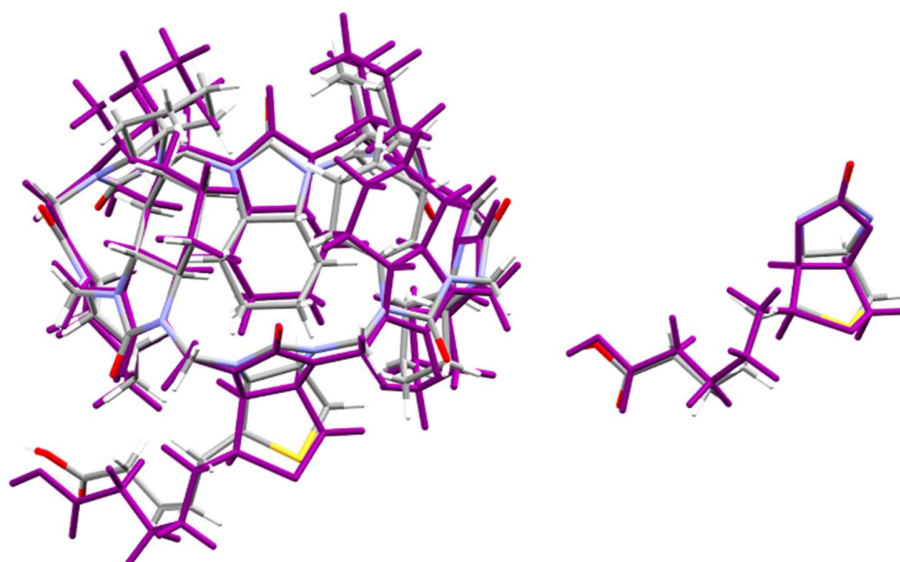


Figure S35. Overlay of SC-XRD and DFT calculation of inclusion complex (left) and closer overlay of biotin thiolane unit (right) (cyclohexyl unit, TBA and PF_6^- are omitted for clarity, DFT calculated structure is presented in purple).

Besides overlaying the structures of the obtained crystal structure and DFT calculated one, measured crystal structure was overlaid with crystal structure of regular cycHC[8] with PF_6^- to visualize the differences or similarities between those two inclusion complexes (Figure S59). Solvent molecules and cation were omitted from molecular overlay for clarity. PF_6^- was taken as center to overlay the structures. As seen, two structures are almost identical in their spatial arrangement.

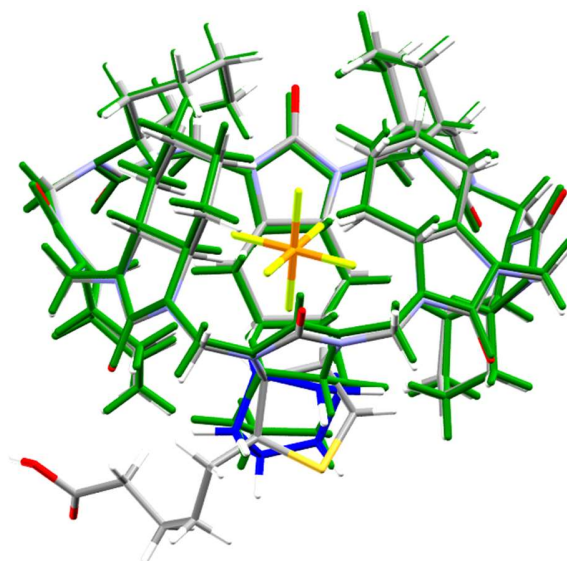


Figure S36. Overlay of SC-XRD of regular cycHC[8] with PF_6^- and $(-)-((S,S,R)(R,R)_7)\text{-mixHC[8]}$ with PF_6^- inclusion complexes (regular cycHC[8] is presented in green).

Analysis of Hirshfeld surfaces and host-guest interactions

Hirshfeld surface analysis was performed to analyze close contacts or intermolecular interactions between moieties present in crystal structure¹¹. This tool generates a surface around a molecule, where its electron density exceeds that from all the neighboring molecules, helping define the space that the molecule is occupying in the crystal. In this work analysis was used to investigate Hirshfeld surface of PF_6^- anion which occupies the cavity of macrocycle. The program CrystalExplorer¹² was used to generate the Hirshfeld surfaces and to highlight the close contacts between the anion and the neighboring host molecule ($\text{C-H}\cdots\text{anion}$). The surfaces were mapped with d_{norm} where a red spot signifies areas with $d(\text{D-H}\cdots\text{A}) \leq \sum r(\text{vdW})[\text{H}, \text{A}]$.

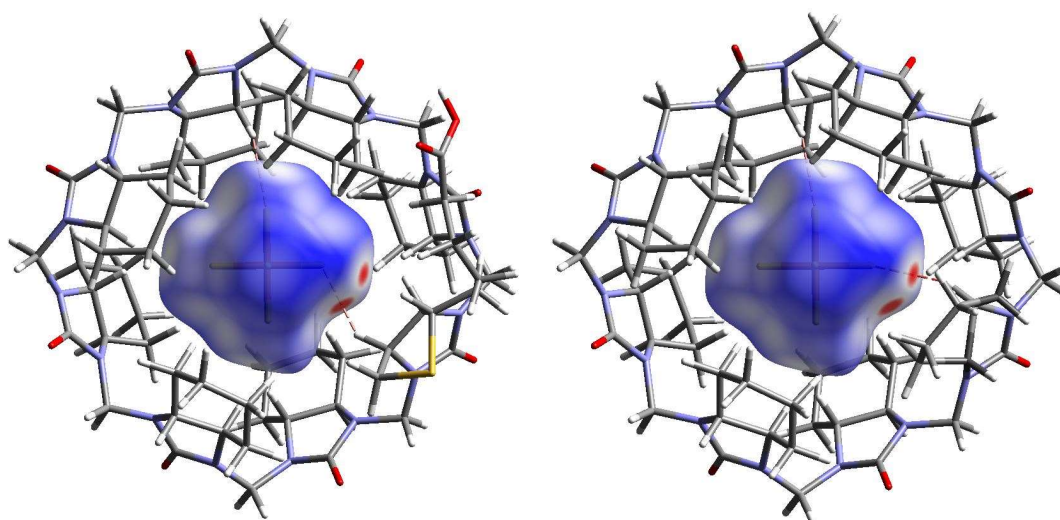


Figure S37. Hirshfeld surface for the encapsulated PF_6^- anion, mapped with d_{norm} over the range -0.1 to 1.0 . Close contacts where $d(\text{DH}\cdots\text{F})$ is shorter than $\sum r(\text{vdW})[\text{H}, \text{A}]$ are displayed with a dashed line. Hirshfeld surface for PF_6^- anion with biotin 5-membered ring as monomeric unit (left) and Hirshfeld surface for PF_6^- anion with cyclohexyl ring as monomeric unit (right)

Shortest distances between the host molecule and the encapsulated anion were investigated using Mercury, the result of which is shown in Tables S21–22. Distances shorter than the sum of van der Waals radii of hydrogen and the acceptor atom $\sum r(\text{vdW})[\text{H}, \text{A}]$ are marked in black, as they indicate influential host-guest interactions.

Hexafluorophosphate (PF₆⁻) – close contacts within PF₆⁻@(-)-((*S,S,R*)(*R,R*)7)-*mixHC*[8], with monomeric unit D being biotin 5-membered ring

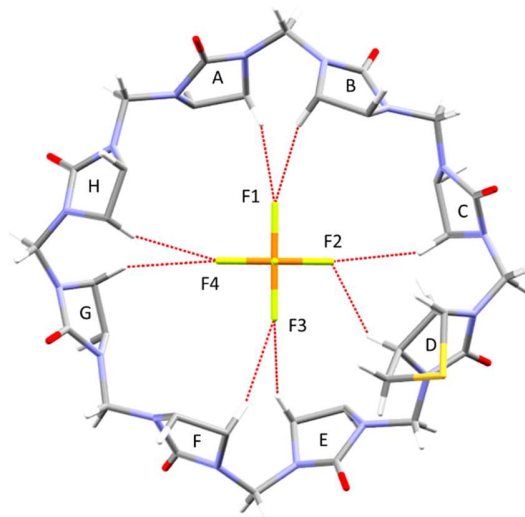


Figure S38. Close contacts within PF₆⁻@(-)-((*S,S,R*)(*R,R*)7)-*mixHC*[8]. (CH₂)₄ groups are omitted for clarity, atoms involved in equalent monomeric units are denoted with suffixes A-H. Monomeric unit D is biotin 5-membered ring.

Table S19. Shortest $d(\text{D-H}\cdots\text{A})$ distances from the crystal structure of ***TBA*(PF₆⁻@(-)-((*S,S,R*)(*R,R*)7)-*mixHC*[8]))**, between the encapsulated PF₆⁻ and the host.

D–H \cdots A	$d(\text{H}\cdots\text{A})$, Å	$\text{D}(\text{H}\cdots\text{A}) - \sum r(\text{vdW})[\text{H}, \text{A}]$, Å
C2A–H2A\cdotsF1	2.53	-0.03
C2B–H2B \cdots F1	2.61	0.05
C2C–H2C \cdots F2	2.81	0.25
C2D–H2D\cdotsF2	2.45	-0.11
C2E–H2E \cdots F3	2.63	0.07
C2F–H2F \cdots F3	2.64	0.08
C2G–H2G \cdots F3	2.92	0.36
C2H–H2H \cdots F3	2.67	0.11

Hexafluorophosphate (PF_6^-) – close contacts within $\text{PF}_6^-@(-)-((S,S,R)(R,R)7)\text{-mixHC}[8]$, with monomeric unit D being cyclohexyl ring

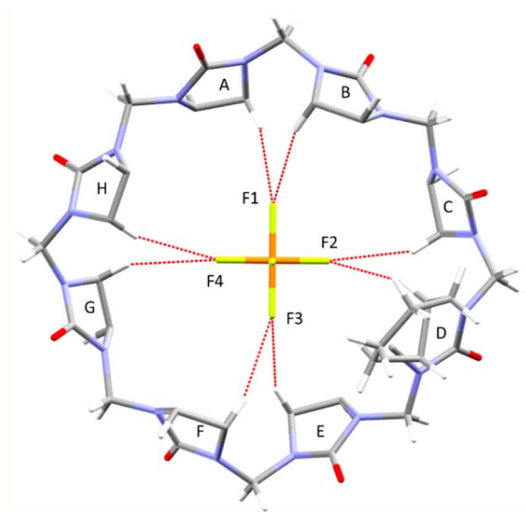


Figure S39. Close contacts within $\text{PF}_6^-@(-)-((S,S,R)(R,R)7)\text{-mixHC}[8]$. $(\text{CH}_2)_4$ groups are omitted for clarity, atoms involved in equalent monomeric units are denoted with suffixes A-H. Monomeric unit D is cyclohexyl ring.

Table S20. Shortest $d(\text{D-H}\cdots\text{A})$ distances from the crystal structure of $\text{TBA}(\text{PF}_6^-@(-)-((S,S,R)(R,R)7)\text{-mixHC}[8])$, between the encapsulated PF_6^- and the host.

$\text{D-H}\cdots\text{A}$	$d(\text{H}\cdots\text{A}), \text{\AA}$	$\text{D}(\text{H}\cdots\text{A}) - \sum r(\text{vdW})[\text{H}, \text{A}], \text{\AA}$
C2A–H2A...F1	2.53	-0.03
C2B–H2B...F1	2.61	0.05
C2C–H2C...F2	2.81	0.25
C2D–H2D...F2	2.50	-0.06
C2E–H2E...F3	2.63	0.07
C2F–H2F...F3	2.64	0.08
C2G–H2G...F3	2.92	0.36
C2H–H2H...F3	2.67	0.11

5. The Computational Study

5.1 Methods

The geometries for (+)-((*S,S,R*)(*S,S*)₇)-mixHC[8] and (–)-((*S,S,R*)(*R,R*)₇)-mixHC[8] were drawn using Chem3D 18.2. The Density Functional Theory (DFT) method used to optimize the geometries was the B3LYP exchange-correlation functional^{13–17} with a 6-31G** basis set^{18–20}. The energy values of the local minima were refined by single point calculations with the inclusion of the Grimme's D3 empirical dispersion correction²¹. Atomic configuration was allowed to relax until the remaining atomic forces reached below 5×10^{-2} eVÅ^{–1}. Calculations were performed with the Gaussian16 program package.²²

5.2 Results

Two conformers were found for both (+)-((*S,S,R*)(*S,S*)₇)-mixHC[8] and (–)-((*S,S,R*)(*R,R*)₇)-mixHC[8] by studying the potential energy surface of the thiolane ring (Figure S64). The conformers had either the sulfur atom in biotin oriented towards the inside or the outside the macrocycle. The relative energy values for the conformers are listed in Table 1. For (+)-((*S,S,R*)(*S,S*)₇)-mixHC[8], the experimentally determined crystal structure was in close agreement with the DFT calculated structure, where the sulfur atom is oriented towards outside the macrocycle. Currently no crystal structure for (–)-((*S,S,R*)(*R,R*)₇)-mixHC[8] have been reported. It should be noted that the differences in the energy of the two conformations (the differences in the sulfur atom orientation) are negligible and the geometry seen in the crystal structure is probably favored due to crystal packing forces, solvent effects, and the guest molecule during crystallization. See optimized geometries as XYZ format files in Data S2.

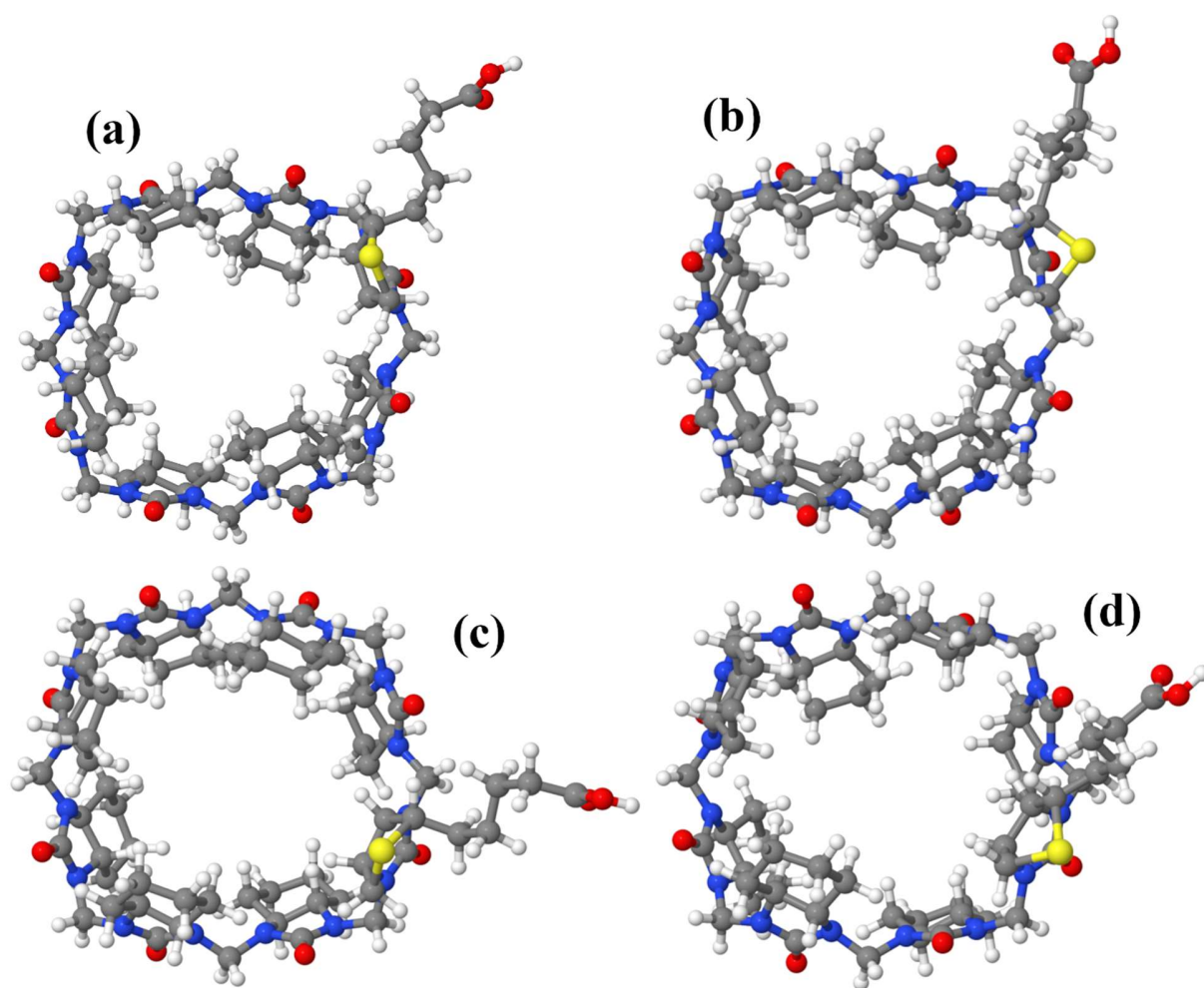


Figure S40. The found conformers: (a) the (-)-mixHC[8] conformer with the sulfur atom oriented towards the centre of the macrocycle, (b) the (-)-mixHC[8] conformer with the sulfur atom oriented towards outside of the macrocycle, (c) the (+)-mixHC[8] conformer with the sulfur atom oriented towards the centre of the macrocycle, (d) the (+)-mixHC[8] conformer with the sulfur atom oriented towards outside of the macrocycle.

Table S21. The relative energies values for the mixHC[8] conformers.

	Sulfur atom oriented towards inside of the macrocycle, ΔE (kJ/mol)	Sulfur atom oriented towards outside of the macrocycle, ΔE (kJ/mol)
(+)-((S,S,R)(S,S) ₇)- mixHC[8]	0.67	0.26
(-)-((S,S,R)(R,R) ₇)- mixHC[8]	0.00	0.28

Table S22. The relative energies values for the PF₆⁻@mixHC[8] conformers.

	Sulfur atom oriented towards inside of the macrocycle, ΔE (kJ/mol)	Sulfur atom oriented towards outside of the macrocycle, ΔE (kJ/mol)
PF ₆ ⁻ @(+)-((S,S,R)(S,S) ₇)- mixHC[8]	11.70	3.50
PF ₆ ⁻ @(-)-((S,S,R)(R,R) ₇)- mixHC[8]	2.10	0.00

4.3 Comparing the Calculated Structure to the Crystal Structure

Previously published results for cyclohexanohemicucurbiturils have shown that the position of the cyclohexyl rings is quite variable and depends on the guest molecule.²³ Furthermore, the structure of the cyclohexyl rings is influenced by the packing forces during crystallization. Thus, in the following study we are comparing structure features such as distances between atoms and angles between bonds, which do not vary due to the aforementioned reasons. The bond lengths (Table 2), which are of interest are the bonds between the carbonyl carbon atom and the nitrogen atom of the monomer, and the bonds between the nitrogen atom of the monomer and the carbon atom of the bridge (–CH₂–). These two bond types also form the angles which will be measured. The angles, however, are not equal as the angles, which are aligned with the fluorine atoms of the PF₆⁻ are more obtuse than the angles, which do not align with the fluorine atoms.

Table S23. The bond lengths of interest. The numbers with the green background show the average bond length.

O=C–N		N–CH ₂	
Crystal Structure	Calculated Structure	Crystal Structure	Calculated Structure
1.339	1.384	1.455	1.453
1.361	1.375	1.469	1.442
1.347	1.398	1.460	1.457
1.36	1.387	1.409	1.453
1.370	1.391	1.421	1.452
1.356	1.394	1.451	1.453
1.384	1.394	1.405	1.451
1.335	1.391	1.454	1.454
1.357	1.391	1.466	1.453
1.386	1.393	1.442	1.452
1.360	1.394	1.433	1.452
1.378	1.390	1.460	1.453
1.361	1.390	1.423	1.454
1.370	1.395	1.435	1.452
1.381	1.394	1.458	1.452
1.387	1.389	1.431	1.451
1.365	1.391	1.442	1.452

The standard deviation values for the O=C–N and the C–CH₂ bond lengths in the crystal structure is 0.020 and 0.016 Å, respectively. The standard deviation values for the same bonds in the calculated structure are 0.003 and 0.005 Å, respectively. The absolute differences between the average bond length for the O=C–N and the C–CH₂ bonds in the crystal and calculated structures were 0.010 and 0.026 Å, respectively.

Table S24. The angles between angles of interest. The numbers with the green background show the average angle value.

O=C–N–CH ₂ (More Obtuse)		O=C–N–CH ₂	
Crystal Structure	Calculated Structure	Crystal Structure	Calculated Structure
115.84	116.20	111.41	114.20
115.19	116.70	111.05	113.80
115.67	116.60	112.20	113.80
115.20	116.60	112.27	113.90
115.48	116.53	111.73	113.93

The absolute differences between the crystal and calculated structures for the more and less obtuse angles were 1.05° and 2.19°, respectively. The difference in the less obtuse angle is small, but noticeable and is most likely caused by the guest, PF₆[−], which forces the structure to contract; thus, reducing the aforementioned “less obtuse” angles.

The overall (meaningful) structural features between the calculated and the crystal structure of the mixHC[8] remain analogous and the differences are likely due to the guest structure and packing forces of the crystal structure. These results indicate that the structure of the mixHC[8] does not vary much in different media nor with different guests (with the exception of the aforementioned cyclohexyl rings, which are known to be flexible). Furthermore, the methods used can be considered suitable for predicting structures for cyclohexanohemicucurbiturils in the future.

Optimized geometry of (-)-((*S,S,R*)(*R,R*)₇)-mixHC[8] sulfur atom oriented towards inside:

194				C	1.04520	-4.74195	-1.08629	H	0.55164	-3.84612	3.39652
E(au) = -4640.58481258				C	-3.06021	-5.23019	2.92310	H	3.90654	-0.20621	4.42376
C	-2.20282	3.41552	-2.94085	C	-4.06930	3.09696	2.06072	H	4.02015	-1.89646	4.93870
H	3.08164	1.81681	-0.54419	C	-0.45129	-4.96982	-1.31071	H	1.58850	-5.61780	-1.48669
C	-4.53445	-4.00508	1.31412	C	1.28863	3.67195	4.66550	H	-2.09491	-5.72038	3.07553
C	5.81785	0.00681	-1.31042	C	1.52188	-3.51424	-1.85167	H	-3.85126	-5.97109	3.09599
C	-5.12963	3.22174	0.97419	C	-1.32763	3.58863	-4.20428	H	-3.54161	4.04512	2.20774
C	3.19806	-1.64348	2.95714	C	-4.63309	-2.74007	2.15703	H	-3.32426	2.34627	1.76788
C	-5.83544	1.88199	0.75392	C	-4.40956	-0.00428	-4.74355	H	-0.97656	-0.41475	-1.13410
C	0.87859	4.83324	2.03296	C	0.13802	3.96810	-3.89474	H	1.05914	2.85279	5.35601
C	4.32807	3.77487	1.09256	C	-0.01267	4.41861	4.29582	H	1.95105	4.35629	5.21268
C	-2.02804	4.67778	-2.10634	C	1.14414	-2.35295	4.88246	H	2.58687	-3.32846	-1.67799
C	-2.05480	-6.48528	0.04248	C	1.25264	-3.78856	-3.34982	H	0.97245	-2.62748	-1.51097
C	4.17624	1.77505	-0.48415	C	2.05764	3.12402	3.44051	H	-1.35036	2.67005	-4.80109
C	-3.89589	-5.00435	-0.67561	C	1.99310	-1.06990	5.03146	H	-1.77517	4.37171	-4.83118
C	2.49767	-3.00309	2.92623	C	-0.70629	-5.38070	-2.75630	H	-5.59241	-2.23589	2.00238
C	2.39802	-4.74364	1.06780	C	-4.80278	2.67256	3.35464	H	-3.84082	-2.03842	1.86567
C	-0.56283	4.86001	-1.70429	C	-6.67553	1.52641	1.97510	H	-4.48352	0.30054	-5.79317
C	5.39953	-0.96769	1.81102	C	-4.47098	-3.17334	3.63272	H	-3.59459	0.59054	-4.30866
C	2.23967	4.28763	2.47451	C	-0.20085	-4.22116	-3.64783	H	0.66755	4.17775	-4.83041
C	4.95403	1.46656	1.71811	C	-3.21179	-4.03149	3.89013	H	0.64413	3.10318	-3.44440
N	1.26954	5.61179	0.85539	C	-5.70382	1.42966	3.17553	H	-0.44456	4.87040	5.19542
C	2.39581	5.03875	0.28702	C	-3.25254	3.26780	-3.21480	H	-0.75225	3.69154	3.93308
N	4.97704	0.22702	1.10668	H	-1.88518	2.53976	-2.36063	H	1.57407	-3.14123	5.51509
N	-0.75351	-5.88735	-0.20748	H	-5.31346	-4.70484	1.66912	H	0.13442	-2.17053	5.26678
C	3.97521	-2.86101	1.14510	H	7.22028	0.41546	-0.82831	H	1.93691	-4.57949	-3.68568
O	-7.31517	-1.28396	0.27106	H	-5.88236	3.95228	1.32405	H	1.50030	-2.89962	-3.94011
N	-4.75040	3.57180	-0.39531	H	2.54755	-0.90810	2.45093	H	3.02253	2.70477	3.74232
N	4.35097	-1.92229	2.10160	H	-5.06411	1.10072	0.63632	H	1.48859	2.32267	2.95058
N	-5.73424	-2.07873	-1.25075	H	0.25315	3.98367	1.70684	H	1.46072	-0.23240	4.55970
N	-5.82215	3.30894	-2.45202	H	4.81272	3.96644	2.05387	H	2.08757	-0.81401	6.09239
O	-0.70259	5.83854	-0.62256	H	4.75094	4.43081	0.32789	H	-1.77109	-5.55767	-2.93090
O	4.62653	2.40351	0.75342	H	-2.31858	5.53832	-2.73701	H	-0.16445	-6.30830	-2.98136
O	-2.30899	6.18144	1.03871	H	-1.92013	-7.16897	0.88165	H	-4.07394	2.48588	4.15127
O	-3.93597	-5.38598	-1.84274	H	-2.36508	-7.04374	-0.84160	H	-5.41932	3.51521	3.69574
N	-4.61160	-3.93297	-0.14579	C	4.78261	2.37279	-1.76938	H	-7.19358	0.57464	1.82924
O	2.88544	5.31819	-0.80358	H	3.03770	-3.68309	3.61050	H	-7.43038	2.30417	2.14803
N	-6.70803	-0.08330	-1.64027	H	2.32491	-5.43485	1.91381	H	-4.45170	-2.28936	4.27997
O	0.03391	-6.07426	1.98512	H	3.19430	-5.07035	0.39119	H	-5.36093	-3.74684	3.92535
N	2.90394	4.08709	1.18109	H	-0.20003	3.90759	-1.27886	H	-0.86747	-3.35995	-3.50260
N	-6.47001	2.12141	-0.54599	H	5.84770	-0.62895	2.74635	H	-0.29015	-4.50202	-4.70293
N	-3.14155	-5.56949	0.34778	H	6.14325	-1.50774	1.22150	H	-3.21873	-4.39146	4.92479
N	2.76591	-3.42338	1.54849	H	2.76986	5.09295	3.01503	H	-2.32042	-3.39649	3.79262
N	1.12312	-4.78189	0.37525	H	3.84483	-0.39291	-0.55608	H	-5.06847	0.54473	3.03295
N	-2.69883	4.81037	-0.81122	H	-6.18778	-2.13482	-3.29374	H	-6.27138	1.25335	4.09580
O	5.19453	1.69582	2.90064	H	-5.86079	1.44022	-3.98983	H	5.79877	-1.05529	-1.56706
O	4.60069	-3.14430	0.12688	H	-6.58601	-0.09571	-4.50404	H	4.07463	2.99937	-2.31284
C	4.65681	0.29730	-0.31419	H	1.33217	5.31765	-2.66079	S	5.26774	0.93738	-2.81439
C	-5.40991	-1.71319	-2.63071	H	-0.07572	6.09369	-3.40924	H	5.66228	2.97780	-1.53529
C	-5.72004	0.35611	-4.00346	H	-0.05799	7.21018	0.74888	H	7.42512	-0.09741	0.11952
C	0.28320	5.17199	-2.93345	H	1.03438	6.98185	-0.64328	H	7.23011	1.48585	-0.59389
C	0.39466	6.47569	0.08118	H	-8.15949	0.90592	-0.58776	C	8.36414	0.10501	-1.80627
C	0.11962	-5.62959	0.84298	H	-7.69710	1.68283	-2.12555	H	9.28318	0.53730	-1.39635
C	-6.65655	-1.15833	-0.75870	H	-3.89778	-3.15306	-2.33387	H	8.17115	0.60907	-2.76164
C	-7.32452	1.17004	-1.23792	H	-3.25449	-1.62496	-2.62038	C	8.59698	-1.39285	-2.05234
C	-4.05415	-2.06960	-3.22675	H	-2.38922	-3.90492	1.38532	C	9.79409	-1.67559	-2.96512
C	-1.93929	5.66553	-0.01325	H	-6.66571	-3.55126	-0.15114	H	7.71034	-1.84588	-2.50985
C	-3.17204	-4.67399	1.50796	H	-5.95525	-4.10740	-1.69799	H	8.75585	-1.90215	-1.09479
C	-5.80704	-3.46475	-0.82445	H	-4.39422	5.58023	0.06746	H	9.81364	-2.73016	-3.26959
C	-4.14776	4.85326	-0.71305	H	-4.57145	5.17896	-1.66876	C	11.13249	-1.39029	-2.31690
C	-5.69561	3.02686	-1.26312	H	-4.69252	0.24943	-2.13170	H	9.73669	-1.10163	-3.89761
C	-5.59456	-0.19496	-2.58765	H	-0.79266	5.91008	2.90458	O	12.14528	-1.46052	-3.21681
C	0.17568	5.50277	3.20838	H	0.78914	6.33013	3.58781	O	11.32487	-1.14788	-1.14496
C	-4.03599	-1.50190	-4.66527	H	-3.04870	-1.65798	-5.11408	H	12.96095	-1.29035	-2.71578
C	1.06536	-2.87989	3.43017	H	-4.74374	-2.07985	-5.27492				
C	3.39842	-1.17556	4.39278	H	0.50576	-2.18484	2.79127				

Optimized geometry of (-)-((*S,S,R*)(*R,R*)₇)-mixHC[8] sulfur atom oriented towards outside

194				C	-1.33593	3.45327	-4.32370	H	1.47156	-2.57449	-1.26299
E(au) = -4640.58470461				C	-4.39682	-3.00118	2.07761	H	-1.20971	2.52386	-4.89017
C	-2.29005	3.21506	-3.12979	C	-3.90290	-0.55711	-4.89213	H	-1.81114	4.16713	-5.00999
H	2.82925	1.87498	-0.32071	C	0.04915	3.99964	-3.90960	H	-5.38800	-2.60838	1.82897
C	-4.10927	-4.28904	1.31654	C	-0.87718	4.42020	4.15992	H	-3.65971	-2.23581	1.80250
C	5.90012	0.75348	-1.02981	C	1.22987	-1.90367	5.16388	H	-3.91500	-0.30639	-5.95848
C	-5.49706	2.80933	0.56826	C	1.98487	-3.83157	-2.98483	H	-3.20035	0.14379	-4.42058
C	3.30048	-1.10424	3.28968	C	1.35327	3.31080	3.46254	H	0.62912	4.24542	-4.80578
C	-6.02279	1.38777	0.35807	C	1.95755	-0.54525	5.28231	H	0.60679	3.20659	-3.39235
C	0.16265	4.95921	1.98858	C	0.12935	-5.54721	-2.40475	H	-1.41759	4.81426	5.02742
C	3.73714	4.14754	1.33335	C	-5.32791	2.40163	2.99306	H	-1.52324	3.64676	3.72209
C	-2.32258	4.50838	-2.32599	C	-6.92490	0.98674	1.51953	H	1.69549	-2.61989	5.85426
C	-1.31860	-6.57680	0.37041	C	-4.30283	-3.34167	3.58326	H	0.19111	-1.79294	5.49445
C	3.90081	2.07985	-0.18899	C	0.59892	-4.41232	-3.34606	H	2.75654	-4.57937	-3.21231
C	-3.22672	-5.31502	-0.56327	C	-2.98680	-4.05033	3.97567	H	2.19894	-2.96811	-3.62456
C	2.72592	-2.52248	3.30506	C	-6.06190	1.05501	2.80221	H	2.32247	2.96722	3.83900
C	2.88074	-4.36848	1.55857	H	-3.29106	2.94498	-3.48152	H	0.89567	2.47682	2.91428
C	-0.92444	4.85853	-1.81201	H	-1.92901	2.39411	-2.49703	H	1.37624	0.21907	4.74829
C	5.52482	-0.31491	2.23020	H	-4.83995	-5.04713	1.65412	H	1.98222	-0.23302	6.33202
C	1.51878	4.50716	2.53529	C	7.16421	-0.00886	-0.62736	H	-0.90122	-5.82982	-2.63612
C	4.71872	1.99766	2.02562	H	-6.35663	3.45985	0.81433	H	0.76258	-6.43592	-2.52223
N	0.59258	5.79566	0.86440	H	2.60652	-0.45794	2.72277	H	-4.65816	2.33545	3.85778
C	1.80641	5.32235	0.38731	H	-5.16021	0.69855	0.34795	H	-6.06458	3.17934	3.23596
N	5.11370	0.81852	1.41853	H	-0.36516	4.07353	1.59296	H	-7.31593	-0.02461	1.37940
N	-0.06059	-5.87736	0.16584	H	4.13591	4.38082	2.32485	H	-7.77581	1.67672	1.58661
C	4.27618	-2.34752	1.59179	H	4.19045	4.81498	0.59642	H	-4.42062	-2.42950	4.17890
O	-7.08905	-1.94672	-0.08178	H	-2.64932	5.31673	-3.00594	H	-5.15017	-3.98945	3.84577
N	-5.03716	3.14489	-0.78021	H	-1.18492	-7.19153	1.26098	H	-0.14692	-3.60625	-3.31162
N	4.50934	-1.31667	2.49292	H	-1.51349	-7.21444	-0.49229	H	0.61139	-4.77304	-4.38036
N	-5.29983	-2.62001	-1.42080	C	4.42937	2.82666	-1.42159	H	-3.03462	-4.35650	5.02642
O	-5.87916	2.67128	-2.90500	H	3.29035	-3.11217	4.05079	H	-2.15840	-3.33213	3.90330
N	-1.25718	5.83957	-0.77551	H	2.80723	-5.00646	2.44524	H	-5.31993	0.24575	2.76075
N	4.11512	2.78126	1.07052	H	3.74793	-4.66582	0.96019	H	-6.68729	0.85153	3.67832
O	-3.02425	6.03717	0.74060	H	-0.49929	3.96067	-1.32924	H	5.48449	0.29877	-1.93769
O	-3.14041	-5.75539	-1.70706	H	5.85889	0.10819	3.17840	H	3.96798	2.40972	-2.32384
N	-4.08157	-4.29645	-0.14704	H	6.35168	-0.83695	1.75354	S	6.23097	2.52701	-1.45701
O	2.36511	5.66767	-0.65072	H	1.93937	5.33724	3.13196	H	4.20165	3.89379	-1.39563
H	-6.44751	-0.76626	-1.99433	H	4.11971	-0.12978	-0.17052	H	6.86985	-1.04225	-0.40443
O	0.57703	-5.84036	2.41392	H	-5.56079	-2.81306	-3.48882	H	7.55739	0.42831	0.29704
N	2.30033	4.38682	1.30125	H	-5.56600	0.74301	-4.33992	C	8.28672	-0.01960	-1.67950
N	-6.55875	1.49612	-1.00234	H	-6.06858	-0.88592	-4.83305	H	9.14294	-0.54839	-1.24745
N	-2.50159	-5.74936	0.54131	H	0.98477	5.49747	-2.62613	H	8.61802	1.00898	-1.87656
N	3.09785	-2.99165	1.96794	H	-0.43034	6.09966	-3.50934	C	7.91266	-0.69477	-3.00597
N	1.66659	-4.56829	0.78793	H	-0.86440	7.26563	0.63650	C	9.06944	-0.73952	-4.00912
N	-3.11009	4.59648	-1.09476	H	0.36033	7.14442	-0.65529	H	7.08165	-0.15860	-3.47823
O	4.87451	2.28875	3.21005	H	-8.09078	0.09233	-1.12530	H	7.57022	-1.71770	-2.81144
O	4.98133	-2.64304	0.62977	H	-7.57845	0.85086	-2.65651	H	8.71675	-1.05488	-4.99982
C	4.73099	0.76057	0.00730	H	-3.18879	-3.56276	-3.18587	C	10.17679	-1.69701	-3.62217
C	-4.89572	-2.27855	-2.78561	H	-2.77201	-1.94794	-2.59875	H	9.51224	0.25247	-4.15824
C	-5.30610	-0.31755	-4.28519	H	-1.99590	-3.96623	1.53071	O	11.25602	-1.56076	-4.43335
C	-0.01641	5.23334	-2.97764	H	-6.15805	-4.13673	-0.32253	O	10.14069	-2.51217	-2.72611
C	-0.28882	6.57871	0.01452	H	-5.27405	-4.67826	-1.78273	H	11.90259	-2.22113	-4.13145
C	0.70770	-5.46920	1.25008	H	-4.94863	5.19675	-0.38754				
C	-6.35834	-1.79040	-1.05711	H	-4.93405	4.71230	-2.11143				
C	-7.23428	0.42336	-1.71393	H	-4.44478	-0.22737	-2.33074				
C	-3.46145	-2.50422	-3.24682	H	-1.65528	5.88138	2.73582				
C	-2.51565	5.54441	-0.26329	H	-0.17351	6.40547	3.55731				
C	-2.70607	-4.80424	1.64317	H	-2.34218	-2.06038	-5.06165				
C	-5.26229	-3.98743	-0.93371	H	-3.95994	-2.67731	-5.34257				
C	-4.55764	4.47443	-1.11122	H	0.67884	-1.89386	3.04113				
C	-5.83042	2.45603	-1.69642	H	0.84059	-3.51336	3.73288				
C	-5.24828	-0.79045	-2.83718	H	3.81363	0.45720	4.71017				
C	-0.68602	5.54293	3.11232	H	4.05059	-1.19129	5.31320				
C	-3.37673	-1.99828	-4.70593	H	2.33671	-5.48738	-0.96962				
C	1.26598	-2.50453	3.73897	H	-1.64978	-5.65329	3.33837				
C	3.39418	-0.55368	4.70741	H	-3.36933	-6.08313	3.25267				
C	1.69297	-4.63835	-0.67422	H	-4.13092	3.86380	1.88858				
C	-2.64525	-5.27409	3.09213	H	-3.68419	2.18511	1.55743				
C	-4.53263	2.85520	1.74647	H	-0.37450	-4.10162	-0.91258				
C	0.24189	-5.01520	-0.98068	H	0.22259	2.91780	5.28187				
C	0.44375	3.76804	4.62710	H	1.00181	4.48872	5.23988				
C	2.11874	-3.42941	-1.49735	H	3.14848	-3.13769	-1.26588				

194				C	5.13666	-3.18749	0.84787	C	-8.48642	0.73558	-2.27270
E(au) = -4640.58455699				C	2.67621	-5.49773	-0.06735	H	-3.71852	3.88282	-1.73415
C	-4.05879	-2.28508	-0.39943	H	5.13612	-3.39107	4.27019	C	-2.12129	3.44536	-3.15782
C	-2.69975	3.01168	2.76101	H	3.84395	-2.79301	3.24475	N	0.19324	5.15052	0.00436
H	-0.74711	-5.70476	2.80576	H	5.20187	-5.86583	-0.15989	N	2.60912	5.00034	0.24389
H	5.47903	-5.30644	-1.83130	H	5.21019	-0.89002	3.96557	C	-2.75017	4.29689	-2.02902
H	6.40320	1.10701	-3.44052	H	6.69076	-1.68115	3.45684	H	-2.91049	5.32945	-2.36495
H	5.72810	4.85806	2.59302	C	5.34039	-3.91987	2.16921	N	-4.43424	-2.82436	0.90541
H	-2.96810	-2.28956	-0.51400	C	5.62791	-1.56125	3.20680	N	-4.95700	-0.66247	1.06705
C	-5.72420	-0.60915	-1.37570	H	6.12930	0.00933	1.76600	O	-4.98783	2.93366	0.10118
C	-9.67189	0.94844	-3.21904	C	4.96941	-5.09073	-0.89132	H	0.44521	2.98684	-1.85798
H	-5.71456	0.35024	2.66850	H	4.48911	-0.62493	1.58353	H	-2.75449	3.49158	-0.45043
H	0.72886	-3.05653	2.44163	C	5.52626	-0.90333	1.81068	H	-2.12072	2.39424	-2.83858
H	1.30731	-5.84870	-2.43077	H	2.80761	-3.28822	-1.74845	H	-0.70600	4.83560	-0.43255
C	2.79572	-4.34150	-2.07965	H	4.72742	-4.82419	2.21389	C	-0.67918	3.86151	-3.52562
H	6.39245	-4.21446	2.27386	H	4.08011	-2.87027	0.79784	H	1.23442	4.38426	-2.60156
H	7.63378	-0.32950	-0.50911	H	7.04154	-2.22491	1.09009	H	-0.26652	3.15146	-4.25089
H	3.32182	0.28519	-5.23901	C	6.01434	-1.93496	0.80147	C	0.26412	3.97274	-2.30485
C	4.43404	3.90454	1.15005	C	5.86716	-2.83208	-1.32922	O	7.17050	1.89708	0.23213
H	-9.60598	0.30221	-4.10244	C	4.93195	-2.93839	3.29370	O	-2.45340	-5.36307	-0.62596
C	-7.13639	-0.97254	-0.88633	C	4.49627	0.14561	-3.41052	O	-0.66128	5.90932	2.04059
H	-6.08927	1.08232	1.08075	C	6.81279	-0.56640	-1.19322	O	3.54441	5.53743	-1.82611
C	-4.83688	-1.83449	1.78516	H	2.78345	2.39030	-4.10580	N	-2.03131	5.05546	0.35142
C	-3.99318	-3.69445	-2.08430	H	3.62644	2.76138	-5.59904	O	6.04769	-2.98388	-2.53494
O	-5.06149	-1.97531	2.98493	C	5.55185	1.01618	-2.74090	O	2.99945	-6.01054	1.00137
H	-7.15506	-2.02051	-0.56641	H	4.39502	4.15904	-3.62332	N	5.97782	2.91460	-1.50164
C	-8.26224	-0.73866	-1.90548	H	5.73107	3.23553	-4.33950	N	-2.77915	-4.53184	1.53205
C	-4.68762	-3.00186	-1.60878	C	4.14004	0.82751	-4.75221	N	6.07690	0.66426	-1.42051
H	-12.84327	0.59753	-2.97793	C	4.78115	3.15098	-3.79624	N	4.79620	4.57653	-0.10188
H	-8.65297	1.32041	-1.36083	H	4.02093	2.31766	-1.98051	C	-0.81881	5.42188	0.92378
H	-7.59302	1.14809	-2.75486	H	4.86965	-0.86980	-3.57761	N	6.00597	-1.63474	-0.63101
H	-5.70319	0.42678	-1.72373	C	5.00171	2.41933	-2.47726	C	-1.76853	4.27834	-0.86283
S	-5.15159	-1.66691	-2.78509	C	6.4810						

Optimized geometry of (+)-((S,S,R)(S,S)7)-mixHC[8] sulfur atom oriented towards outside

194				H	-5.71605	5.43594	-0.58504	N	5.07136	1.18196	1.35246
E(au) = -4640.58471172				H	-5.58039	0.62359	3.71678	O	5.33994	-2.44728	0.59156
C	3.81633	2.52428	-0.15852	H	-7.08542	1.24299	3.06268	H	0.05980	-3.01834	-1.68365
C	2.91276	-2.55180	3.12161	C	-5.86147	3.56493	1.79469	H	3.42437	-3.38887	-3.64437
H	0.03945	5.76947	2.77882	C	-5.99908	1.22394	2.90131	H	2.63164	-2.28109	-2.53876
H	-5.82566	4.80721	-2.25094	H	-6.22275	-0.43547	1.49072	H	1.48517	-4.88606	-3.67184
H	-5.97281	-1.72517	-3.67415	C	-5.36264	4.66720	-1.27338	C	1.35232	-3.89116	-3.22590
H	-5.34634	-5.15363	2.54419	H	-4.64440	0.35723	1.41091	H	-0.57278	-4.51129	-2.39010
H	2.75051	2.31507	-0.32312	C	-5.71918	0.53505	1.54519	H	0.93558	-3.25623	-4.01573
C	5.80625	1.25367	-1.10194	H	-3.00089	3.06005	-1.96031	C	0.34282	-4.00971	-2.06007
C	8.89991	-0.06105	-4.23807	H	-5.34407	4.52646	1.85011	O	-6.92925	-2.46742	-0.03689
H	5.73117	0.31154	3.07221	H	-4.39755	2.60475	0.56769	O	1.97244	5.58112	-0.54076
H	-1.20703	3.01924	2.32476	H	-7.29446	1.67115	0.65673	O	1.12681	-5.63227	2.43877
H	-1.68645	5.73441	-2.58796	C	-6.22362	1.47820	0.46042	O	-2.82613	-5.80843	-1.69579
C	-3.05903	4.10629	-2.30835	C	-5.99512	2.31633	-1.68701	N	2.53516	-4.76352	0.78948
H	-6.94221	3.75595	1.80554	C	-5.45195	2.66680	2.98643	O	-6.09257	2.41003	-2.90821
H	-7.56145	-0.32851	-0.90487	C	-4.17985	-0.57142	-3.54913	O	-3.61042	5.78359	0.72471
H	-2.86601	-0.65014	-5.28417	C	-6.71676	-0.02924	-1.53341	N	-5.51296	-3.41302	-1.63785
C	-4.05394	-4.14318	1.13895	H	-2.20331	-2.64947	-4.03085	N	2.22799	4.75699	1.62957
H	9.35333	0.93356	-4.32369	H	-2.89270	-3.15531	-5.56292	N	-5.84425	-1.18338	-1.65602
C	7.06829	0.45191	-0.77596	C	-5.18948	-1.52333	-2.92039	N	-4.27015	-4.89753	-0.09962
H	6.29050	-0.49351	1.58268	H	-3.66062	-4.55808	-3.59033	C	1.31951	-5.19364	1.30748
C	4.64541	2.29980	2.04534	H	-5.02574	-3.80168	-4.43527	N	-6.06959	1.13419	-0.95401
H	3.88505	3.01030	-2.26115	C	-3.65905	-1.25746	-4.83364	C	2.29481	-4.07674	-0.48196
O	4.80752	2.50783	3.24594	C	-4.13189	-3.60131	-3.83073	N	-1.82767	5.07650	-0.60571
H	7.48402	0.82473	0.16663	H	-3.59612	-2.63347	-2.00131	C	-3.13290	-3.80423	3.87631
C	8.17022	0.50036	-1.84878	H	-4.63966	0.39412	-3.78305	N	3.84369	-3.21674	2.20738
C	4.35081	3.35752	-1.33230	C	-4.52209	-2.85252	-2.56148	H	2.03077	-3.02452	-0.27367
H	11.71362	-1.55914	-4.51412	C	-6.17506	-2.36789	-1.00174	C	-2.11431	-3.94654	2.72130
H	7.41151	-1.10533	-3.08382	H	-7.07800	0.26262	-2.52462	N	0.14735	5.04433	0.81607
H	6.92982	0.50305	-3.62876	H	-4.47616	-1.28568	-5.56717	N	4.38125	-1.02192	2.17487
H	5.37118	0.87289	-2.03477	H	-3.35893	-0.38424	-2.84493	N	-3.92724	4.86072	-1.39904
S	6.14976	3.05047	-1.39670								
H	4.04156	0.31482	-0.24925								
H	9.02689	-0.06821	-1.47154								
H	4.12363	4.41905	-1.23112								
O	11.07175	-0.86931	-4.75379								
H	4.59453	-4.75863	1.09594								
H	4.11708	4.66021	2.49766								
C	1.56119	-2.23236	5.16064								
H	1.21689	3.01573	2.21937								
C	1.32469	4.06480	2.54825								
C	5.44115	-0.01917	2.07166								
H	2.54894	3.54480	4.26595								
H	1.68878	5.08430	4.41706								
H	4.04371	5.20492	0.80493								
C	1.60584	4.05502	4.04553								
H	0.53421	3.36184	5.80883								
H	3.02248	-0.93346	6.09750								
H	0.46705	2.26128	4.44326								
C	0.42068	3.32368	4.71995								
H	1.91313	-4.15712	4.18917								
C	2.20864	-0.84434	5.36528								
H	1.47651	-0.15813	5.80538								
H	-1.75111	3.25679	4.75671								
H	-1.08743	4.88028	4.77357								
C	-0.96437	3.88534	4.32486								
C	3.64781	4.48898	1.52787								
H	-0.25529	6.45410	-0.63009								
C	-1.17154	4.00945	2.79676								
H	0.40248	4.37451	-2.33642								
H	-0.58787	2.93614	-2.05690								
C	0.01418	4.79671	2.25400								
H	-0.59524	4.74174	-4.54897								
H	-0.02597	3.08366	-4.49109								
C	-1.71164	4.77775	-2.03412								
C	-0.77661	3.76639	-4.07752								
H	-2.29763	2.22356	-4.16553								
C	1.50333	5.17073	0.51787								
H	-2.30134	3.29793	-5.55275								
C	-2.19058	3.27577	-4.46310								
H	-2.11653	4.51541	2.57370								
C	-0.81779	5.85234	0.09106								
H	-1.34378	6.50980	0.79078								
H	-4.30044	3.61329	-4.01892								
H	-3.36182	5.10863	-4.19764								
C	-3.33620	4.08323	-3.80712								
C	-0.56780	3.91534	-2.55228								
C	-5.48077	2.81430	0.52364								
C	-3.17390	5.29082	-0.31256								
H	-5.77905	3.12791	3.92478								
H	-4.35458	2.63133	3.02879								

Optimized geometry of $\text{PF}_6^-@(-)((\text{S},\text{S},\text{R})(\text{R},\text{R})_7)\text{-mixHC}[8]$ sulfur atom oriented towards outside

201				C	4.52787	-2.46510	1.57758	H	0.78080	5.28760	3.21349
E(au) = -5581.34704297				C	-0.84054	4.63413	-0.85740	H	2.45441	5.85599	3.29966
C	2.52159	-2.80125	-2.94756	C	-0.00588	-3.32683	4.44186	H	4.25305	-3.51308	1.73624
H	-2.49125	-1.89465	0.02947	C	-2.61709	2.89417	-1.21675	H	3.62236	-1.92077	1.28849
C	3.48809	4.37575	1.25254	C	1.46091	-2.93052	-4.06632	H	-0.20094	3.77355	-0.60338
C	-5.52243	-1.02893	-1.07495	C	3.85752	3.04469	1.89498	H	0.13016	-2.39499	5.00175
C	5.58855	-2.34097	0.49088	C	3.49484	0.66758	-4.66100	H	-0.40296	-4.06238	5.15630
C	-3.56310	0.83785	3.26439	C	0.11758	-3.51218	-3.57301	H	-3.65451	2.60681	-1.01362
C	5.94712	-0.87128	0.25982	C	1.36249	-3.81678	3.91811	H	-1.95989	2.11892	-0.81064
C	0.26932	-4.71530	1.90471	C	-1.42526	1.74872	5.00326	H	1.28731	-1.95075	-4.52495
C	-3.39989	-4.37249	1.39715	C	-2.39474	3.05788	-2.73895	H	1.86263	-3.57668	-4.86034
C	2.62403	-4.16711	-2.28075	C	-1.04887	-3.11176	3.31969	H	4.90425	2.79275	1.69426
C	0.55192	6.48141	0.31853	C	-1.99394	0.31451	5.09181	H	3.22992	2.24507	1.48812
C	-3.53707	-2.21982	-0.01298	C	-0.65800	4.93352	-2.34059	H	3.43526	0.37573	-5.71614
C	2.62310	5.49647	-0.58406	C	5.14669	-1.87457	2.86635	H	2.92574	-0.08343	-4.09961
C	-3.14221	2.30737	3.33275	C	6.68625	-0.32186	1.47448	H	-0.55692	-3.65678	-4.42509
C	-3.55833	4.18055	1.63818	C	3.62488	3.20750	3.41555	H	-0.35821	-2.77730	-2.91172
C	1.27595	-4.57402	-1.68121	C	-1.00454	3.62889	-3.09783	H	2.02606	-4.02935	4.76451
C	-5.71852	-0.16350	2.26934	C	2.21284	3.72735	3.76628	H	1.82745	-3.00446	3.34623
C	-1.09959	-4.40382	2.51569	C	5.72373	-0.45347	2.67921	H	-1.89619	2.37004	5.77857
C	-4.67667	-2.37520	2.05271	H	3.48664	-2.50305	-3.37081	H	-0.35395	1.72979	5.23167
N	-0.11269	-5.71569	0.89824	H	2.22373	-2.04716	-2.21216	H	-3.17214	3.72436	-3.13984
C	-1.40321	-5.44362	0.46739	H	4.11193	5.16262	1.71859	H	-2.52985	2.09084	-3.23636
N	-5.11315	-1.20351	1.45288	C	-6.91091	-0.43899	-0.81651	H	-2.02972	-2.88405	3.75153
N	-0.65185	5.68735	0.14980	H	6.49648	-2.86768	0.84232	H	-0.75664	-2.27808	2.67305
C	-4.81513	2.06491	1.74386	H	-2.85909	0.31632	2.59546	H	-1.38944	-0.34250	4.45447
O	6.93084	2.59953	-0.22415	H	5.00672	-0.30744	0.14442	H	-1.88732	-0.06127	6.11622
N	5.30861	-2.77787	-0.87551	H	0.62987	-3.80859	1.39355	H	0.36660	5.24824	-2.56047
N	-4.86187	0.96096	2.59257	H	-3.78088	-4.64688	2.38652	H	-1.32843	5.74938	-2.64333
N	4.97508	3.02084	-1.42313	H	-3.81041	-5.05908	0.65082	H	4.39469	-1.86085	3.66309
O	6.24570	-2.26484	-2.94878	H	2.89483	-4.90708	-3.05821	H	5.94844	-2.54433	3.20931
N	1.70079	-5.64995	-0.77509	H	0.36614	7.11313	1.18935	H	6.97089	0.72365	1.32435
N	-3.85928	-0.32340	1.16339	H	0.70841	7.10432	-0.56428	H	7.60405	-0.90077	1.64453
O	3.57872	-5.93487	0.59109	C	-3.80046	-2.93670	-1.34434	H	3.79631	2.24972	3.91939
O	2.55526	6.03076	-1.69035	H	-3.68999	2.78734	4.16608	H	4.37499	3.90570	3.81442
N	3.55419	4.54116	-0.19857	H	-3.51541	4.85338	2.50135	H	-0.24596	2.87489	-2.85479
O	-1.96876	-5.94658	-0.50311	H	-4.44453	4.40790	1.03544	H	-0.94521	3.80177	-4.17891
N	6.25882	1.27687	-2.03352	H	0.90067	-3.72864	-1.08316	H	2.14270	3.90428	4.84605
O	-1.40955	5.94862	2.34806	H	-6.02637	-0.66594	3.18793	H	1.48419	2.94331	3.52590
N	-1.95946	-4.50771	1.33532	H	-6.59208	0.25804	1.77381	H	4.89285	0.24804	2.53317
N	6.61806	-0.95710	-1.04406	H	-1.36323	-5.22625	3.20776	H	6.23591	-0.14046	3.59670
N	1.79213	5.74808	0.50290	H	-3.97503	-0.06054	0.10249	H	-5.03251	-0.46270	-1.87666
N	-3.69351	2.80777	2.07435	H	5.00322	3.14620	-3.50894	H	-3.24156	-2.43758	-2.14289
N	-2.35268	4.40893	0.87158	H	5.34675	-0.41334	-4.24023	S	-5.59566	-2.78734	-1.66150
N	3.50915	-4.36480	-1.13324	H	5.60504	1.24165	-4.82081	H	-3.49651	-3.98547	-1.32552
O	-4.97125	-2.75762	3.18483	H	-0.69280	-5.16666	-2.39362	H	-6.77813	0.59353	-0.47073
O	-5.62652	2.33609	0.85958	H	0.64345	-5.63764	-3.45457	H	-7.37710	-0.99962	0.00125
C	-4.52463	-1.00698	0.12743	H	1.45119	-7.08033	0.65589	C	-7.86353	-0.45429	-2.02492
C	4.47609	2.57377	-2.72173	H	0.17786	-7.06855	-0.59753	H	-8.84117	-0.09032	-1.68962
C	4.96707	0.61113	-4.18697	H	7.98869	0.61248	-1.17524	H	-8.01174	-1.48854	-2.36463
C	0.27101	-4.84149	-2.79561	H	7.55841	-0.21615	-2.69843	C	-7.40203	0.40526	-3.20970
C	0.80622	-6.44724	0.04353	H	2.60646	3.64152	-2.99315	C	-8.35111	0.34595	-4.41072
C	-1.46228	5.40612	1.24490	H	2.42799	2.01934	-2.30526	H	-6.41609	0.07182	-3.55186
C	6.13919	2.32698	-1.12537	H	1.41526	3.82397	1.26791	H	-7.29506	1.44691	-2.88642
C	7.17296	0.18080	-1.75772	H	5.64617	4.61039	-0.31285	H	-7.90090	0.82960	-5.28817
C	2.98588	2.61550	-3.03638	H	4.73894	5.07145	-1.78807	C	-9.68090	1.03137	-4.18497
C	2.99244	-5.37572	-0.33503	H	5.40012	-4.83861	-0.49510	H	-8.54846	-0.68863	-4.71546
C	2.01854	4.71133	1.51872	H	5.30805	-4.33351	-2.21193	O	-10.56490	0.74279	-5.17843
C	4.78292	4.37382	-0.94434	H	4.30137	0.51366	-2.15268	O	-9.96799	1.77236	-3.27043
C	4.93705	-4.13894	-1.19965	H	2.24359	-5.31741	2.59014	H	-11.37046	1.24224	-4.96265
C	6.07282	-2.02493	-1.75468	H	0.90670	-5.93331	3.57293	F	2.21346	-0.01153	-0.23974
C	4.98770	1.13212	-2.75444	H	1.75928	1.97156	-4.71421	F	0.30704	-1.22699	-0.79085
C	1.26390	-5.06297	3.00569	H	3.25861	2.76100	-5.17808	F	1.07140	-1.19112	1.39800
C	2.82370	2.04578	-4.46526	H	-1.07190	1.91585	2.84549	P	0.66319	-0.04657	0.29228
C	-1.65160	2.41847	3.62726	H	-1.33545	3.46638	3.65879	F	0.25869	1.09585	-0.81325
C	-3.47123	0.20014	4.64489	H	-3.78562	-0.84848	4.62033	F	1.00042	1.13147	1.38447
C	-2.29426	4.24098	-0.58017	H	-4.13243	0.72836	5.34477	F	-0.89314	-0.08640	0.82765
C	1.81780	5.01254	2.99954	H	-2.95194	5.00178	-1.04278				

201		C	-0.63194	4.59765	-1.18034	H	4.01418	-3.52035	2.06068
E(au) = -5581.34626015		C	-0.55349	-3.26889	4.33410	H	3.46089	-1.93714	1.49391
C	2.72712	-2.93579	-2.76062		C	-2.40904	2.85947	-1.53807	
H	-2.50693	-2.02686	-0.26612		C	1.77158	-3.07379	-3.96956	
C	3.53923	4.40188	1.21650		C	3.83225	3.10432	1.95897	
C	-5.39921	-0.63943	-1.28710		C	3.93032	0.40234	-4.52560	
C	5.48393	-2.42261	0.90136		C	0.38154	-3.63116	-3.59225	
C	-3.55043	1.08646	2.98131		C	0.85964	-3.77064	3.96499	
C	5.89339	-0.96986	0.64740		C	-1.47983	2.09079	4.74156	
C	-0.02697	-4.70740	1.86824		C	-2.09091	2.91762	-3.05051	
C	-3.62355	-4.38413	0.95314		C	-1.47443	-3.07040	3.10663	
C	2.75097	-4.28959	-2.06193		C	-2.02773	0.65157	4.86793	
C	0.71622	6.49798	-0.03663		C	-0.35242	4.79628	-2.66537	
C	-3.58310	-2.19231	-0.38345		C	4.83110	-1.85139	3.20432	
C	2.82259	5.42683	-0.73596		C	6.52545	-0.38314	1.90424	
C	-3.14882	2.56178	2.99561		C	3.51562	3.36882	3.44943	
C	-3.49955	4.33077	1.17101		C	-0.67274	3.44882	-3.35728	
C	1.34756	-4.66989	-1.58457		C	2.09991	3.94304	3.67978	
C	-5.61327	-0.00596	1.93840		C	5.45043	-0.44834	3.01570	
C	-1.45195	-4.37756	2.32394		H	3.73050	-2.65755	-3.09975	
C	-4.71990	-2.29886	1.67975		H	2.37470	-2.16444	-2.06822	
N	-0.30517	-5.73212	0.85414		H	4.15183	5.20121	1.67621	
C	-1.54113	-5.47132	0.28185		C	-6.76865	-1.31747	-1.09820	
N	-4.89493	-1.01848	1.19081		H	6.34413	-2.94979	1.35692	
N	-0.48883	5.71216	-0.23228		H	-2.82624	0.54398	2.35309	
O	-4.75618	2.21574	1.35571		H	4.98017	-0.39540	4.02078	
C	7.00842	2.46609	0.11063		H	0.38961	-3.81367	1.37678	
N	5.32435	-2.91001	-0.46746		H	-4.11583	-4.69980	1.87948	
N	-4.83252	1.16504	2.27255		H	-3.92161	-0.54570	0.13559	
N	5.17446	2.86908	-1.27295		H	3.08503	-5.04757	-2.79617	
O	6.46318	-2.49932	-2.46090		H	0.48690	7.18879	0.77707	
N	1.67148	-5.73051	-0.62102		H	0.94179	7.05835	-0.94597	
N	-4.08844	-3.03871	0.69807		C	-3.87904	-2.71937	-1.80250	
O	3.40532	-6.00175	0.92609		H	-3.72899	3.07560	3.78545	
O	2.84028	5.89543	-1.87331		H	-3.50416	5.06285	1.98570	
N	3.70397	4.47868	-0.23358		H	-4.34996	4.51301	0.50486	
O	-2.00635	-6.00656	-0.72206		H	0.92886	-3.80821	-1.04105	
N	6.46634	1.07481	-1.69066		H	-5.95778	-0.49940	2.84905	
O	-1.37721	6.12507	1.89281		H	-6.47399	0.36146	1.37315	
N	-2.18117	-4.50331	1.05763		H	-1.79330	-5.18469	2.99965	
N	6.68283	-1.12137	-0.58231		H	-3.64890	-0.02331	-0.18550	
N	1.92756	5.75932	0.27623		H	5.38181	2.89906	-3.35171	
N	-3.66348	2.99231	1.69515		H	5.71489	-0.69233	-3.89942	
N	-2.25198	4.50530</							

Optimized geometry of $\text{PF}_6^-@(+)-((\text{S},\text{S},\text{R})(\text{S},\text{S})_7)\text{-mixHC}[8]$ sulfur atom oriented towards outside

201				H	2.01523	2.72296	5.27899	H	-7.46694	0.09641	5.48465
E(au) = -5581.34569817				C	2.01797	2.83981	4.18883	C	-9.24803	-0.28243	4.43096
C	-3.25309	2.79815	-0.06216	H	2.67467	4.31345	-2.42055	C	-2.58382	-3.00193	-4.32532
C	-3.10893	-2.32167	-3.06641	C	1.36753	5.97672	-0.17093	C	-4.27907	-4.25337	-1.78918
H	0.63789	5.66198	-2.95013	H	2.00339	6.55649	-0.84846	H	-2.97515	0.99036	-4.08456
H	6.04727	4.25370	2.47226	H	4.18906	3.00644	3.99638	H	-1.83974	0.11500	-3.03826
H	5.17717	-2.16590	3.81309	H	3.37659	4.55904	4.26014	H	-3.39820	-3.11924	-5.05307
H	4.56724	-5.15568	-2.49300	C	3.29778	3.59034	3.74845	C	-2.57306	0.00050	-3.84439
H	-2.20474	2.47870	-0.03238	C	0.67421	3.86259	2.22867	H	-4.37367	-1.07155	-4.27476
C	-5.21463	1.65999	1.09185	C	5.47126	2.31415	-0.29873	H	-2.26231	-2.17223	-2.37733
C	-7.94709	0.47691	4.57293	C	3.62159	5.18647	0.42428	C	-3.68593	-0.94757	-3.41705
H	-5.62417	0.85958	-3.13328	H	5.65116	2.52518	-3.71610	C	-4.94285	-1.88305	-1.71059
H	1.64140	2.93400	-2.00421	H	4.22416	2.20902	-2.74198	O	-9.50916	-1.12157	3.59718
H	1.95304	5.53776	2.60099	H	6.09637	4.92626	0.81776	H	-0.62200	-2.10757	-4.19611
C	3.18230	3.80839	2.24431	H	5.16971	0.06608	-3.43392	H	-1.10371	-2.49954	-5.84056
H	6.97713	3.05024	-1.66022	H	6.77047	0.51585	-2.86615	H	-6.41577	-0.06194	0.63900
H	7.27854	-1.00985	1.17979	C	5.88195	2.99063	-1.60184	C	-4.21317	1.55500	-0.10058
H	2.05669	-0.60365	4.91743	C	5.69726	0.62777	-2.65504	H	-7.71066	2.12547	2.36404
C	3.25254	-4.32793	-0.99053	H	5.80183	-1.01292	-1.21943	C	-7.00899	0.34599	3.36883
H	-8.18559	1.52618	4.78317	C	5.61902	4.19306	1.47022	H	-4.70712	-2.98487	1.04117
C	-6.57829	0.99098	0.90164	H	4.32053	-0.05230	-1.08741	C	-3.12013	-2.80368	2.53407
H	-6.28126	0.15178	-1.63353	C	5.39930	0.00397	-1.27139	N	-1.09815	-5.18994	-0.37075
C	-4.35262	2.71702	-2.15491	H	3.04994	2.82567	1.76294	N	1.30512	-5.39844	-0.36888
H	-3.01172	3.23751	2.03718	H	5.48641	4.00878	-1.66089	C	-3.86500	-3.57295	1.41729
O	-4.62999	2.96884	-3.32687	H	4.37264	2.22097	-0.28974	H	-4.26423	-4.52222	1.79894
H	-7.07606	1.46015	0.04576	H	7.14039	0.97190	-0.49266	N	-3.54541	3.46637	-1.33101
C	-7.51947	1.07228	2.11682	C	6.06498	0.90516	-0.23900	N	-4.80103	1.62367	-1.43606
C	-3.56690	3.63981	1.18318	C	6.03076	1.80111	1.89919	O	-5.82804	-2.02202	-0.86752
H	-10.92100	-0.48656	5.24540	C	5.31770	2.12258	-2.75235	H	-0.44674	-3.02295	1.39027
H	-6.86161	-0.711606	3.14172	C	3.61303	-0.76363	3.40524	H	-3.79366	-2.64104	3.38377
H	-6.03482	0.75045	3.66496	C	6.43774	-0.62350	1.76628	H	-2.85558	-1.80874	2.15216
H	-4.70296	1.20343	1.94843	H	1.31641	-2.49758	3.55871	H	-2.11215	-4.41463	3.57629
S	-5.36136	3.46573	1.48672	H	1.64467	-3.07164	5.18938	C	-1.83360	-3.50830	3.01954
H	-3.64389	0.62390	-0.00404	C	4.55381	-1.87079	2.94717	H	-0.05030	-4.51169	2.26300
H	-8.48231	0.63614	1.82839	H	2.52241	-6.44025	3.39896	H	-1.30752	-2.86027	3.72917
H	-3.28355	4.68719	1.06670	H	3.82977	-4.04358	4.43270	C	-0.87584	-3.90784	1.87208
O	-10.13626	0.06554	5.40136	C	2.80949	-1.33290	4.59790	O	6.53579	-3.12120	0.34439
H	-5.24196	-4.33715	-1.28197	C	3.07620	-3.74351	3.69191	N	-1.47939	6.09275	0.24770
H	-3.57193	4.96334	-2.69968	H	2.97332	-2.75414	1.79726	O	-1.96191	-5.81121	-2.44513
C	-1.47021	-2.08984	-4.89204	H	4.17554	0.12421	3.71243	O	2.03564	-6.27605	1.66508
H	-0.76598	3.10881	-2.06313	C	3.75795	-3.09612	2.49178	N	-3.21185	-4.61452	-0.87422
C	-0.78383	4.09690	-2.54861	C	5.67737	-2.89395	1.19602	O	6.18502	1.90549	3.11526
C	-5.37410	0.48883	-2.13435	H	6.77213	-0.38735	2.78236	O	4.21202	5.72642	-0.51034
H	-1.95006	3.41641	-4.25409	H	3.49100	-1.46766	5.45024	N	4.78754	-3.81893	1.73377
H	-0.95503	4.84306	-4.57062	H	2.94425	-0.47819	2.58616	N	-1.68410	4.98297	-1.80245
H	-3.47910	5.55003	-1.01957	H	5.52803	-5.31239	0.56007	N	5.43546	-1.66697	1.79920
C	-0.98059	3.87995	-4.04320	H	4.42068	-5.87284	1.84537	N	3.47914	-5.20747	0.16495
H	0.12461	2.82447	-5.59629	C	4.59505	-5.10616	1.08803	C	-2.07558	-5.26453	-1.35139
H	-2.63066	-0.57951	-5.92999	C	2.12032	-2.67923	4.28284	N	5.95200	0.61202	1.18830
H	0.04323	1.97659	-4.05355	C	3.71148	-3.24830	-3.15466	C	-2.84260	-3.84374	0.31978
C	0.17686	2.96441	-4.51008	H	5.23618	-3.74199	-1.66393	N	2.24576	5.10270	0.57730
H	-2.19031	-3.99818	-4.10218	H	0.41408	-4.47490	-2.98251	C	2.34326	-3.73175	-3.68487
C	-1.91433	-0.62455	-5.09710	H	1.02701	-3.09624	-2.05285	N	-4.23511	-2.90380	-3.22632
H	-1.05186	-0.02015	-5.39840	C	4.31648	-4.17298	-2.07075	H	-2.41397	-2.87869	0.00401
H	2.33391	2.75504	-4.40028	H	2.30278	-5.87343	-2.14477	C	1.31759	-4.01948	-2.56336
H	1.79456	4.39844	-4.70992	C	1.99591	-4.96929	-1.58441	N	0.36010	5.25512	-0.91650
C	1.57553	3.49519	-4.12214	H	2.48889	-4.64882	-4.27416	N	-4.49445	-0.66615	-2.22533
C	-3.11663	4.79455	-1.72198	C	2.24961	-5.68869	0.60512	N	4.21439	4.56205	1.51968
H	0.83444	6.65335	0.50624	H	-0.05792	-6.69237	-1.30132	F	1.75131	1.09075	0.04469
C	1.70855	3.83729	-2.61897	H	4.41555	-3.14730	-3.98914	F	-0.50292	0.75569	0.48062
H	-0.21682	4.45498	1.99571	H	0.01796	-6.74474	0.48816	F	0.25987	0.76391	-1.70769
H	0.64373	2.95320	1.61913	C	0.03497	-6.09064	-0.39059	P	0.65293	-0.06537	-0.34161
C	0.55964	4.78023	-2.28570	H	2.98411	-3.32118	-0.63142	F	1.03593	-0.98917	1.01891
H	0.57078	4.45054	4.30989	H	1.93480	-2.98384	-4.37360	F	1.81204	-0.88240	-1.16853
H	-0.14310	2.87748	3.98807	H	3.58286	-2.24760	-2.72477	F	-0.44336	-1.22281	-0.73910
C	1.94396	4.65340	1.93540	H	-2.14372	-5.56796	1.40108				
C	0.70697	3.52185	3.73730	C	-1.70203	-4.70374	0.86903				
H	2.05139	1.82716	3.76794	H	-4.22643	-4.97469	-2.60673				
C	-0.98784	5.50606	-0.71628	N	5.91689	2.85287	0.99275				

Optimized geometry of PF₆⁻@(+)-((S,S,R)(S,S)7)-mixHC[8] sulfur atom oriented towards inside

201

E(a.u) = -5581.34257696

C	-3.53826	-2.73091	-0.28698
C	-3.03011	2.62421	2.73788
H	0.01116	-5.78228	2.78832
H	5.85094	-4.60388	-2.20770
H	5.76467	1.82850	-3.50138
H	4.80105	4.89108	2.74088
H	-2.44921	-2.61361	-0.30403
C	-5.23003	-1.14724	-1.37374
C	-8.92028	1.05338	-2.90538
H	-5.68357	-0.44051	2.74115
H	1.22943	-3.09036	2.00089
H	1.69494	-5.54628	-2.65346
C	3.01499	-3.92578	-2.14382
H	6.55523	-3.57029	2.02077
H	7.44911	0.49429	-0.67472
H	2.64355	0.60370	-4.95549
C	3.58409	4.13881	1.12132
H	-8.42236	0.98790	-3.87999
C	-6.67021	-1.62349	-1.10384
H	-6.19465	0.23594	1.16728
C	-4.57773	-2.47068	1.81995
H	-3.22147	-4.07616	-2.00203
O	-4.90822	-2.69120	2.98391
H	-6.70248	-2.71795	-1.12056
C	-7.68921	-1.05557	-2.10649
C	-3.99855	-3.44373	-1.57253
H	-11.79546	0.49797	-4.19209
H	-8.65936	0.42230	-0.86638
H	-7.19855	1.01515	-1.62971
H	-5.24012	-0.09745	-1.67887
S	-4.43977	-2.10188	-2.75090
H	-3.43977	-0.54720	-0.31539
H	-8.59283	-1.67437	-2.09740
H	-4.87579	-4.06635	-1.37233
O	-10.90646	0.89099	-4.20260
H	-4.87921	4.63855	0.65850
H	-4.12142	-4.85140	2.33747
C	-1.56638	2.40112	4.70683
H	-1.19504	-3.12876	1.90588
C	-1.29481	-4.12723	2.36168
C	-5.34161	-0.11936	1.75206
H	-2.52110	-3.42412	4.01417
H	-1.62740	-4.91425	4.34726
H	-3.96030	-5.43936	0.65788
C	-1.56827	-3.93759	3.84800
H	-0.50385	-2.98709	5.49365
H	-2.88023	0.99554	5.70936
H	-0.44005	-2.09754	3.97407
C	-0.39187	-3.10286	4.40912
H	-2.11495	4.30262	3.77544
C	-2.09831	0.96855	4.93679
H	-1.29347	0.33989	5.33333
H	1.77641	-3.02002	4.43716
H	1.12361	-4.63595	4.66327
C	0.99495	-3.70551	4.09120
C	-3.61107	-4.70102	1.38424
H	0.36413	-6.65956	-0.69032
C	1.20174	-4.01281	2.58907
H	-0.42899	-4.33443	-2.14889
H	0.50260	-2.91496	-1.64631
C	0.02402	-4.87527	2.15407
H	0.51177	-4.28722	-4.40381
H	-0.11065	-2.68118	-4.05251
C	1.70188	-4.68884	-1.95337
C	0.67309	-3.39618	-3.77994
F	1.66748	-1.29720	0.11036

H	2.13385	-1.80660	-3.64103
C	-1.46086	-5.45782	0.46815
H	2.13713	-2.63103	-5.19317
C	2.05724	-2.79472	-4.11196
H	2.14847	-4.54165	2.43583
C	0.89231	-6.04821	0.04997
H	1.43918	-6.69670	0.74290
H	4.19387	-3.13636	-3.79228
H	3.28694	-6.60881	-4.17493
C	3.24664	-3.65805	-3.62631
C	0.51410	-3.79715	-2.29455
C	5.23786	-2.67398	0.56249
C	3.22963	-5.39919	-0.35838
H	5.11717	-2.95937	3.97648
H	3.81197	-2.49061	2.89767
H	5.73201	-5.31512	-0.57298
H	4.89685	-0.46150	3.71856
H	6.48879	-1.05361	3.26769
C	5.47845	-3.40806	1.87684
C	5.43032	-1.05766	2.96991
H	5.80295	0.59095	1.58770
C	5.36122	-4.53051	-1.23500
H	4.25377	-0.22295	1.31828
C	5.30452	-0.38412	1.58302
H	2.91975	-2.95583	-1.62957
H	4.98915	-4.38647	1.87976
H	4.15703	-2.47788	0.47093
H	7.00427	-1.49938	0.91694
C	5.96295	-1.32650	0.58341
C	6.01624	-2.17929	-1.57194
C	4.90413	-2.51030	2.99918
C	4.02333	0.60742	-3.27280
C	6.64240	0.18904	-1.34986
H	1.96239	2.59059	-3.70871
H	2.56013	3.10147	-5.28002
C	5.02304	1.60947	-2.70940
H	3.36502	4.57577	-3.37548
H	4.71951	3.84182	-4.25085
C	3.43214	1.24767	-4.55065
C	3.85445	3.62589	-3.60941
H	3.42358	2.66520	-1.74493
H	4.51378	-0.34131	-3.51338
C	4.31653	2.91595	-2.34151
C	6.04784	2.52103	-0.84053
H	7.05719	-0.07114	-2.32989
H	4.21900	1.29197	-5.31729
H	3.23780	0.40755	-2.53513
H	6.05359	4.94957	-0.19465
H	5.12724	5.60747	-1.57366
C	5.16555	4.82227	-0.81641
C	2.86905	2.66813	-4.32152
C	3.76700	3.04668	3.32027
H	5.45221	3.43097	1.97875
H	0.58566	4.47580	2.83720
H	1.19287	3.05195	1.97550
C	4.52879	3.92348	2.29755
H	2.62357	5.74806	2.17428
C	2.31727	4.85834	1.59107
H	2.53890	4.53355	4.31539
C	2.82357	5.54781	-0.56358
H	0.40786	6.71114	1.08729
H	4.38228	2.90586	4.21681
H	0.64223	6.70092	-0.68886
C	0.54624	6.07552	0.20565
H	3.29005	3.14850	0.73627
H	1.87273	2.90784	4.37022
H	3.61368	2.05337	2.88133
H	-1.48565	5.57812	-1.76277

C	-1.14106	4.71933	-1.15540
H	-3.96168	5.30068	2.04127
N	5.73354	-3.22985	-0.70356
H	-9.04770	2.12654	-2.70880
C	-10.31275	0.47997	-3.04977
C	-2.57890	3.33908	4.00637
C	-3.97493	4.53696	1.26148
H	-3.15549	-0.63992	3.90714
H	-1.89644	0.12879	2.92419
H	-3.44448	3.53126	4.65480
C	-2.68420	0.31815	3.66126
H	-4.45293	1.50077	3.89401
H	-2.13744	2.39788	2.13383
C	-3.70557	1.30011	3.10284
C	-4.76010	2.20217	1.24494
O	-10.88637	-0.23628	-2.25760
H	-0.66318	2.34566	4.08652
H	-1.26012	2.83780	5.66462
H	-6.97028	-1.33448	-0.09034
C	-4.20817	-1.31822	-0.20986
H	-7.27227	-1.12947	-3.12050
C	-8.08707	0.39764	-1.80084
H	-4.20270	3.13847	-1.53038
C	-2.49907	2.81029	-2.86120
N	-0.62826	5.23435	0.11406
N	1.77300	5.31602	0.31262
C	-3.30145	3.66773	-1.85356
H	-3.61585	4.61522	-2.31196
N	-3.97284	-3.36495	0.95663
N	-4.76389	-1.28902	1.13388
O	-5.55622	2.33162	0.31489
H	0.06271	2.95328	-1.48869
H	-3.09985	2.63782	-3.76179
H	-2.31988	1.82370	-2.41470
H	-1.32177	4.32420	-3.87312
C	-1.14124	3.43203	-3.25610
H	0.61754	4.38045	-2.37969
H	-0.58864	2.72715	-0.88677
C	-0.27133	3.83685	-2.04242
O	6.82887	2.66468	0.09891
O	-1.92723	-5.97093	-0.54797
O	-1.64594	6.00702	2.06577
O	2.74909	6.14156	-1.63868
N	-2.80780	4.79219	0.43859
O	6.25819	-2.27666	-2.77441
O	3.71483	-6.01462	0.59025
N	5.32035	3.53089	-1.46490
N	-2.19276	-4.94609	1.53844
N	5.74889	1.32206	-1.47365
N	3.97455	4.99876	-0.00505
C	-1.68715	5.40747	0.99220
N	5.99086	-0.99923	-0.84120
C	-2.37130	3.94362	-0.67824
N	1.87685	-5.20919	-0.59810
C	2.39008	3.62132	3.71934
N	-4.05683	3.22016	1.87149
H	-2.02564	2.97642	-0.27958
C	1.49352	3.96082	2.50554
N	-0.11639	-5.29021	0.75772
N	-4.42633	0.99931	1.86403
N	3.93847	-4.78124	-1.38575
F	-0.31515	1.25681	0.70076
F	1.19885	0.70852	-0.97157
F	1.87308	0.71424	1.24766
P	0.67500	-0.02146	0.39824
F	-0.52319	-0.75750	-0.44131
F	0.14477	-0.74874	1.77596

6. Anion Binding Studies

Anion binding was studied in solution by ITC, and via SPE of perchlorate using silica material functionalized with mixHC[8].

6.1 Isothermal Calorimetric Titration

The titration was carried out by addition of 0.5 μL or 0.7 μL portions of guest compound solution to mixHC[8] solution in the cell with 60 s or 90 s spacing. The heat of dilution was obtained by introduction of guest solution to the solvent (CH_3OH or $\text{CH}_3\text{OH} : \text{H}_2\text{O}$ 1 :1 mixture). The first smaller addition (0.4 μL) used to compensate diffusion of guest compound from the injector during system equilibration was discarded prior to fitting procedure. Before data analysis, the heat of dilution was subtracted from the corresponding total heat of the interaction. The obtained data was processed by MicroCal PEAQ-ITC analysis software (Malvern) and fitted using one set of sites binding model.

The complexation between mixHC[8] and NaSbF_6 was studied using reversed approach: mixHC[8] solution was placed in the cell and titrated by 1 μL additions of NaSbF_6 solution with 60 s spacing.²⁴

Table S25. Summary of ITC results for binding of anions to mixHC[8] (average values). For experimental error see results of particular titrations.

Guest	Solvent	(-)-mixHC[8]			(+) -mixHC[8]		
		K_a (M^{-1})	ΔH (kJ/mol)	$-T\Delta S$ (kJ/mol)	K_a (M^{-1})	ΔH (kJ/mol)	$-T\Delta S$ (kJ/mol)
(TBA) ClO_4	CH_3OH	$(4.60 \pm 0.05) \cdot 10^2$	-30.5 ± 0.4	15.3 ± 0.4	$(9.7 \pm 0.2) \cdot 10^2$	-33.8 ± 0.7	16.8 ± 0.6
	$\text{CH}_3\text{OH}:\text{H}_2\text{O}$ 50:50	$(1.90 \pm 0.03) \cdot 10^2$	-30.8 ± 0.3	17.8 ± 0.3	$(4.56 \pm 0.02) \cdot 10^2$	-40.7 ± 0.8	25.5 ± 0.8
(TBA) PF_6	CH_3OH	$(1.05 \pm 0.07) \cdot 10^4$	-38.5 ± 0.6	15.6 ± 0.4	$(1.59 \pm 0.04) \cdot 10^4$	-41.7 ± 0.5	17.6 ± 0.6
	$\text{CH}_3\text{OH}:\text{H}_2\text{O}$ 50:50	$(0.63 \pm 0.02) \cdot 10^4$	-44 ± 2	22 ± 2	$(1.4 \pm 0.3) \cdot 10^4$	-60.3 ± 0.5	37 ± 1
NaSbF_6	CH_3OH	$(2.7 \pm 0.2) \cdot 10^4$	-41.5 ± 0.7	25.3 ± 0.2	$(3.7 \pm 0.4) \cdot 10^4$	-41 ± 1	26.1 ± 0.2
MgSO_4	$\text{CH}_3\text{OH}:\text{H}_2\text{O}$ 50:50	N/A	–	–	N/A	–	–

(TBA)ClO₄ binding to (–)-mixHC[8] in CH₃OH

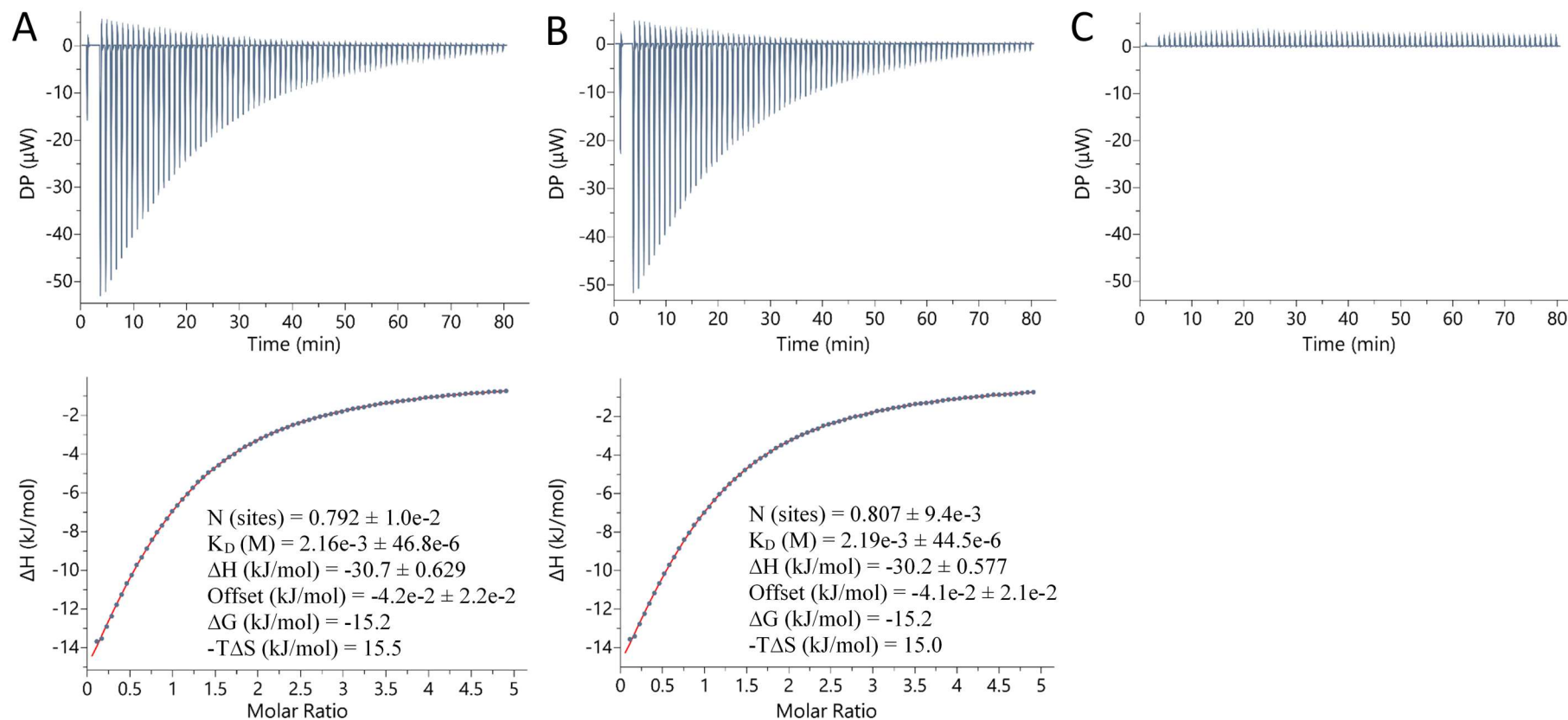


Figure S41. ITC of (TBA)ClO₄ binding to (–)-mixHC[8] in CH₃OH at 298 K (A, B) and control experiment (C). *Top:* Data obtained from the sequential injections of 0.5 μL of (TBA)ClO₄ (60.0 mM) to (–)-mixHC[8] (2.5 mM) (A,B) or to the pure solvent (C) with 60 s spacing. *Bottom:* Plot of the total heat released as a function of total guest concentration for the titration shown in the upper panel. The red solid line represents least-squares fit of the data.

(TBA)ClO₄ binding to (-)-mixHC[8] in CH₃OH:H₂O 1:1 mixture

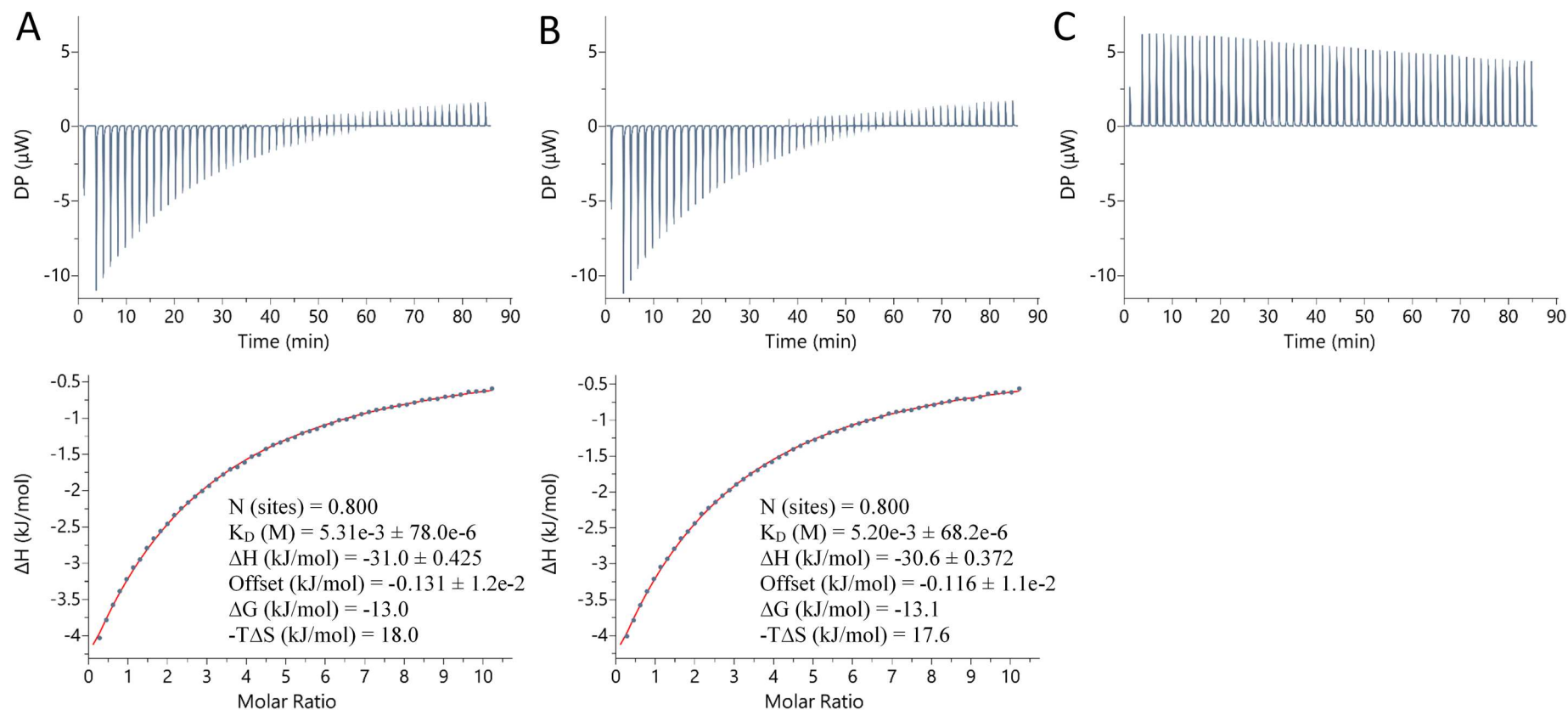


Figure S42. ITC of (TBA)ClO₄ binding to (-)-mixHC[8] in CH₃OH : H₂O 1:1 mixture at 298 K (A, B) and control experiment (C). *Top:* Data obtained from the sequential injections of 0.7 μL of (TBA)ClO₄ (50.0 mM) to (-)-mixHC[8] (1.0 mM) (A,B) or to the pure solvent mixture (C) with 90 s spacing. *Bottom:* Plot of the total heat released as a function of total guest concentration for the titration shown in the upper panel. The red solid line represents least-squares fit of the data.

(TBA)PF₆ binding to (–)-mixHC[8] in CH₃OH

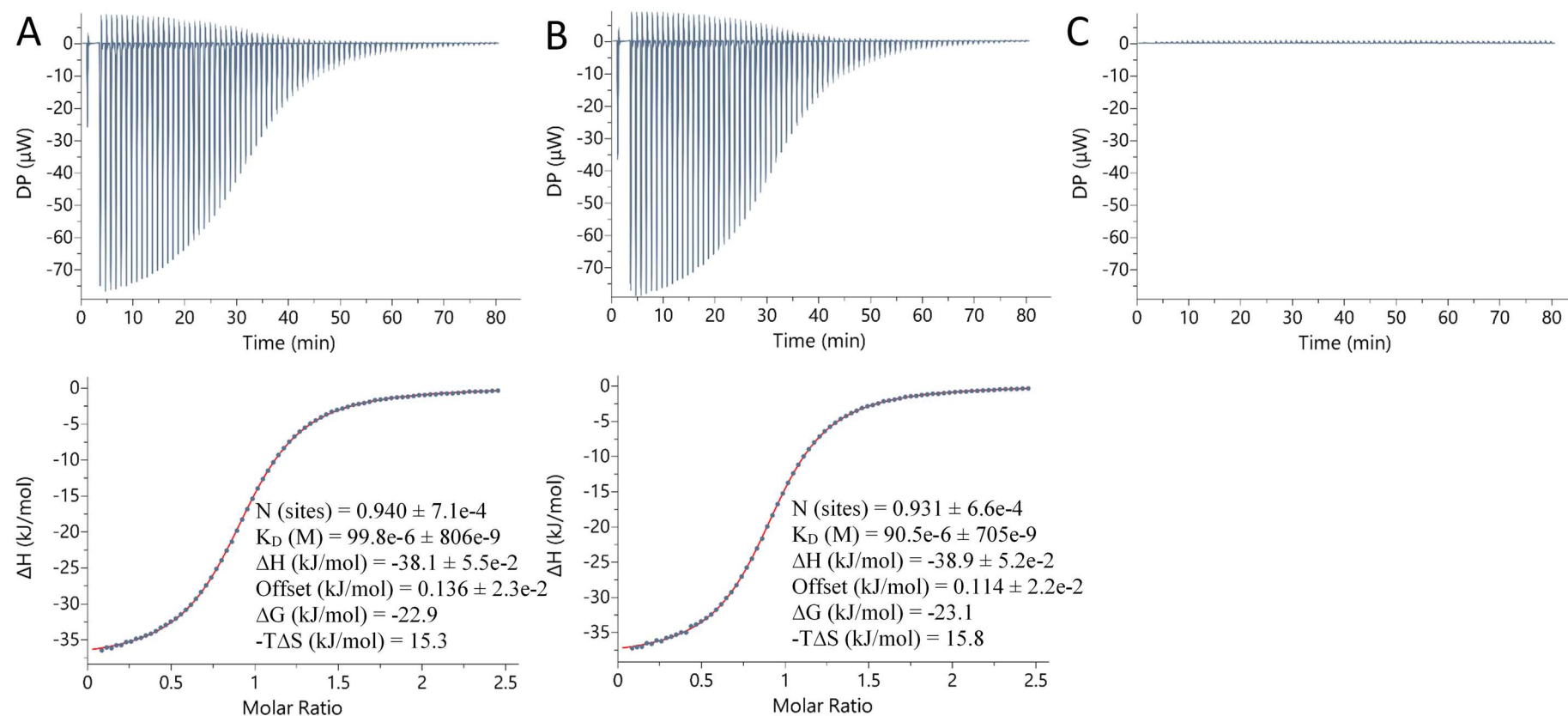


Figure S43. ITC of (TBA)PF₆ binding to (–)-mixHC[8] in CH₃OH at 298 K (A, B) and control experiment (C). *Top:* Data obtained from the sequential injections of 0.5 μL of (TBA)PF₆ (30.0 mM) to (–)-mixHC[8] (1.00 mM) (A,B) or to the pure solvent mixture (C) with 60 s spacing.

Bottom: Plot of the total heat released as a function of total guest concentration for the titration shown in the upper panel. The red solid line represents least-squares fit of the data.

(TBA)PF₆ binding to (-)-mixHC[8] in CH₃OH:H₂O 1:1 mixture

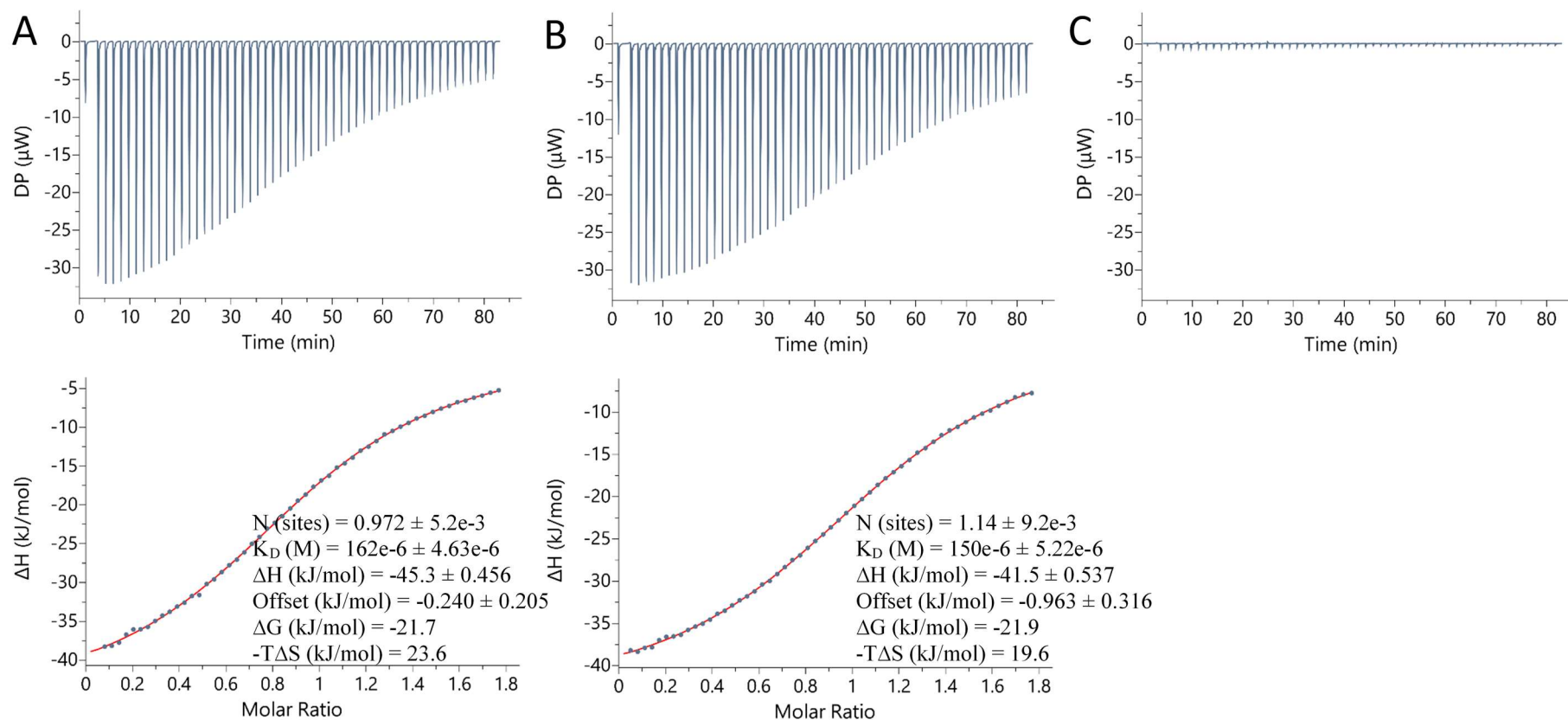


Figure S44. ITC of (TBA)PF₆ binding to (-)-mixHC[8] in CH₃OH : H₂O 1:1 mixture at 298 K (A, B) and control experiment (C). *Top:* Data obtained from the sequential injections of 0.7 μL of (TBA)PF₆ (9.0 mM) to (-)-mixHC[8] (1.0 mM) (A,B) or to the pure solvent mixture (C) with 90 s spacing. *Bottom:* Plot of the total heat released as a function of total guest concentration for the titration shown in the upper panel. The red solid line represents least-squares fit of the data. Note: subtracted dilution heat (C) is negligible in comparison to heat produced by complexation event.

(-)-mixHC[8] binding to NaSbF₆ in CH₃OH

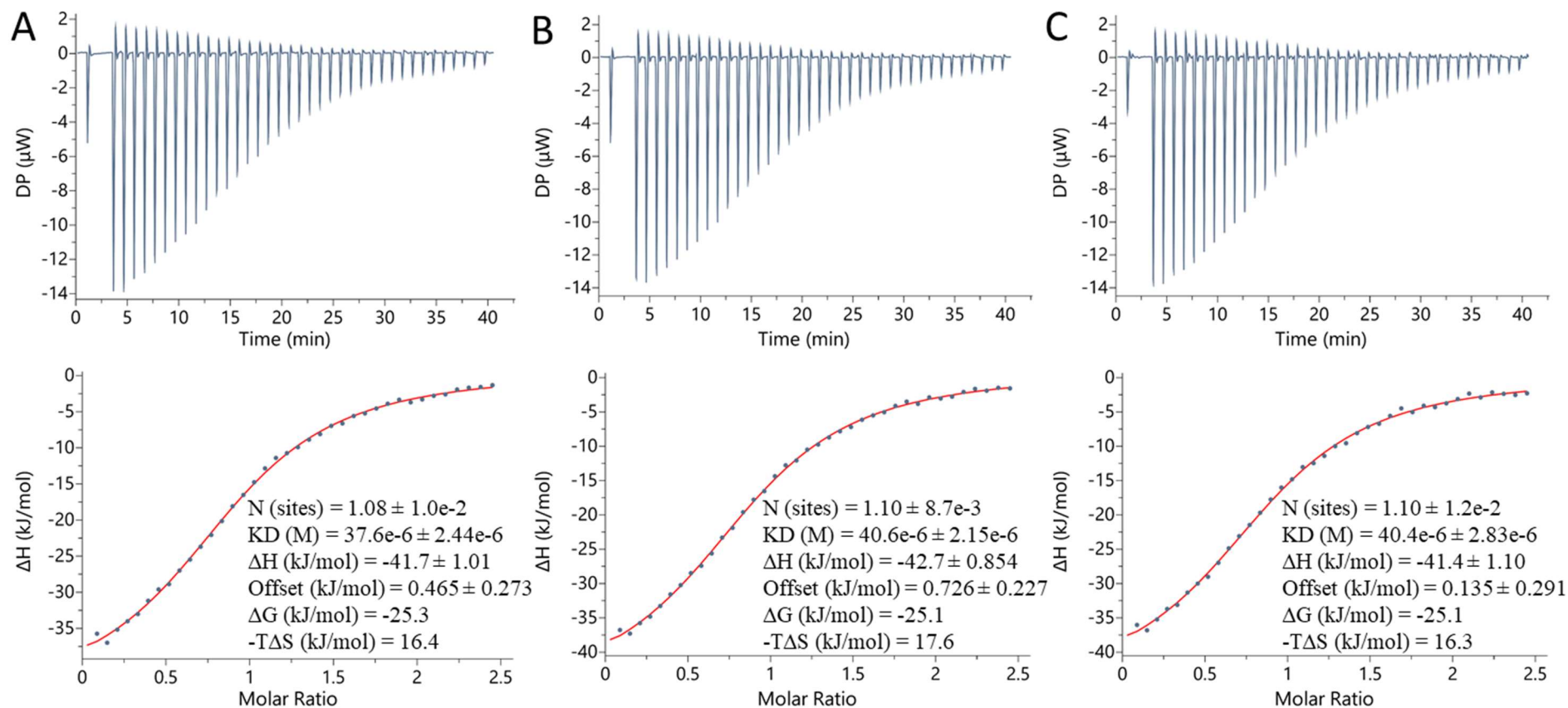


Figure S45. ITC of (-)-mixHC[8] binding to NaSbF₆ in CH₃OH at 298 K (A, B, C – parallel titrations). Top: Data obtained from the sequential injections of 1 μL of (-)-mixHC[8] (2.5 mM) to NaSbF₆ (0.2 mM) with 60 s spacing. Bottom: Plot of the total heat released as a function of total guest concentration for the titration shown in the upper panel. The red solid line represents least-squares fit of the data.

(-)-mixHC[8] binding to NaSbF₆ in CH₃OH

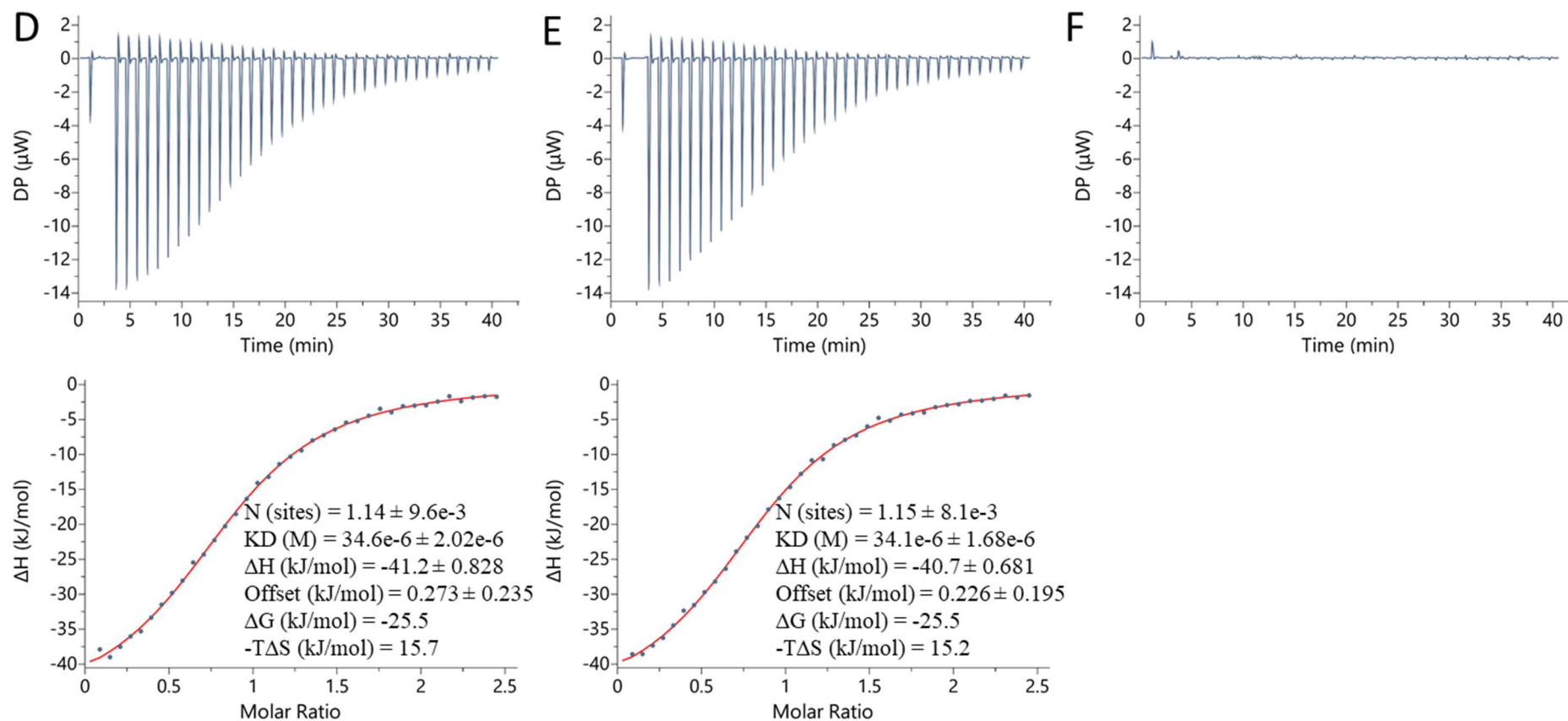


Figure S46. ITC of (-)-mixHC[8] binding to NaSbF₆ in CH₃OH at 298 K (D, E) and control experiment (F). Top: Data obtained from the sequential injections of 1 μL of (-)-mixHC[8] (2.5 mM) to NaSbF₆ (0.2 mM) (D, E) or to the pure solvent (F) with 60 s spacing. Bottom: Plot of the total heat released as a function of total guest concentration for the titration shown in the upper panel. The red solid line represents least-squares fit of the data.

MgSO₄ binding to (–)-mixHC[8] in CH₃OH:H₂O 1:1 mixture

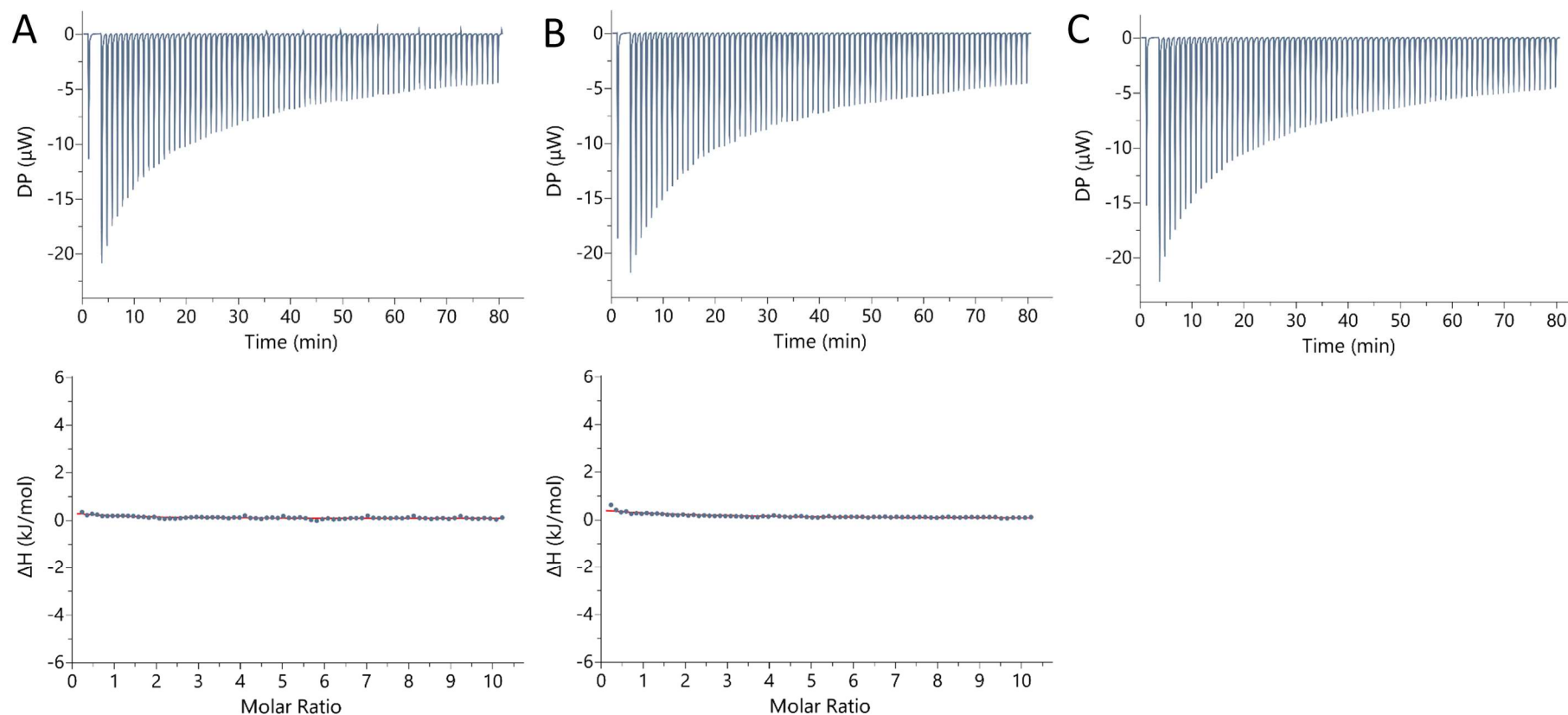


Figure S47. ITC of MgSO₄ binding to (–)-mixHC[8] in CH₃OH : H₂O 1:1 mixture at 298 K (A, B) and control experiment (C). *Top:* Data obtained from the sequential injections of 0.5 μL of MgSO₄ (50.0 mM) to (–)-mixHC[8] (1.1 mM) (A,B) or to the pure solvent mixture (C) with 60 s spacing. *Bottom:* Plot of the total heat released as a function of total guest concentration for the titration shown in the upper panel. The red solid line represents least-squares fit of the data.

(TBA)ClO₄ binding to (+)-mixHC[8] in CH₃OH

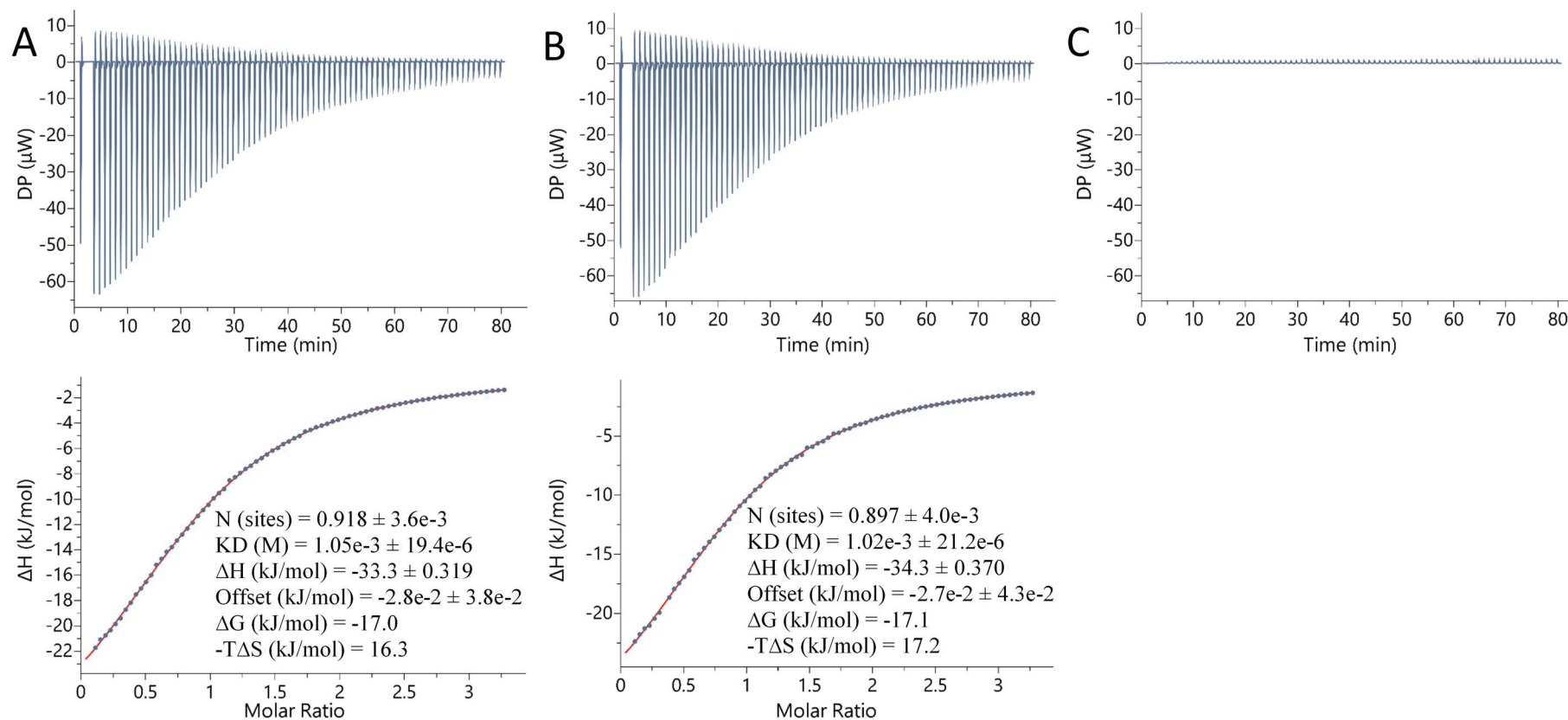


Figure S48. ITC of (TBA)ClO₄ binding to (+)-mixHC[8] in CH₃OH at 298 K (A, B) and control experiment (C). *Top:* Data obtained from the sequential injections of 0.5 μ L of (TBA)ClO₄ (40.0 mM) to (+)-mixHC[8] (2.6 mM) (A,B) or to the pure solvent mixture (C) with 60 s spacing. *Bottom:* Plot of the total heat released as a function of total guest concentration for the titration shown in the upper panel. The red solid line represents least-squares fit of the data.

(TBA)ClO₄ binding to (+)-mixHC[8] in CH₃OH:H₂O 1:1 mixture

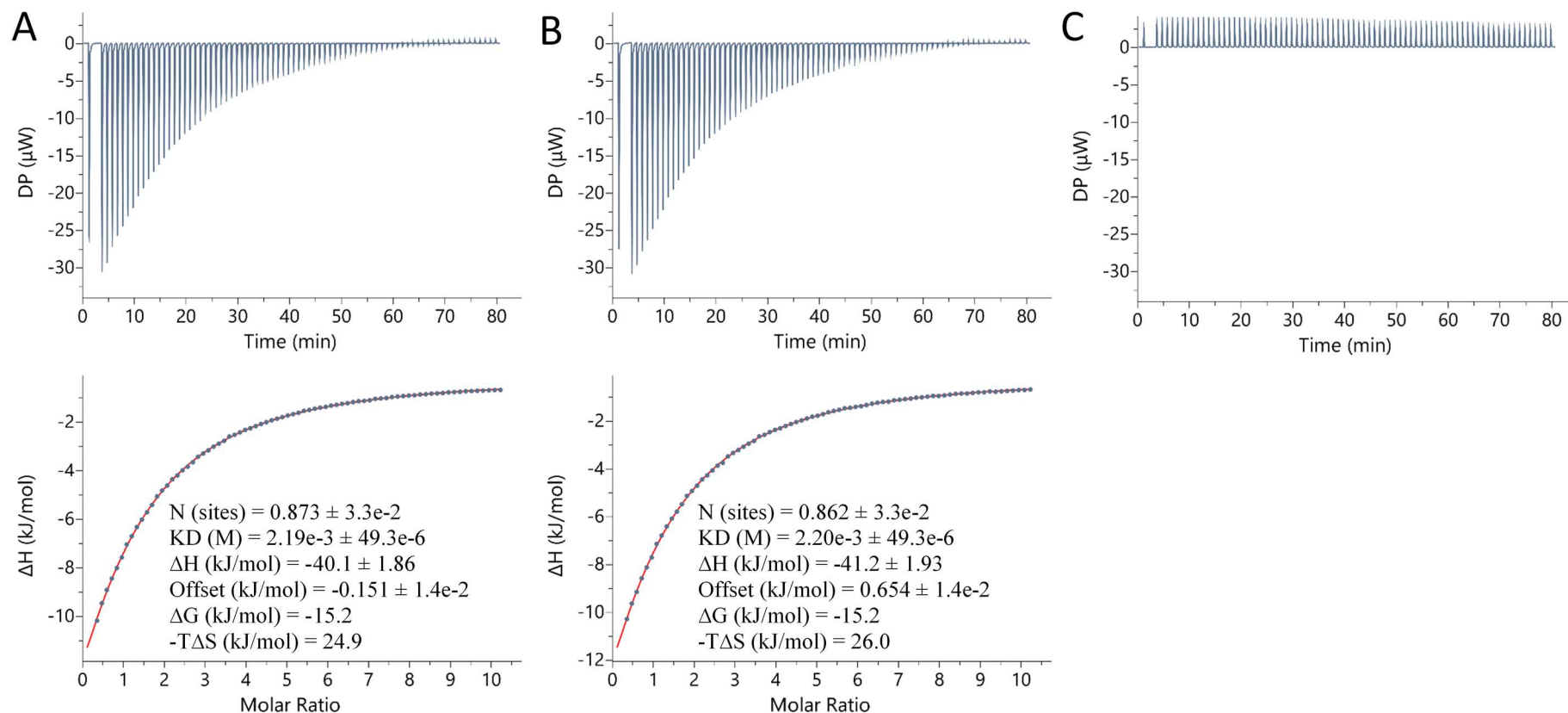


Figure S49. ITC of (TBA)ClO₄ binding to (+)-mixHC[8] in CH₃OH : H₂O 1:1 mixture at 298 K (A, B) and control experiment (C). *Top:* Data obtained from the sequential injections of 0.5 μL of TBAClO₄ (50.0 mM) to (+)-mixHC[8] (1.1 mM) (A,B) or to the pure solvent mixture (C) with 60 s spacing. *Bottom:* Plot of the total heat released as a function of total guest concentration for the titration shown in the upper panel. The red solid line represents least-squares fit of the data.

(TBA)PF₆ binding to (+)-mixHC[8] in CH₃OH

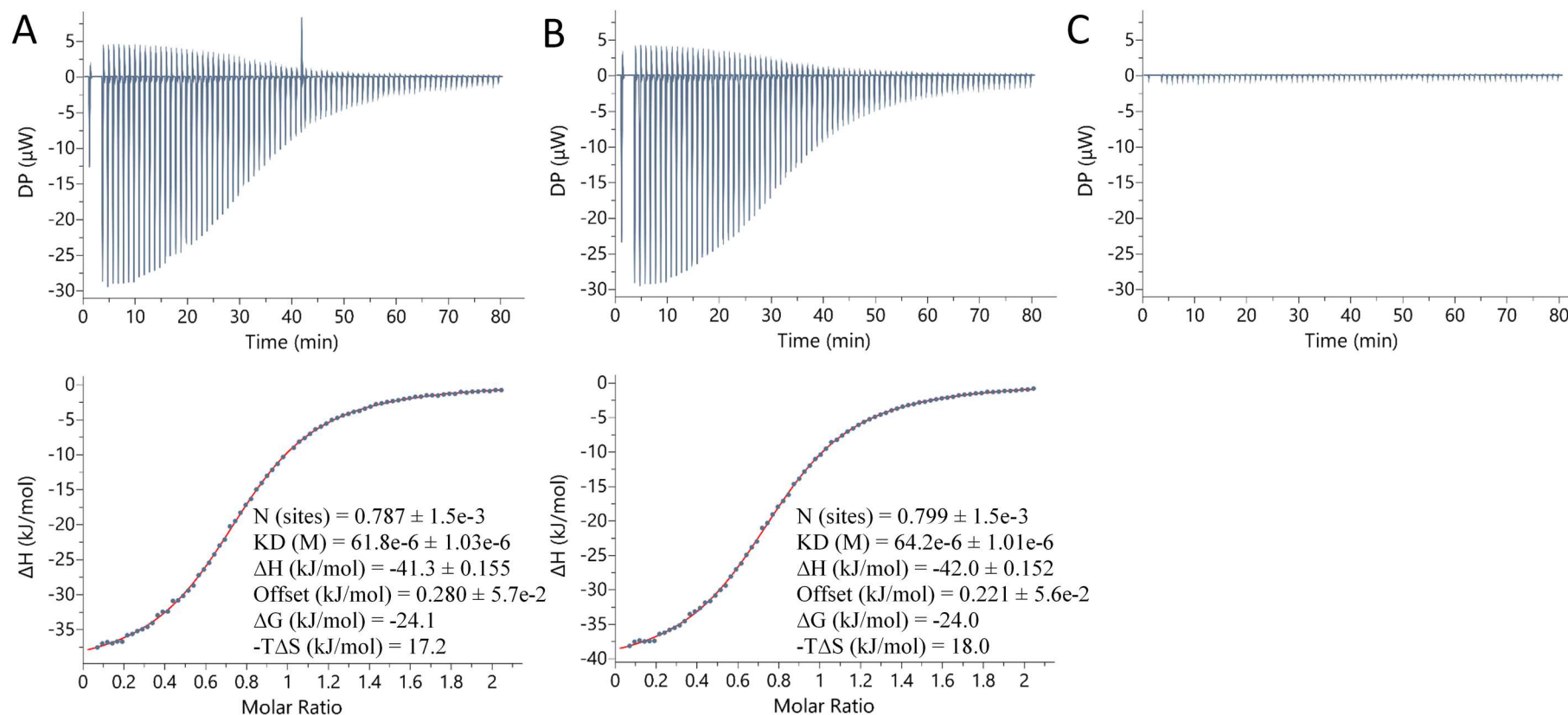


Figure S50. ITC of (TBA)PF₆ binding to (+)-mixHC[8] in CH₃OH at 298 K (A, B) and control experiment (C). *Top:* Data obtained from the sequential injections of 0.5 μL of (TBA)PF₆ (10.0 mM) to (+)-mixHC[8] (1.1 mM) (A,B) or to the pure solvent mixture (C) with 60 s spacing. *Bottom:* Plot of the total heat released as a function of total guest concentration for the titration shown in the upper panel. The red solid line represents least-squares fit of the data.

(TBA)PF₆ binding to (+)-mixHC[8] in CH₃OH:H₂O 1:1 mixture

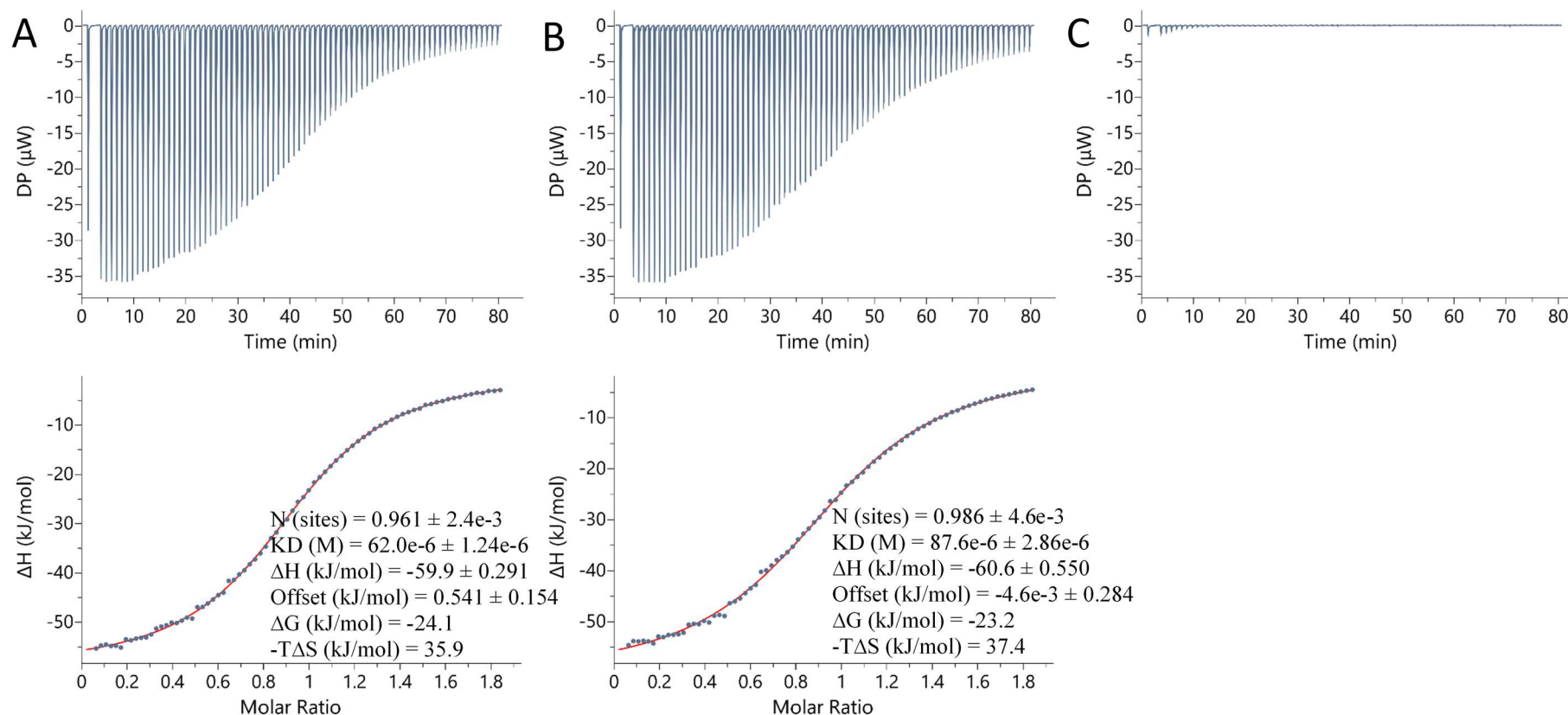


Figure S51. ITC of (TBA)PF₆ binding to (+)-mixHC[8] in CH₃OH : H₂O 1:1 mixture at 298 K (A, B) and control experiment (C). *Top:* Data obtained from the sequential injections of 0.5 μL of (TBA)PF₆ (9.0 mM) to (+)-mixHC[8] (1.1 mM) (A,B) or to the pure solvent mixture (C) with 60 s spacing. *Bottom:* Plot of the total heat released as a function of total guest concentration for the titration shown in the upper panel. The red solid line represents least-squares fit of the data.

(+)-mixHC[8] binding to NaSbF₆ in CH₃OH

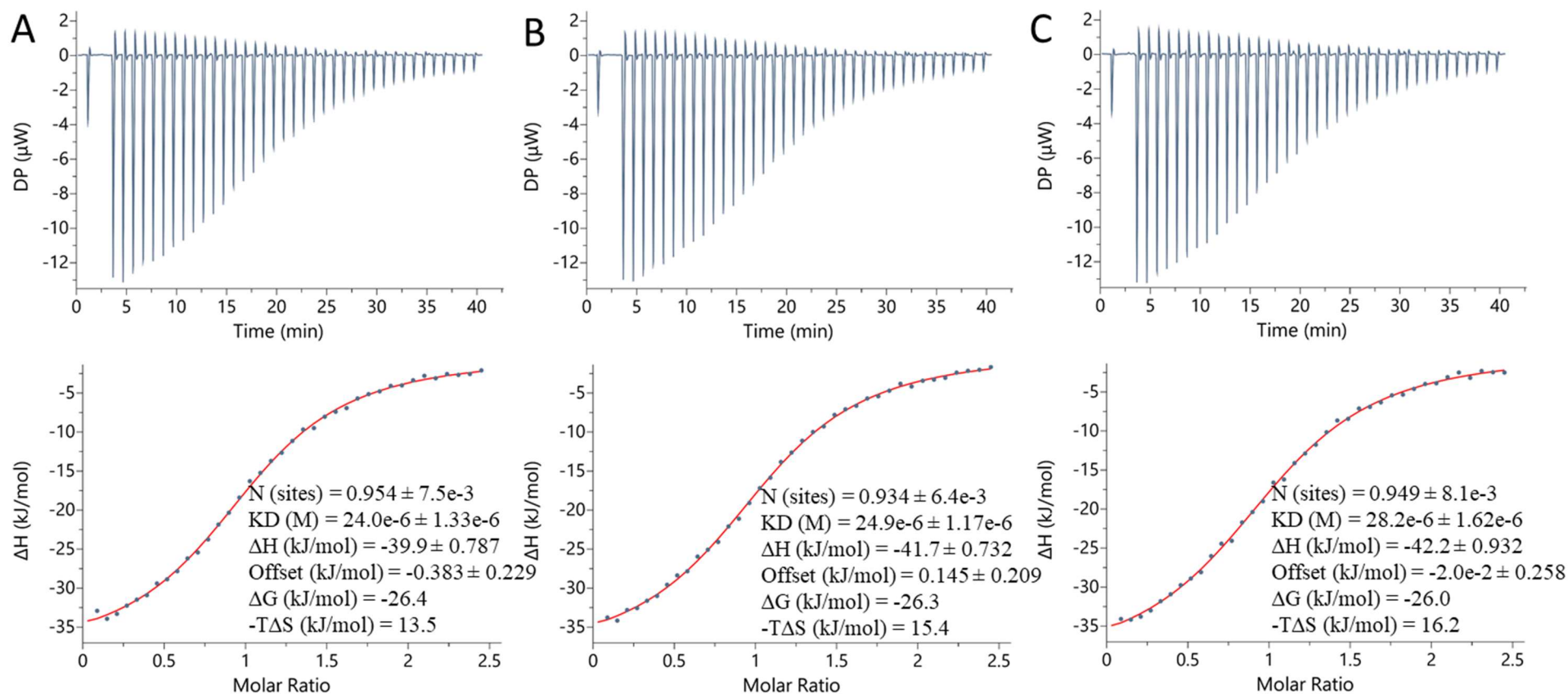


Figure S52. ITC of (+)-mixHC[8] binding to NaSbF₆ in CH₃OH at 298 K (A, B, C – parallel titrations). Top: Data obtained from the sequential injections of 1 μ L of (+)-mixHC[8] (2.5 mM) to NaSbF₆ (0.2 mM) with 60 s spacing. Bottom: Plot of the total heat released as a function of total guest concentration for the titration shown in the upper panel. The red solid line represents least-squares fit of the data.

(+)-mixHC[8] binding to NaSbF₆ in CH₃OH

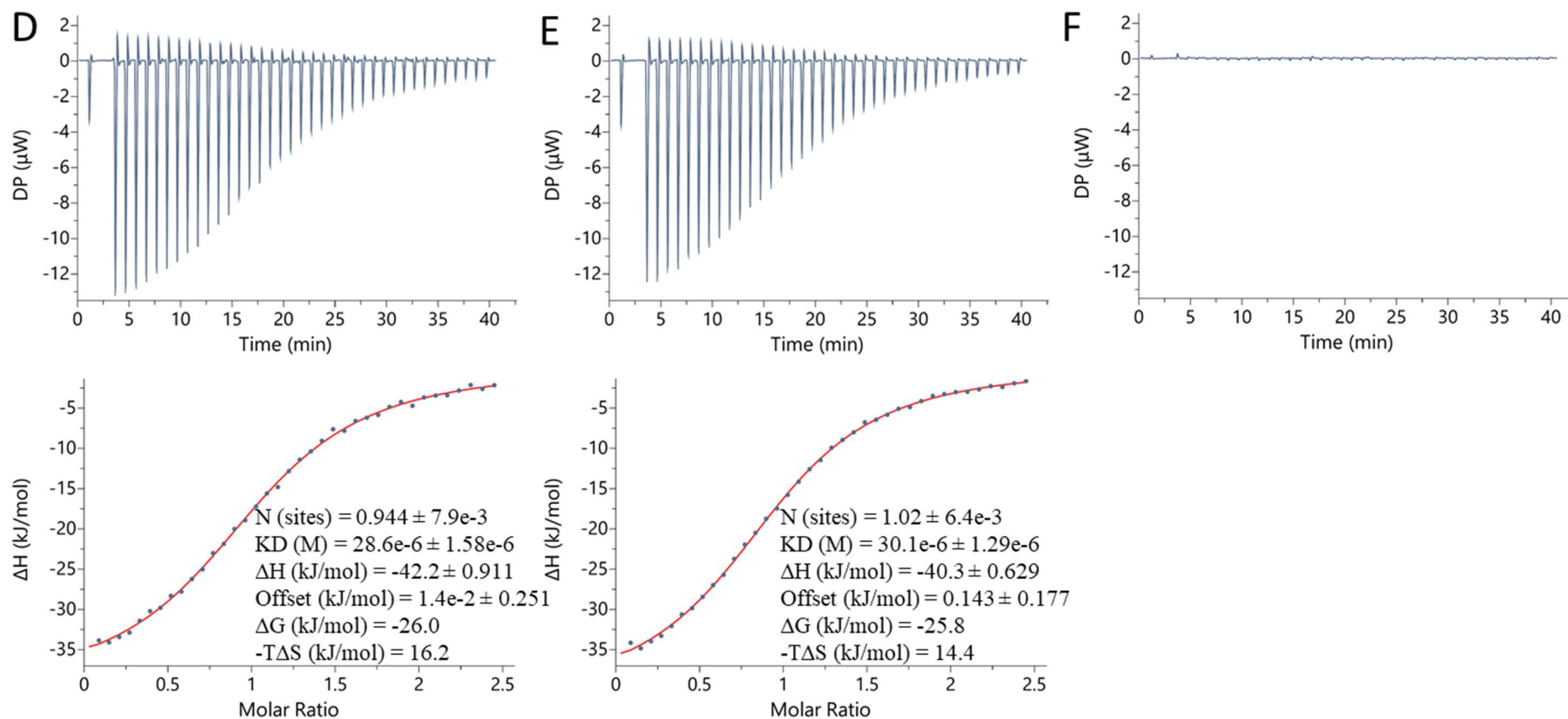


Figure S53. ITC of (+)-mixHC[8] binding to NaSbF₆ in CH₃OH at 298 K (D, E) and control experiment (F). Top: Data obtained from the sequential injections of 1 μL of (+)-mixHC[8] (2.5 mM) to NaSbF₆ (0.2 mM) (D, E) or to the pure solvent (F) with 60 s spacing. Bottom: Plot of the total heat released as a function of total guest concentration for the titration shown in the upper panel. The red solid line represents least-squares fit of the data.

MgSO₄ binding to (+)-mixHC[8] in CH₃OH:H₂O 1:1 mixture

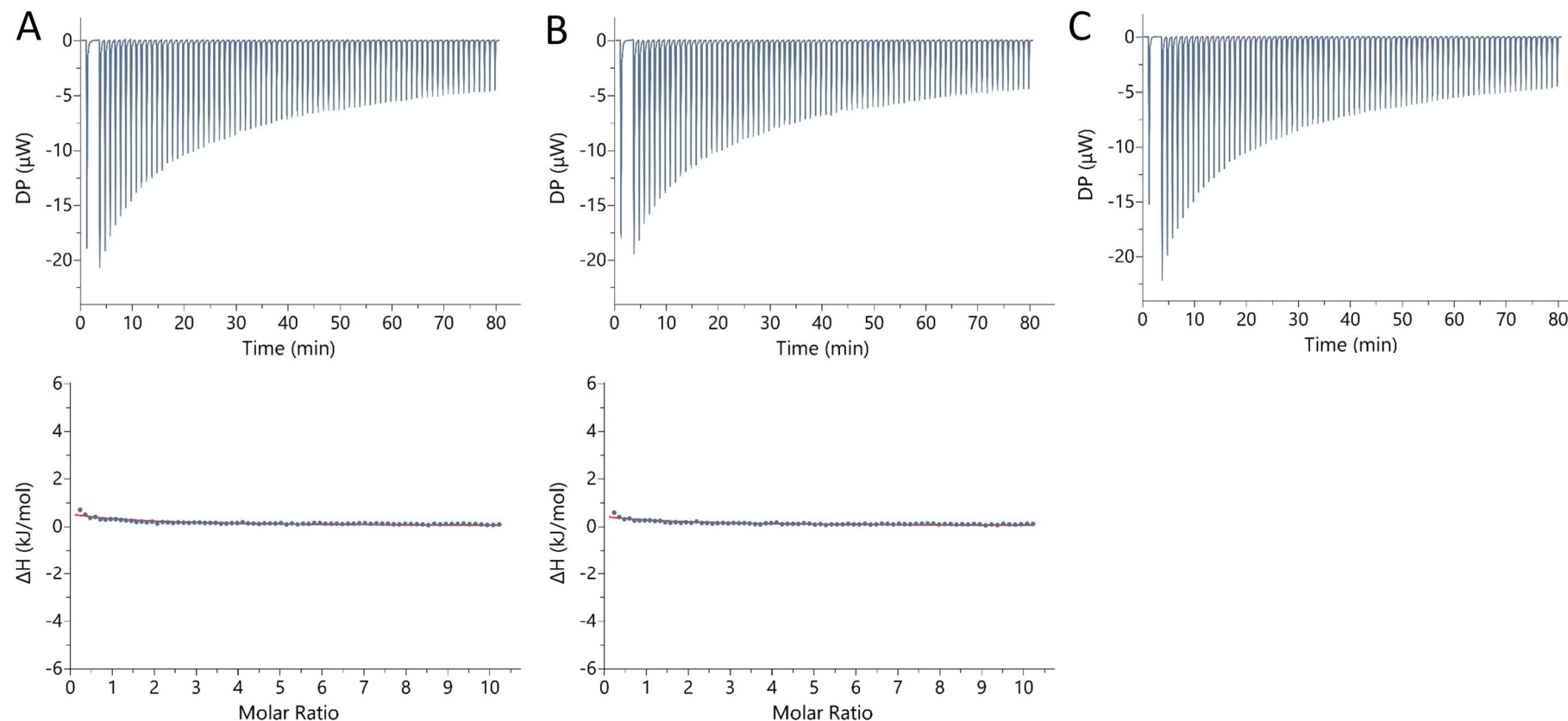


Figure S54. ITC of MgSO₄ binding to (+)-mixHC[8] in CH₃OH : H₂O 1:1 mixture at 298 K (A, B) and control experiment (C). *Top:* Data obtained from the sequential injections of 0.5 μL of MgSO₄ (50.0 mM) to (+)-mixHC[8] (1.1 mM) (A,B) or to the pure solvent mixture (C) with 60 s spacing. *Bottom:* Plot of the total heat released as a function of total guest concentration for the titration shown in the upper panel. The red solid line represents least-squares fit of the data.

6.2 Immobilization of mixHC[8] on APS

APS (49.9 mg, corresponding to 0.050 mmol NH_2 -groups, 1 eq.), (–)-mixHC[8] (82.0 mg, 0.056 mmol, 1.1 eq.), DIC (7.9 μl [6.4 mg, P=99%], 0.050 mmol, 1 eq.) and 10 ml DCM were placed into 25 ml round bottom flask. The mixture was stirred at 700 rpm and 50 °C under argon atmosphere with reflux for 7 days. To wash the product (mixHC[8]-APS), the reaction mixture was transferred on the cotton placed into a glass Pasteur pipette. The solid was filtered out and rinsed with 5×1 ml DCM and additional 0.5 ml DCM. The last portion of DCM after rinsing was analyzed by HPLC and no peaks belonging to the macrocycle were detected. The solid product was dried with air, transferred into the vial and dried on rotovap, final weight: 43.1 mg.

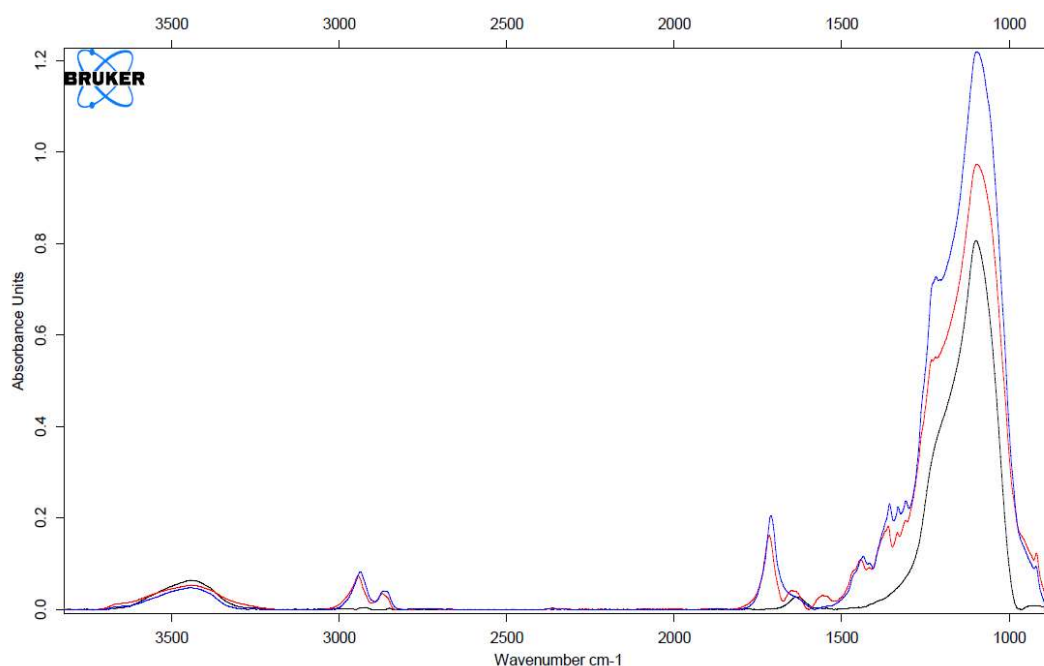


Figure S55. IR absorption spectra of APS (black), mixHC[8]-APS (red) and mixHC[8] + APS reference mixture (blue). Rough quantitation based on the carbonyl peak (1711 cm^{-1}) absorption provided mixHC[8] loading on modified APS ca. 12% by mass.

The obtained mixHC[8]-APS was tested for leaching: the solid material was stirred in methanol, which was further analyzed by HPLC-UV-MS and no macrocycle was detected.

6.3 Removal of Perchlorate from Methanol Solutions

General extraction procedure

Solid sorbent (mixHC[8]-APS or non-modified APS) was dispersed in guest methanol solution and stirred on orbital shaker for 60 min. The supernatant was filtered and clear filtrate was analysed for the guest content by IC.

Removal percentage (R , %) of the guest upon extraction was calculated using formula (3):

$$R(\%) = \frac{S_0 - S_i}{S_0} \cdot 100 \quad (3)$$

where S_0 – guest peak area in reference solution in the absence of host, $\mu\text{S}/\text{cm}$; S_i – guest peak area in experimental solution (mixed with solid host and filtered), $\mu\text{S}/\text{cm}$.

Removal experiments

The removal experiments were carried out for solid-phase extraction of ClO_4^- from its individual solution (*a*), as well as from its mixture with SO_4^{2-} (selectivity studies, *b*) and in presence of complex matrix – MGS-1 (*c*).

Table S26. Exolith Mars Global Soil Simulant (MGS-1) mineralogy^{25,26}

Mineral	Wt. %
Anorthosite	27.1
Glass-rich basalt	22.9
Pyroxene (Bronzite)	20.3
Olivine	13.7
Mg-sulfate	4.0
Ferrihydrite	3.5
Hydrated silica	3.0
Magnetite	1.9
Anhydrite	1.7
Fe-carbonate	1.4
Hematite	0.5

Stock solution of guest compound. 5 mg/L ClO_4^- in methanol (*a*); 5 mg/L ClO_4^- + 4 mg/L SO_4^{2-} in methanol (*b*); 495 mg MGS-1 + 17 mg (TBA) ClO_4 (corresponding to 5 mg ClO_4^- , or 1% by mass) was stirred in 5 ml methanol on orbital shaker for 60 min, the solution was then filtered and diluted 200 times providing ca. 4–5 mg/L ClO_4^- in methanol (*c*).

Blank suspension ($\times 1$) of host compound. 5 mg mixHC[8]-APS or non-modified APS in 2 ml methanol.

Reference solution ($\times 2$). 2 ml of stock solution.

Experimental suspension ($\times 2$). 5 mg mixHC[8]-APS or non-modified APS and 2 ml of stock solution.

Reference solution and blank and experimental suspensions were each placed into a 4 ml vial and stirred on orbital shaker at 500 rpm for 1 hr. The samples were then filtered through Minisart RC 13 mm, 0.45 μm syringe filter. The clear filtrate was analysed for the ionic content by IC.

IC analysis

IC analysis was performed on 761 Compact IC ion chromatograph with chemical suppression of eluent conductivity (Metrohm Ltd) using METROSEP A Supp 5 column (150 mm \times 4.0 mm). A mixture of 1.0 mM NaHCO_3 + 3.2 mM Na_2CO_3 was used as the mobile phase with the flow rate 0.7 ml/min; the samples were injected manually via 20 μl sampling loop.

For calibration studies, all solutions were filtered with Whatman FP 30 / 0.45 μM CA syringe filters. The samples were prepared and diluted with bi-distilled water.

Method linearity was investigated for a series of solutions of known concentrations.

ClO_4^- : 0.5 mg/L, 1 mg/L, 5 mg/L, 10 mg/L, 25 mg/L, 50 mg/L, 200 mg/L.

SO_4^{2-} : 0.01 mg/L, 0.05 mg/L, 0.1 mg/L, 0.5 mg/L, 1 mg/L, 6 mg/L, 10 mg/L, 12 mg/L, 30 mg/L, 60 mg/L, 120 mg/L.

Table S27. Analytical method characteristics.

Analyte	Linear regression	R^2	LoD, mg/L
ClO_4^-	$Y=5.1068x$	0.9995	0.5
SO_4^{2-}	$y = 14.588x$	0.9975	0.01

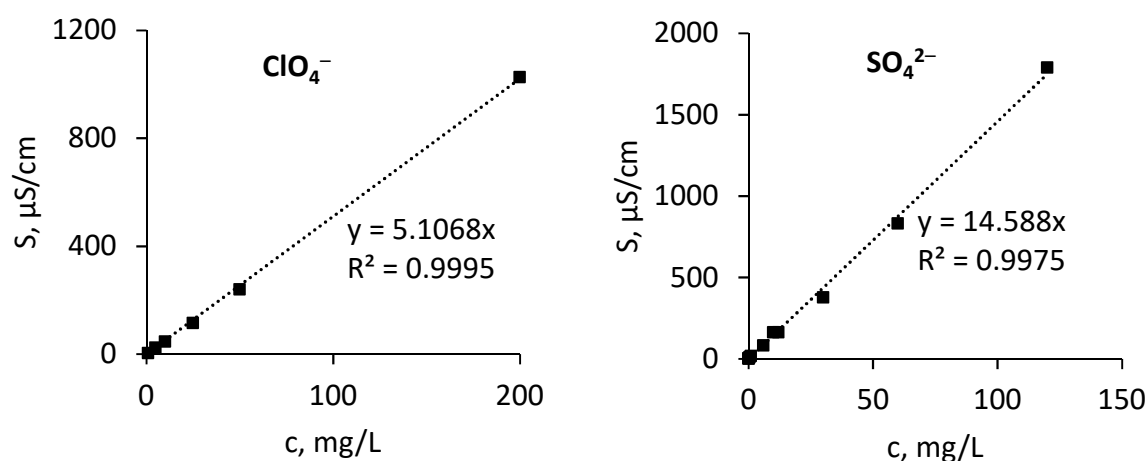


Figure S56. Calibration graph for determination of ClO_4^- and SO_4^{2-} concentration and linearity studies.

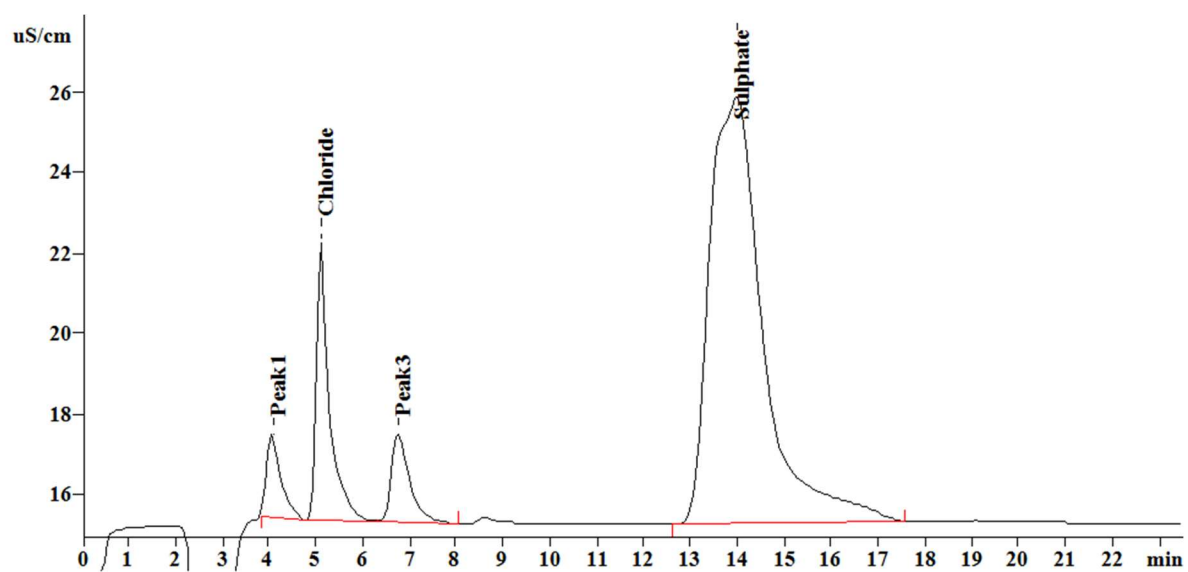


Figure S57. IC chromatogram of MGS-1 methanolic extract.

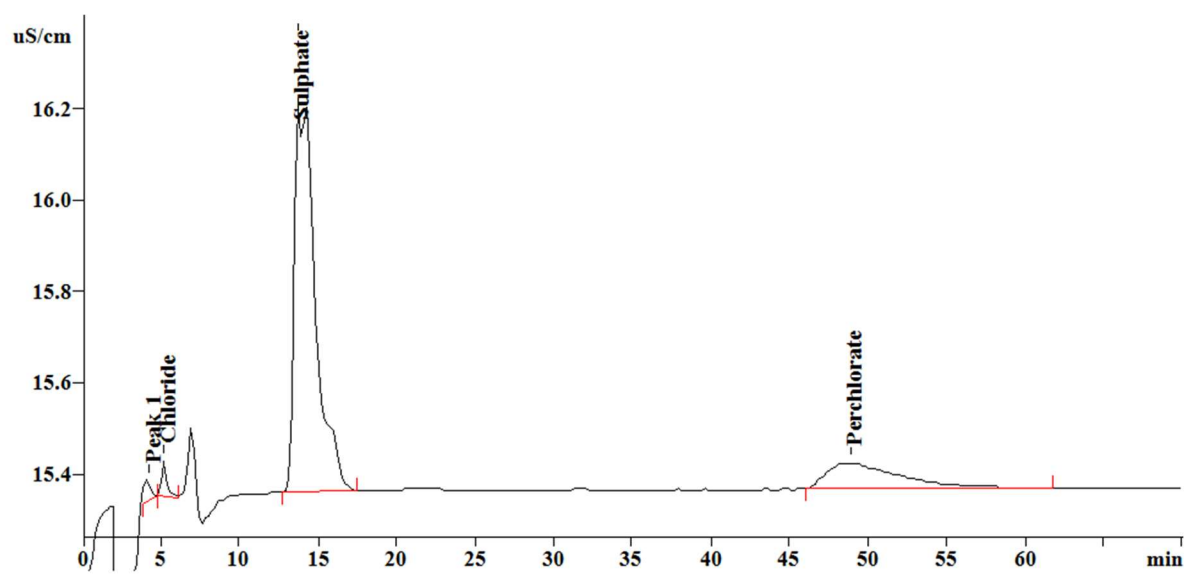


Figure S58. IC chromatogram of MGS-1 methanolic extract spiked with ClO_4^- .

Table S28. Removal of perchlorate and sulfate anions from methanol by 5 molar excess of mixHC[8], immobilized on APS, compared to non-modified APS.

Experiment	Guest	Host	m_{host} , mg	$n_{\text{mixHC[8]}}$, μmol	c_{guest} , mg/L	n_{guest} , μmol	R , % ^a
ClO ₄ ⁻ solution	ClO ₄ ⁻	mixHC[8]-APS	5.0	0.5	5.0	0.10	100±0
		APS		—			22±2
ClO ₄ ⁻ + SO ₄ ²⁻ solution (selectivity)	ClO ₄ ⁻	mixHC[8]-APS		0.5	4.9	0.10	100±0
		APS		—			14±2
	SO ₄ ²⁻	mixHC[8]-APS		0.5	3.8	0.08	97.3±0.1
		APS		—			89.5±0.3
MGS-1 + ClO ₄ ⁻ (spiked martian soil)	ClO ₄ ⁻	mixHC[8]-APS		0.5	4.7	0.09	100±0
		APS		—			15±2
	SO ₄ ²⁻	mixHC[8]-APS		0.5	6.4	0.13	96.7±0.5
		APS		—			85±1

[a] The average R value is provided as mean result ± standard deviation between parallel experiments ($n \geq 2$)

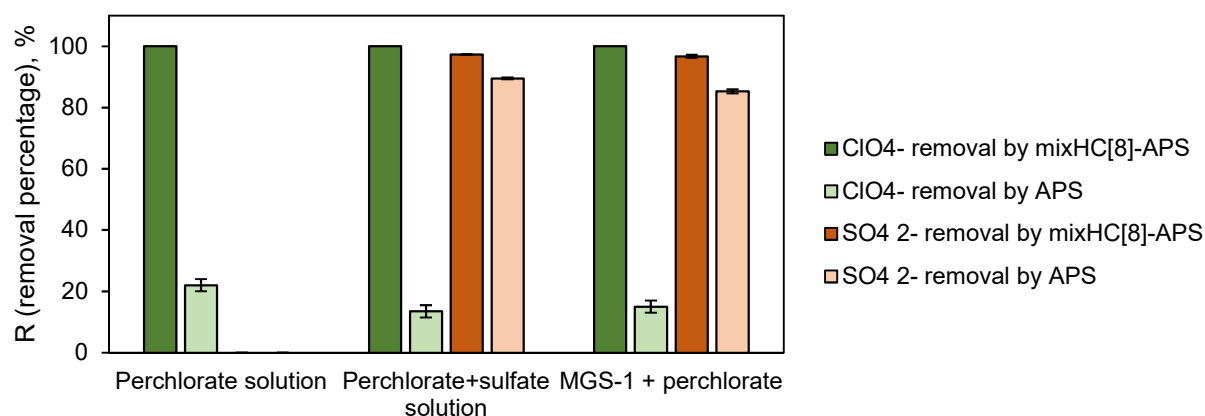


Figure 59. Removal percentage upon extraction of perchlorate and sulfate anions from methanol by mixHC[8]-APS and non-modified APS. The error bars represent standard deviation between parallel experiments ($n \geq 2$).

References

1. Aav, R., Shmatova, E., Reile, I., Borissova, M., Topić, F., & Rissanen, K. (2013). New chiral cyclohexylhemicucurbit[6]uril. *Organic Letters*, 15(14), 3786–3789. 10.1021/ol401766a.
2. Prigorchenko, E., Öeren, M., Kaabel, S., Fomitšenko, M., Reile, I., Järving, I., Tamm, T., Topić, F., Rissanen, K., & Aav, R. (2015). Template-controlled synthesis of chiral cyclohexylhemicucurbit[8]uril. *Chemical Communications*, 51(54), 10921–10924. 10.1039/C5CC04101E.
3. Fuentes de Arriba, Á. L., Seisdedos, D. G., Simón, L., Alcázar, V., Raposo, C., & Morán, J. R. (2010). Synthesis of monoacylated derivatives of 1,2-cyclohexanediamine: Evaluation of their catalytic activity in the preparation of Wieland–Miescher ketone. *Journal of Organic Chemistry*, 75(23), 8303–8306. 10.1021/jo101723v.
4. Stat-Ease. Understanding Lack of Fit: When to Worry. <https://www.statease.com/blog/understanding-lack-of-fit-when-to-worry/>
5. Kaabel, S., Stein, R. S., Fomitšenko, M., Järving, I., Friščić, T., & Aav, R. (2019). Size-control by anion templating in mechanochemical synthesis of hemicucurbiturils in the solid state. *Angewandte Chemie International Edition*, 58(19), 6230–6234. 10.1002/anie.201813431.
6. MatchMass. <https://matchmass.taltech.ee/>
7. Morpheus. <https://software.broadinstitute.org/morpheus/>
8. Fomitšenko, M., Peterson, A., Reile, I., Cong, H., Kaabel, S., Prigorchenko, E., Järving, I., & Aav, R. (2017). A quantitative method for analysis of mixtures of homologues and stereoisomers of hemicucurbiturils that allows us to follow their formation and stability. *New Journal of Chemistry*, 41(6), 2490–2497. 10.1039/C6NJ03050E.
9. Sheldrick, G. M. (2015). SHELXT – Integrated space-group and crystal-structure determination. *Acta Crystallographica Section A*, 71(1), 3–8. 10.1107/S2053273314026370.
10. Dolomanov, O. V., Bourhis, L. J., Gildea, R. J., Howard, J. A. K., & Puschmann, H. (2009). OLEX2: A complete structure solution, refinement and analysis program. *Journal of Applied Crystallography*, 42(2), 339–341. 10.1107/S0021889808042726.
11. Spackman, M. A., & Jayatilaka, D. (2009). Hirshfeld surface analysis. *CrystEngComm*, 11(1), 19–32. 10.1039/B818330A.
12. Spackman, P. R., Turner, M. J., McKinnon, J. J., Wolff, S. K., Grimwood, D. J., Jayatilaka, D., & Spackman, M. A. (2021). CrystalExplorer: A program for Hirshfeld surface analysis, visualization and quantitative analysis of molecular crystals. *Journal of Applied Crystallography*, 54(3), 1006–1011. 10.1107/S1600576721002910.
13. Becke, A. D. (1993). Density-functional thermochemistry. III. The role of exact exchange. *The Journal of Chemical Physics*, 98(7), 5648–5652. 10.1063/1.464913.
14. Lee, C., Yang, W., & Parr, R. G. (1988). Development of the Colle-Salvetti correlation-energy formula into a functional of the electron density. *Physical Review B*, 37(2), 785–789. 10.1103/PhysRevB.37.785.

15. Vosko, S. H., Wilk, L., & Nusair, M. (1980). Accurate spin-dependent electron liquid correlation energies for local spin density calculations: A critical analysis. *Canadian Journal of Physics*, 58(8), 1200–1211. 10.1139/p80-159.
16. Stephens, P. J., Devlin, F. J., Chabalowski, C. F., & Frisch, M. J. (1994). Ab initio calculation of vibrational absorption and circular dichroism spectra using density functional force fields. *The Journal of Physical Chemistry*, 98(45), 11623–11627. 10.1021/j100096a001.
17. Dewar, M. J. S., Zoebisch, E. G., Healy, E. F., & Stewart, J. J. P. (1985). Development and use of quantum mechanical molecular models. 76. AM1: A new general purpose quantum mechanical molecular model. *Journal of the American Chemical Society*, 107(13), 3902–3909. 10.1021/ja00299a024.
18. Hariharan, P. C., & Pople, J. A. (1973). The influence of polarization functions on molecular orbital hydrogenation energies. *Theoretica Chimica Acta*, 28(3), 213–222. 10.1007/BF00533485.
19. Ditchfield, R., Hehre, W. J., & Pople, J. A. (1971). Self-consistent molecular-orbital methods. IX. An extended Gaussian-type basis for molecular-orbital studies of organic molecules. *The Journal of Chemical Physics*, 54(2), 724–728. 10.1063/1.1674902.
20. Hehre, W. J., Ditchfield, K., & Pople, J. A. (1972). Self-consistent molecular orbital methods. XII. Further extensions of Gaussian-type basis sets for use in molecular orbital studies of organic molecules. *The Journal of Chemical Physics*, 56(5), 2257–2261. 10.1063/1.1677527.
21. Grimme, S., Ehrlich, S., & Goerigk, L. (2011). Effect of the damping function in dispersion corrected density functional theory. *Journal of Computational Chemistry*, 32(7), 1456–1465. 10.1002/jcc.21759.
22. Frisch, M. J., Trucks, G. W., Schlegel, H. B., Scuseria, G. E., Robb, M. A., Cheeseman, J. R., Scalmani, G., Barone, V., Petersson, G. A., Nakatsuji, H., Li, X., Caricato, M., Marenich, A. V., Bloino, J., Janesko, B. G., Gomperts, R., Mennucci, B., Hratchian, H. P., Ortiz, J. V., Izmaylov, A. F., Sonnenberg, J. L., Williams, I.; Ding, F., Lipparini, F., Egidi, F., Goings, J., Peng, B., Petrone, A., Henderson, T., Ranasinghe, D., Zakrzewski, V. G., Gao, J., Rega, N., Zheng, G., Liang, W., Hada, M., Ehara, M., Toyota, K., Fukuda, R., Hasegawa, J., Ishida, M., Nakajima, T., Honda, Y., Kitao, O., Nakai, H., Vreven, T., Throssell, K., Montgomery, J. A., Peralta, J. E., Ogliaro, F., Bearpark, M. J., Heyd, J. J., Brothers, E. N., Kudin, K. N., Staroverov, V. N., Keith, T. A., Kobayashi, R., Normand, J., Raghavachari, K., Rendell, A. P., Burant, J. C., Iyengar, S. S., Tomasi, J., Cossi, M., Millam, J. M., Klene, M., Adamo, C., Cammi, R., Ochterski, J. W., Martin, R. L., Morokuma, K., Farkas, O., Foresman, J. B., & Fox, D. J. (2016). Gaussian 16 Rev. C.01.
23. Öeren, M., Shmatova, E., Tamm, T., & Aav, R. (2014). Computational and ion mobility MS study of (All-S)-cyclohexylhemicucurbit[6]uril structure and complexes. *Physical Chemistry Chemical Physics*, 16(36), 19198–19205. 10.1039/C4CP02202E.
24. Kaabel, S., Adamson, J., Topić, F., Kiesilä, A., Kalenius, E., Öeren, M., Reimund, M., Prigorchenko, E., Löökene, A., Reich, H. J., Rissanen, K., & Aav, R. (2017). Chiral hemicucurbit[8]uril as an anion receptor: Selectivity to size, shape, and charge distribution. *Chemical Science*, 8(3), 2184–2190. 10.1039/C6SC05058A.

25. Cannon, K. M., Britt, D. T., Smith, T. M., Fritsche, R. F., & Batcheldor, D. (2019). Mars global simulant MGS-1: A rocknest-based open standard for basaltic Martian regolith simulants. *Icarus*, 317, 470–478. 10.1016/j.icarus.2018.08.019.
26. Mars Global (MGS-1) High-fidelity Martian dirt simulant. Exolith Lab. <https://exolithsimulants.com/products/mgs-1-mars-global-simulant>